

**Hosam M. Saleh
Amal I. Hassan**

**Geochemistry
and
Mineral Resources**

A Review on Elemental and Isotopic Geochemistry

Riyam N. Khalef, Amal I. Hassan and Hosam M. Saleh

Abstract

Geochemistry is the study of the development, and distribution of chemical elements on Earth, which are found in rock-forming minerals and their byproducts, as well as in living beings, water, and the environment. The elemental geochemical variation of sediments is used to recognize the mechanisms controlling the estuarine environment and serves as a baseline for assessing the environmental effect in the future. Geochemistry is a unique field that deals with the study of mineral deposits. It also addresses the interconnections between the structures of rock, soil, water, and air, which vary according to different places. Furthermore, groundwater is the solely accessible water supply in many desert basins, particularly in developing nations. Geochemical indicators are proper instruments for addressing a diversity of hydrological issues, particularly in arid and semi-arid settings. Thermodynamically, the fugacity of oxygen (f_{O_2}) in solid earth varies by many orders of magnitude. Enstatite chondrites can have high levels of hydrogen abundance, hydrogen, and nitrogen isotope compositions like those of the earth's mantle. The chapter deals with the basic concept of geochemistry and its types, as well as the development of geochemistry. It also explains elemental and isotopes geochemistry, human health, and medical geochemistry.

Keywords: geochemistry, analytical geochemistry, elemental geochemistry, medical geochemistry

1. Introduction

Christian Friedrich Schönbein, a German-Swiss scientist, coined the word “geochemistry” in 1838 [1]. Geochemistry is the study of the chemistry of natural earth materials, and chemical processes that occur within and on the earth's surface today and in the past. Geochemical investigations can thus cover a wide range of minerals and analyses, and they can be carried out in a variety of situations, including industrial, environmental, and educational [2]. The study of chemical processes that occur in natural sources of earth materials such as rocks, as well as the evaluation of their compositions and structures, is called geochemistry. Most geological materials are composed of inorganic minerals. The earth has hundreds of natural minerals [3]. Maybe the greatest explanation is that in geochemistry, we use chemical techniques to address geological issues; scientists use chemistry to comprehend the earth and how it operates. The basic components of the earth are the core (both

inner and outer), mantle, and crust. The latter is composed of igneous, sedimentary, and metamorphic rocks. These rocks are frequently silicates rich in Mg and Fe. Scientists may find rocks with these qualities as xenoliths in lavas; they are Mg- and Fe-rich silicate rocks composed principally of olivine and pyroxenes [4]. Quartz, feldspars, amphiboles, pyroxenes, olivines, biotite, garnets, clay minerals, and calcite are among the naturally occurring minerals that make up most of the earth's crust. Except for calcite, all these minerals are silicates. Most rock-forming minerals of the earth's crust are made of Al, Si, and O. The fundamental primal material of soil is rock, which is broken down by weathering to generate loose debris known as soil parent material, the physical and chemical characteristics of which alter. Earlier research has discovered that the soil parent material is a significant natural source of heavy metals, determining the initial heavy metal level in the soil. Soils of various sorts are found in many geological formations. Indeed, many kinds of soils can exist within the same geological unit. Soil heavy metal contamination is distinguished by its concealment, irreversibility, and long-term nature, which complicates heavy metal pollution control [5].

Heavy metals (HMs) are naturally present in soils, and their quantity reflects the composition of the parent rocks from which they are created. Excessive or high-level concentrations of certain of these metals in soil offer major environmental concerns, including health threats to plant, animal, aquatic, and human life. Therefore, understanding the geochemical and mineralogical composition of sediments may be required to predict the fate of discharged contaminants [6]. Owing to their typical coherent behavior and sensitivity to changes in pH, redox potential, and adsorption/desorption processes, rare earth elements (REEs) compositions are often used as a proxy in groundwater geochemical studies [7]. Geochemical technologies are used in the process of mass prospecting for mineral resources. Their participation significantly improves the efficacy of geological exploration activity and helps geological scientific-technical advancement. Finding previously unknown mineral deposits needs a geochemical investigation. To emphasize the geographical relationship of geochemical patterns, create elemental correlations, or extract geochemical anomalies induced by mineralization, several approaches have been used to analyze geochemical exploration data. In recent decades, there has been a lot of interest in the normal, lognormal, power-law, multimodal, and sophisticated distribution laws of geochemical element concentrations. Methods including classic statistics, multivariate statistics, geostatistics, fractal/multifractal, machine learning, and deep learning algorithms that follow distribution laws have been used to identify geochemical anomalies associated with targeted mineralization [8].

Elemental geochemical characteristics and their ratios are extensively used to evaluate paleoenvironmental conditions, ancient water compositions, paleotectonic settings, and sedimentary rock origin.

This chapter describes the geochemistry of elemental and isotopes and their impact on the environment and humans.

2. Analytical geochemistry

Analytical geochemistry generally focuses on 5 approaches: (1) major element geochemistry; (2) trace element geochemistry; (3) mass fractionation determination; (4) age dating; and (5) radionuclides isotopes for geochemical probes. When

geochemistry first began, the idea was to use conventional wet chemistry to identify the bulk main elements. One of the most prevalent methods for classifying igneous rocks was to use a total alkali versus silica) diagram. The classification of rocks is straightforward yet crucial, although an exact determination of the primary constituents is necessary. X-ray fluorescence spectroscopy was created to replace the time-consuming and difficult conventional wet chemistry, and it has been widely utilized since then.

Geochemical analyses are performed for industrial, environmental, or academic reasons; thus, involve a diverse range of materials and analytes of interest such as air, volcanic gas, water, dust, soil, rock, or biological hard tissues (particularly ancient biological tissues), as well as anthropogenic materials, such as industrial effluent and sewage sludge [9]. The analytical approaches used in geochemistry are categorized based on the physical principles into eight methods, as illustrated in **Figure 1**. Methods like mass spectroscopy dominate fields like isotope geochemistry, despite their wide range of sample types and machine preparation [11]. Whether the composition of rocks, glass chemistry or minerals is important in areas like sedimentary, igneous rocks, metamorphic geochemistry, as well as other domains of geochemistry directly related to petroleum research, a variety of analytical methods are frequently used. The process of figuring out the chemical interactions that exist between mineral grains is known as mineral analysis. To analyze major and trace elements, analytical techniques with high precision such as X-ray spectroscopy, ionic radiation techniques, and laser ablation processes are frequently used [12].

Aside from minerals, the study of fluid inclusions (small drops of fluid trapped inside crystals during the initial growth of the solution or later) has aided in the development of modern theories of ore origin, reproduction, formation, oil migration, accumulation, as well as our understanding of the importance of the liquid stage in a variety of geological processes [13]. Fission path analysis is a specialized method

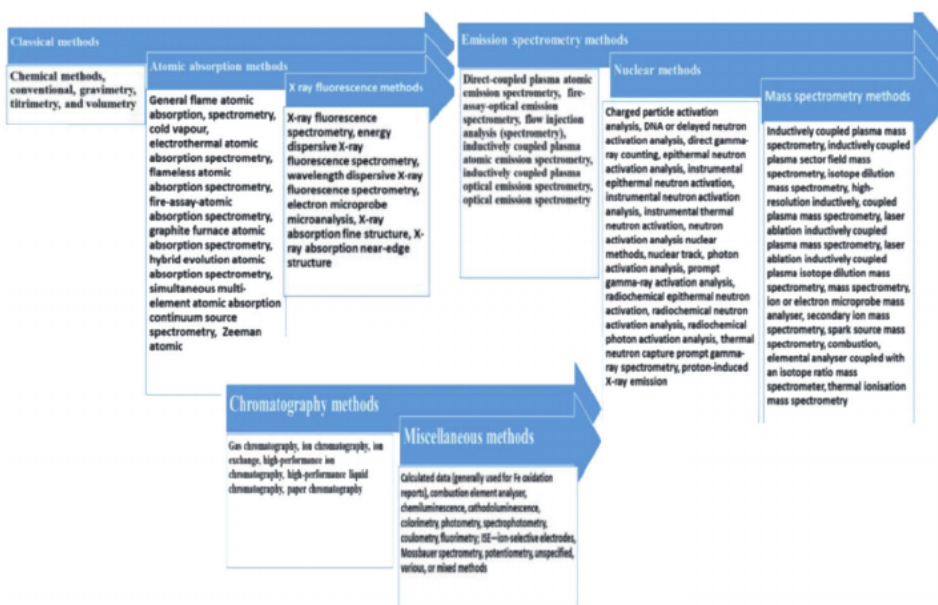


Figure 1.
 Geochemical analyses modified from [10].

for extracting information from minerals that analyses the signs of physical damage caused by the spontaneous fission of the original nucleus to the crystal network. When the rate of spontaneous fission is known, the accumulation of these fission pathways can be used as a dating tool in other geological studies [14].

X-ray Fluorescence Spectrometer (XRF) is mostly used to analyze solid materials. A 100 mg sample is diluted 10 times with a flux made of pure LiBO_2 and $\text{Li}_2\text{B}_4\text{O}_7$ and melted into a glass bead in a Pt crucible [15]. Because the absorption of X-rays rises with mass number, lithium borate is a good material for making the glass bead for measuring the emitted X-rays [15]. The chamber is kept under a vacuum to reduce the loss of secondary X-rays. The mass numbers of N_2 and O_2 in the air are greater than those of Li or B. As a result, X-rays were absorbed or dispersed by these gases. As a result, X-rays were absorbed or dispersed by these gases. A vacuum is also wanted to prevent the diffracting crystals from deliquescence. To correctly find the principal elements, measurements of H_2O (–), H_2O (+), LOI (loss on ignition), and the ferric/ferrous ratio (Fe(II)/Fe(III)) are necessary. The weight of absorbed water is denoted by H_2O (). The weight difference between the sample at room temperature and after heating it to 105°C was measured. This is insignificant for hard silicate rock, but it becomes significant for new deep-sea sediments. The weight difference between the raw sample and that heated at 1000°C in a porcelain crucible is referred to as the LOI.

3. The evolution of geochemistry

Geochemistry developed from the same metallurgy and alchemy roots as chemistry and emerged as a distinct subfield of chemistry and geology in the nineteenth century [16]. Clarke Goldschmidt and Vernadsky's works laid the groundwork for the field's subsequent development and progress in the 20th and 21st centuries [17]. Geochemistry has become an integral part of all aspects of earth and planetary sciences over that time, greatly enriching our understanding of the nature and evolution of our planet [17]. Geochemistry is a modern science and belongs to the group of earth sciences that studies the composition and geological history of the earth. Geochemistry arose because of the accumulation of large numbers of geological and chemical studies, and the urgent need to solve many of the issues associated with the exploration of useful ores reservoirs [18]. The field of geochemistry has expanded, and branches such as organic geochemistry have emerged. Organic materials are the cornerstone of this branch of geochemistry means organic geochemistry in two main divisions: a) oil chemistry, asphalt, coal, humic acids, and other organic components that are found in sedimentary rocks; b) the role of organic processes and living organisms in fixing inorganic elements. This type of study is sometimes called biogeochemistry. Geochemistry also blends with other branches of science such as mathematics, physics, and statistics and has become a quantitative trend in recent years. Thermodynamics is considered the backbone of experimental geochemistry to predict the chemical reactions between minerals [19]. As for statistics, it is possible to describe the chemical composition of large groups of land units of the crust, even the interactions of igneous rocks, at statistical rates. Geochemistry has also benefited from contemporary methods in determining the properties of solid materials. These methods can be divided into chemical analysis and structural analysis techniques. The latter includes the technical method that extends to understanding the nature of chemical bonds. The ancient chemical methods of analyzing minerals and rocks depended on using acids and other chemicals to determine the proportion of major elements. There has been a

tremendous development in this field, where the use of emission X-ray spectroscopy is an alternative method for the analysis of major and trace elements [9].

Elemental geochemistry is concerned with studying the distribution of chemical elements, their forms of existence, and their concentration rates in metals, rocks, and earth's mantle [20]. This branch has made it possible to reveal many facts about the distribution of chemical elements.

Biogeochemistry studies the distribution of chemical elements and their concentrations in organic matter, the role of living organisms in the movement of these elements, and their distribution in the earth's various atmospheres [21]. Although the weight of living organisms is estimated at 0.01% of the weight of earth's crust, they have a significant role in geological processes, which are called biogeochemical processes. We cite as an example that iodine is obtained mainly from some types of marine plants that extract it from seawater and concentrate it in their tissues in proportions hundreds of times higher than its concentration in water. These processes also include photosynthesis and the liberation of oxygen under the influence of solar energy, which is stored in the form of fossil fuels (coal, oil, and gas). One of the crucial topics in this science is the study of the biogeochemical provinces, which are areas in which the concentrations of chemical elements change from their general rates, increasing or decreasing [21]. It was found that there are at least thirty chemical elements involved in the formation of these zones. The iodine-poor provinces, which spread in high areas, the interior parts of the continents and others, the regions poor in fluorine, which causes tooth decay, and the provinces rich in fluorine and volcanic areas and the areas of the spread of apatite rocks, and usually, cause osteoporosis.

Isotope geochemistry studies the distribution of isotopes in the chemical elements that make up natural bodies (rocks, metals, water, and organic matter) [22]. Another aspect of this science is finding the absolute ages of bodies and natural phenomena using radioactive elements such as uranium, thorium, and potassium (K40). Cosmochemistry is concerned with studying the distribution of chemical elements and their concentrations in celestial bodies, especially meteorites. It also interests the effect of cosmic rays on the components of the earth's atmosphere, especially the gaseous atmosphere, which causes the formation of some elements such as carbon-14 [23]. Cosmological studies are helpful in verifying information about the origin and development of the earth and the evolution of geological processes. Isotopes are atoms of the same element with differing numbers of neutrons. Differences in the number of neutrons among distinct isotopes of an element indicate that the isotopes have different masses. Isotopes of the same element have the same number of protons. All isotopes of oxygen contain 8 protons, but an oxygen atom with a mass of 18 (denoted ^{18}O) has two more neutrons than oxygen with a mass of 16 (^{16}O).

Nuclear reactions in stars determine the primordial isotopic compositions of planetary systems. Radioactive decay, cosmic ray interactions, mass-dependent fractionations that go with inorganic and biological reactions, and anthropogenic activities such as nuclear fuel processing, reactor accidents, and nuclear-weapons testing can change isotopic compositions in terrestrial environments over time. Nuclides (isotope-specific atoms) that spontaneously break down over time to generate other isotopes are known as radioactive (unstable) isotopes. Radioactive isotopes release alpha or beta particles, as well as gamma rays, during disintegration. On geologic time scales, stable isotopes do not appear to decay to other isotopes, yet they can be generated by the decay of radioactive isotopes. Therefore, the main target of this chapter is the geochemistry of elemental and isotopes and their impact on the environment and humans. Fractionating processes cause changes in the stable isotope compositions of

metals and metalloids. Radiogenic processes can cause metal stable isotope variations in some elements, such as the radioactive decay of unstable to stable isotopes [24]. Strontium (Sr) and lead (Pb), both of which have four stable isotopes, are the most important examples of environmental studies. For Sr, one isotope is influenced by radiogenic processes (^{87}Rb , ^{87}Sr decay), whereas the other three are only influenced by stable isotope fractionation (e.g., $^{88}\text{Sr}/^{86}\text{Sr}$), allowing Sr. isotope signatures to be used as two-dimensional tracers by investigating radiogenic processes and stable isotope fractionation in parallel [25]. While radiogenic Sr. isotope variations have been studied for decades and applied in many fields, such as ecosystem research, natural water studies, and archaeology, stable Sr. isotope fractionation research is still in its infancy. Three of the four stable isotopes of Pb are byproducts of radioactive U-Th decay chains. As a result, stable Pb isotope fractionation in natural samples cannot be detected because there is no ratio between two isotopes that is unaffected by radiogenic processes [25]. Depending on the geochemical composition and age of the source materials, relatively large Pb isotope variations between environmental samples can be observed, and these are generally thought to outnumber potentially occurring mass-dependent and nuclear-volume effects of Pb isotopes by a factor of up to 200 [26]. Natural (e.g., $^{210}\text{Pb}_{25}$) and anthropogenic nuclear processes produce some radioactive metal isotopes (e.g., ^{137}Cs). Finally, metal stable isotopes used as enriched tracers (or “spikes”) have a wide range of applications in environmental research [27].

Groundwater geochemistry studies the groundwater, which is a vital water resource that must be protected to preserve its long-term viability. Aquifer resource evaluation needs a right report on the origin, age, source, and migratory passages of groundwater. To determine provincial impacts in an aquifer using just hydrogeologic procedures, data from several wells, time-series analysis of water levels, discharge monitoring, and permeability and aquifer boundary measurements are frequently required. Deep under the Earth, water reduces the melting temperature of rock, resulting in magma that forms the continents. Deep crustal fluids, such as chloride-rich brine, transport gold, and other metals to create ore deposits. The water of the ancient oceans served as a crucible for the evolution of early life, and freshwater is the foundation of life on earth. Homogeneous hydrogeochemical reactions include only one phase, whereas heterogeneous reactions involve two or more phases, such as gas and water, water and solids, or gas and solids. In contrast to open systems, closed systems can only interchange energy with the environment, not components. Multi-tracer studies are often used to estimate hydrodynamic characteristics such as groundwater flow, mixing patterns between different groundwater sources, and recharge rate and such data are required to better water-resource management. However, in arid areas, estimation of groundwater recharge remains complicated because of spatial variability of rainfall and a low amount of recharge.

4. An insight into isotope geochemistry: history and importance

Because of their suitable geochemical and nuclear properties, isotopes are used as tracers and chronometers to study a wide range of topics, including rock and mineral chronology, reconstruction of sea-level changes, rock water interactions, and magmatic processes [28]. Isotopic observations have revealed time scales of mixing processes in the seas and atmosphere and the residence durations of marine components and gases in the atmosphere. Isotope geochemistry is a branch of geology that studies the natural fluctuations in the relative abundance of isotopes

of certain elements [29]. Isotope ratio mass spectrometry measures variations in isotope abundance and can give information about the ages and origins of rocks, air, and water bodies, as well as their mixing processes. The geochemistry of radioactive isotopes is concerned with Nucleosynthesis, Radiogenic, and Stable Isotopes (**Figure 2**). Nucleosynthesis (i.e., the origin of elements) in stars can generate “new” heavy isotopes like Proton-proton (H to He), Helium burning (He to C), s-process (neutron capture), and p-process (proton capture). Plutonium isotopes, $^{239}\text{-Pu}$, $^{240}\text{-Pu}$, and $^{241}\text{-Pu}$ are produced in nearly all nuclear reactors by neutron capture on naturally occurring uranium $^{238}\text{-U}$ [30].

The measurement of the age of the earth and our solar system is arguably the most significant milestone in the use of isotopes in earth science. Isotope-based dating methods are the gold standard and are utilized to confirm non-isotope-based dating methods. Stable isotope tests of organic materials, and phosphate in bones and teeth in recovered fossils, give evidence for dietary sources ingested by humans and other animals.

The isotope geochemistry domain began after Henri Becquerel discovered a radioactivity item in 1896 [31]. Within a few years, following this astounding finding, Rutherford reported an exponential decline in radioactive material activity with time and created the notion of half-lives, paving the way for the age determination of natural compounds containing radioactive elements (Rutherford 1900) [31]. Soddy coined the term “isotope” in 1913 (Soddy 1913). Soddy (1913) and Fajans (1913) developed the principles regulating the transformation of elements during radioactive decay at the same time (1913). Rutherford determined the first radiometric age of a geologic sample on a pitchblende sample in 1905, and the ages of the number of other minerals were later determined by Strutt (1905) and Boltwood (1907) using the U-He and U-Pb techniques. The full ^{238}U and ^{232}Th chain, which is still in use today, was formed in 1913 [28]. The disequilibria between members of the U-Th series caused by differences in the geochemical properties of different elements within the chain opened a new field of study to investigate different geochemical processes like rock-water interaction, dating of inorganic precipitates, detrital and biogenic sediments, and archeological objects. One of the most important findings in this field was the discovery of substantial fractionations of ^{238}U and ^{234}U in rocks, rock leachates, and natural waters [32]. Protons, alpha particles, electrons, helium, nuclei of other elements, and subatomic particles are charged particles (including high-energy charged particles) that make up cosmic rays. The high-energy charged particles that reach the atmosphere interact with atmospheric components (e.g., N, O, Ar, and so on) to form a variety of cosmogenic radioactive isotopes with half-lives ranging from a few

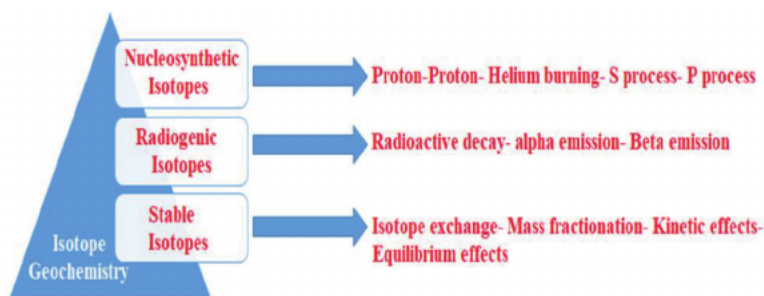


Figure 2.
Types of isotope geochemistry.

minutes to millions of years [33]. Some cosmogenic isotopes (e.g., ^{14}C , ^{10}Be , ^7Be) have been used to quantify processes in earth surface reservoirs such as air-sea exchange, atmospheric mixing, ocean circulation and mixing, scavenging, sediment accumulation and mixing rates in aqueous systems, erosion rates, exposure ages, changes in cosmic ray production rates, and human civilization history. Murphy and Urey (1932), Nier and Gulbransen (1939), Dole and Slobod (1940), and Urey (1948) were among the first to quantify stable isotopes in terrestrial materials, long before the discovery of cosmogenic isotopes like ^7Be , ^{10}Be , and ^{14}C . Urey (1947) and Bigeleisen and Mayer (1947) used statistical quantum mechanics and statistical thermodynamics to give the theoretical underpinning for isotopic fractionation. Stable isotope geothermometry is used at low temperatures, that is, non-magmatic temperatures, due to the dependency of the equilibrium constant on the inverse square of temperature. The fractionations are often minor at temperatures over 800°C or thereabouts, making precise temperature determination problematic [34]. However, even at temperatures in the upper mantle (1000°C or higher), fractionations remain considerable, albeit minor. Fractionation factors for minerals in the temperature range of 600° to 1300°C were obtained experimentally and matched with theoretical estimates.

Radioactive and stable isotopes have consequences on humans, both directly and as tracers of processes, that affect their well-being. Human activities such as nuclear weapons, testing, and accidents have released certain radioactive isotopes into the environment [35]. The majority are naturally formed, both from the earth's original composition and through the ongoing synthesis of U isotopes and Th by cosmic rays, which produce a variety of radioactive daughters and ^{40}K in biological systems and the environment.

5. The elemental geochemistry

The elemental geochemistry of clastic sedimentary rocks offers critical information for recognizing sedimentary histories, such as chemical weathering history, nature and composition of sediment origin, sediment transit, and diagenetic history. Geochemical apprehension of these challenges constrains many basic geological topics, including paleoclimates, tectonic linkages, basin formation, diagenetic fluid movement, and crust-mantle evolution. Geochemical apprehension of these concerns constrains many basic geological topics, including paleoclimates, tectonic linkages, basin formation, diagenetic fluid movement, and crust-mantle evolution. Experience from the Mars Exploration Rovers Spirit and Opportunity, orbital spectroscopy, and experiments with Mars-like compositions, demonstrate that such approaches apply to sedimentary environments on Mars, where primary igneous compositions and aqueous conditions may differ from our terrestrial experience. The elemental geochemistry index is currently a reliable predictor of marine and lake habitats. The variation in elemental geochemical characteristics indicates the lithofacies of the shale and the sedimentary environment. Wang et al. [36] discovered that lake-water depth fluctuates from deep to shallow in a high-frequency sequence unit, and element ratios in shales shift regularly, particularly near the high-frequency cycle interface [36]. Chemostratigraphy is the study of inorganic/organic chemical changes within sedimentary sequences, depending on the rock's elemental or isotopic composition [37]. It is a significant device for the discovery and exploitation of unconventional resources. A rock's chemistry changes depending on its mineral makeup. Because rock chemistry is so easily measurable, the rocks may be put in a chronostratigraphic

sequence framework [38]. Because the $\text{Al}_2\text{O}_3/\text{TiO}_2$ ratio grows from 3 to 8 for mafic igneous rocks, 8 to 21 for intermediate rocks, and 21 to 70 for felsic igneous rocks, the $\text{Al}_2\text{O}_3/\text{TiO}_2$ ratio of most clastic rocks is used to infer the source rock compositions [39]. Source rock composition, length of weathering, climatic conditions, and rates of tectonic uplift of the source location mainly controlled the chemical weathering of source rocks. About 75% of the upper crust's labile material comprises feldspars and volcanic glass, and the chemical weathering of these components eventually culminates in the production of clay minerals [40, 41]. Ca, Na, and K are mainly eliminated from source rocks during chemical weathering. The quantity of these elements that survive in soil profiles and sediments produced from them is a sensitive indicator of chemical weathering severity. If the alkali contents ($\text{K}_2\text{O} + \text{Na}_2\text{O}$) and $\text{K}_2\text{O}/\text{Na}_2\text{O}$ ratios in silica clastic sedimentary rocks are devoid of alkali-related post-depositional changes, then they are regarded credible indicators of the source material's weathering severity [42].

Recently, the sequential stratigraphy of shale has been studied in many regions around the world. Those investigations revealed that, even in an environment conducive to organic matter accumulation, the characteristics and distribution of source rocks changed systemically both vertically and laterally. This alteration can vary from a few centimeters to hundreds of meters and can be laminae to super-sequence [43]. The sedimentary environment and stratigraphic stacking patterns affect the transition, which occurs at both sequence and para-sequence scales. The primary unit of characterizing organic matter enrichment is the para-sequence, and the interior rock characteristics (or litho-faces/facies) of the para-sequence also underwent systematic modifications. Previous research has found a unique association between shale formation division and its sequence hierarchy [43]. Previous studies found that the high-frequency sequence separation of lake-facies sediments occurred mostly during the deposition of coarse debris sediments [44]. Coarse-grained silt shows evident lithologic alterations, making detection of progradation and retrogradation as well as high-frequency sequence division simple. However, dividing shale sequence stratigraphy (particularly high-frequency sequence) is a tough task and a difficult point in the study of high-frequency sequence. Previous studies found that the high-frequency sequence separation of lake-facies sediments occurred mostly during the deposition of coarse debris sediments [45]. Coarse-grained silt shows evident lithologic alterations, making detection of progradation and retrogradation as well as high-frequency sequence division simple. However, dividing shale sequence stratigraphy (particularly high-frequency sequence) is a tough task and a difficult point in the study of high-frequency sequence. The elemental geochemistry index is now a reliable indicator for marine and lake ecosystems. The variation in elemental geochemical parameters reflects the lithofacies of shale and the sedimentary environment [46]. Wang et al. discovered that lake-water depth fluctuates from deep to shallow in a high-frequency sequence unit, and element ratios in shales shift regularly, particularly near the high-frequency cycle interface [36]. The periodic vertical change of organic geochemical parameters in the lacustrine basin serves as a foundation for sequence stratigraphic unit categorization and linkage. Jin et al. [47] discovered strong correlations between the vertical change of geochemical elements and para-sequence cycle changes in lake-facies shales, and the cyclic change of geochemical elements can also be used to classify the stratigraphy division of high-frequency sequences in shales. Their research established the importance of employing geochemical components in high-frequency shale sequence stratigraphic division studies, which has significant implications for shale gas and oil exploration and production.

6. Light elements in the earth

The light elements found in the earth's core are yet unknown; however, they might include silicon, oxygen, sulfur, carbon, and hydrogen [48]. Knowledge of the earth's building blocks, planetary accretion and core formation processes, and subsequent chemical and thermal development of the core requires an understanding of the nature of the light elements in the core. Hydrogen, carbon, oxygen, silicon, and sulfur are possibly the primary light elements [49]. The earth's core is mostly made up of iron and nickel alloyed with lighter elements including oxygen, silicon, Sulfur, carbon, and hydrogen in amounts of 5–10 wt. %. Because oxygen is the most representative element on earth, it has been postulated as a possible main light element [50].

The density deficit of elements, such as silicon, sulfur, or oxygen was assigned. Over the years, several researchers have investigated several elements lighter than iron, such as silicon, sulfur, oxygen, hydrogen, and carbon, either alone or in combination. The existence and significance of a freezing point depression at the inner core boundary (ICB), on which major questions in geophysics and geochemistry hinge, such as to what extent are light elements released at the ICB, thus inducing compositional convection thought to power the geodynamic the temperature at the ICB lower than the melting temperature [51]. When compared to pure iron, the presence of significant amounts of low atomic number 'light' elements like sulfur, silicon, oxygen, carbon, and hydrogen in the earth's outer and inner cores result in a density deficit. Core composition estimates may only be obtained indirectly due to their inaccessibility, by combining results from high-pressure tests and theoretical calculations with seismic data [51]. Restrictions on individual light element concentrations in the core might provide insights into the nature of earth's building blocks and the path of accretion. More oxidized material from the outer Solar System is thought to have been added near the end of accumulation. Although the amounts of Si, O, and H in the core are still constrained, they would be significant inputs into such a scenario. Although core amounts of Si, O, and H are still constrained, they would be important inputs in such a scenario [52]. The behavior of core-mantle (metal-silicate) element partitioning is affected by metal composition, specifically S, Si, and O concentrations. Recognizing the core, light element concentrations would lead to a better understanding of earth's core-mantle element partitioning and core formation conditions. The presence of H in the core suggests that H₂O was not only delivered in the final stage of accretion but was also incorporated into core-forming metals via a hydrous magma ocean. The upper bound of 900 ppm H in the bulk earth corresponds to 8100 ppm H₂O, implying that up to 35 times the current ocean mass of water could have been brought to our planet. This high-water content agrees with upper estimates for the number of oceans on earth derived from ab initio calculations of hydrogen partitioning between silicate melt and liquid iron at core-forming conditions.

Metal-silicate partitioning data should assist limit each light element's concentrations in core-forming metals and abundances in the bulk silicate earth (albeit uncertainties remain due to unknowns regarding the degree of chemical equilibrium²⁰) (BSE) [52].

Recognizing earth accretion, core formation, and the maintenance of the earth's magnetic field requires constraining the core's composition. The presence of significant amounts of low atomic number "light" elements such as sulfur, silicon, oxygen, carbon, and hydrogen in the earth's outer and inner cores results in a density deficit relative to pure iron. The following is a display of these elements:

1. Oxygen

The oxygen fugacity of gas of solar composition is calculated using the procedure $H_2 + 12O_2 \rightarrow H_2O$ after accounting for the oxygen connected to carbon in CO and other less prevalent oxides. The bulk of the Solar System's rocky planets, including earth, developed with DIW five orders of magnitude bigger than that of solar gas, according to meteorite research. Oxygen fugacity was likely strong during the early phases of rock formation in the Solar System, as evidenced by significant levels of iron linked to oxygen in silicates in chondrite meteorites. Sublimation of water-rich and/or rock-rich dust at high dust/gas ratios may cause an increase in oxygen fugacity during rocky body formation. In this regard, we'd like to know if the mechanisms that cause rock oxidation in the Solar System are replicated in other planetary systems, and if rocky exoplanets exist as a result geophysical and geochemical characteristics of the earth are shared [53]. Geophysical and geochemical characteristics of the earth are shared. As a result, whether rocky exoplanets reflect or not, the earth's geophysical and geological characteristic is an open question. Carbonate oxygen and carbon isotopes are often utilized as tracers of mineral precipitation temperatures and fluid sources, and bulk rock techniques are typically used to study them. The oxygen and carbon isotopic compositions of Wade Dima carbonates were examined utilizing two complementary techniques, ranging from mm-scale micro-bulk-rock investigations to m-scale in situ isotopic analyses [54].

In solid earth, the thermodynamic property of oxygen fugacity (fO_2) varies by many orders of magnitude. The capacity of fayalite-magnetite-quartz to link to equilibrium, depending on the relative concentrations of ferric and ferrous iron, is commonly portrayed. Arc magmas contain more Fe^{3+} (and hence greater estimated oxygen fugacity) than mid-ocean ridge basalts, as well as a lot of water and other volatile elements (e.g., S, C, F). They vary from MORB in that they have greater chalcophile (sulphur-loving) element concentrations and are typically found in Cu-Au-Ag ore deposits [55].

Because large-scale oxygen isotope fractionation occurs only near the earth's surface, deviations from the average $\delta^{18}O$ of mantle-derived rocks, whether positive or negative, are usually attributed to the presence of recycled crustal material in the mantle source or the interaction of mantle-derived melts with crustal material during ascent. Valley *et al.* [56] find that the $\delta^{18}O$ of magmatic zircons have remained relatively constant (and similar to modern mantle) throughout time, back to 4.4 billion years ago (4.4 Ga). This suggests that the $\delta^{18}O$ content of the mantle has stayed relatively stable throughout the earth's history. Upper mantle and crust melting produce Hadean and Archaean zircons [57]. As a result, this composition of carbonate isotope ratios may be a proxy for limnological conditions. Furthermore, the differential accumulation of certain trace elements during source rock deposition may preserve information about paleoclimate conditions during source rock deposition, which can be used to categorize sedimentary environments [58].

2. Hydrogen

The core may contain the world's largest H reservoir. The H partition coefficient between iron and silicate, which melts at high pressures and temperatures, was recently calculated by combining ab initio molecular dynamics with thermodynamic integration, and it was proven that under core-formation conditions, H prefers to partition into the iron liquid. The amount of water dissolved into the silicate mantle

during core-mantle differentiation determines the optimal quantity of H in the core, which is linked to water in the materials accreting to build earth and its accretion processes. New research suggests that enstatite chondrites (EC), which are assumed to be representative of the materials that formed the earth, may contain high levels of hydrogen and have hydrogen and nitrogen isotope compositions similar to the earth's mantle [59].

Kerogen is described as the fraction of sedimentary organic constituents of sedimentary rocks that are insoluble in common organic solvents. Kerogens are derived from organic materials such as algae, pollen, wood, vitrinite, and structureless material. Different kerogens have varying amounts of hydrogen concerning carbon and oxygen. The hydrogen content of kerogen determines the oil vs. gas yields from primary hydrocarbon-generating reactions [60].

The first hydrogen index (HI) of hydrogen-rich kerogen is higher, while the initial hydrogen index of hydrogen-poor kerogen is lower. As a result, the early HI levels of marine shales are linked to paleo productivity, terrestrial input, and preservation. The photosynthetic intensity of phytoplankton in the photic zone influences paleo productivity, which can be estimated using a range of geochemical proxies such as organic P (Porg), and biogenic Ba (Babio), excess Si (EXSiO₂), and trace elements. In theory, inorganic geochemical techniques can be used to approximate the original TOC contents and recover the original HI values of high to over-mature marine shales. Because shale formation is so complicated, it's crucial to consider all of the influencing variables, such as the shale's formation mechanism and depositional or diagenetic settings, as these have varying effects on geochemical parameters. Examine the inorganic proxies and use a preservation or redox perspective to compute the original hydrogen index [60].

Much experimental research has been undertaken to examine the mechanisms of hydrogen incorporation in olivine under various thermodynamic settings, because the viscosity of olivine-rich rock may decrease as impurities such as H, Fe, or Ti are integrated (e.g., pressure, temperature, f_{O_2} , f_{H_2O} , a SiO₂, and chemical composition). A new experimental approach involves doping olivine with a high proportion of atomic impurity before or after hydration. While these studies reveal a distinct method of H incorporation, the findings aren't always applicable to the earth's upper mantle [61].

3. Silicon

Silicon is the third most abundant element on the planet (atomic weight: 28.08553). (16.1% Si; since it is lithophile and reacts incompatibly with other elements during mantle melting, the oceanic and continental crusts are richer in Si than the mantle). In terrestrial conditions, silicon has a single valence state (Si⁴⁺) and does not produce volatile compounds. On the silicate earth, native Si is rare; instead, Si is almost usually bonded to O as the SiO tetrahedron. Si is a crucial cation in the silicate earth and is essential in the biosphere, with diatoms accounting for more than half of ocean primary production. It is also a result of successful continental erosion, which feeds the marine ecosystem. As a result, it's not surprising that the early uses of Si isotopes, which were within the scope of low-precision technology, were centered on the earth's supergene semiconductor environment [62].

At first, silicon was assumed to be a light component in the core. Since then, silicon has advanced to become one of the most promising materials. The earth's mantle has a higher Mg/Si ratio than chondrites ("missing Si"), which can be explained by a large amount of silicon in the core. The absorption of Si into the core also explains

why bulk earth has a higher Si isotopic composition than chondrites, but the explanation for such a disparity in Si isotope composition and Si isotopic fractionation factor remains a mystery. Furthermore, because silicon and iron are known to form a wide solid solution, a Fe–Si alloy could approximate the density and compressional-wave velocity of the inner core. Previous theoretical investigations and observations on the Fe–Si binary system at 21 GPa, on the other hand, have shown that the variation in Si concentration between coexisting liquid and solid is far too small to account for the observed density rise at this temperature [63].

The first technique used to precisely identify silicon isotope compositions of interest in geochemistry was gas source mass spectrometry. This method entails breaking down the sample with HF, followed by a series of chemical conversion procedures which vary across authors to generate SiF₄, it can then be injected into a mass spectrometer with a gas source for isotopic analysis. Because sample breakdown and subsequent purification usually result in isotopic fractionation, it is critical to develop a silicon purification yield that is as near to 100% feasible. Following that, the Apollo lunar sample return mission generated d³⁰Si values that were repeated or quadrupled and claimed to fall within an “average deviation” of 0.11 or better if sample fluorination with the F₂ gas was utilized [64].

Silicon could be a light element component for geophysical and geochemical reasons. Lin et al. [65] used the Fe_{0.85}Si_{0.15} Fe-rich Fe–Si alloy as an example to investigate the effect of a light element on the physical properties of Fe. This is done for several reasons, including the ones listed below: (1) in the core, the abundance of light element(s) is only 10% by weight. (2) Most light elements, such as oxygen and sulfur, have limited solubility in Fe and form intermediate compounds with Fe (such as FeO, FeS, and Fe₃S₂) over a narrow pressure-temperature range; (3) silicon readily forms alloys with Fe under ambient conditions; and (4) Fe-rich Fe–Ni and Fe–Si alloys adopt the hexagonal close-packed (hcp) structure at high pressures, imposing a significant restriction on the crystal structure of the inner core [66].

Figure 3 depicts the general pattern of ³⁰Si fluctuations in numerous geological processes in terrestrial reservoirs. The fractionation of the silicon thermodynamic isotope induced by low-temperature geological processes such as chemical weathering, biogenic/non-biogenic precipitation, adsorption, and biological absorption is smaller at elevated temperatures. Silicon isotope geochemistry provides critical geochemical constraints for tracing bio-physicochemical processes in terrestrial environments, mineral deposit formation, hydrothermal fluid activities, meteorite and planetary evolutions, and a better understanding of the mechanisms underlying silicon isotope fractionation in common geological processes [68].

Silicon (Si) is the second most prevalent element in earth’s lithosphere crust, and it is used in a variety of geochemical and biochemical processes. This “Si biosphere” is fed by chemical weathering, which produces secondary minerals with considerable negative Si isotope fractionation and a heavy Si fluid phase. The exact Si isotope content of the protolith, i.e., the continental crust, is unknown; however, it can currently be determined using inductively coupled plasma mass spectrometry with many detectors (MC-ICPMS). The exact and accurate analysis of all three stable isotopes (²⁸Si, ²⁹Si, and ³⁰Si) at high mass resolution has been made possible by these methods. Igneous processes cause minor isotope differences [69].

Silicon (Si) is a crucial nutrient for photosynthetic marine diatoms and, as a result, indirectly influences the oceanic CO₂ storage capacity. Rivers transmit 85% of the silicon dissolved (DSi) that enters the ocean (**Figures 3 and 4**). Chemical weathering of continental silicate provides for 45% of the riverine dissolved load. Importantly,

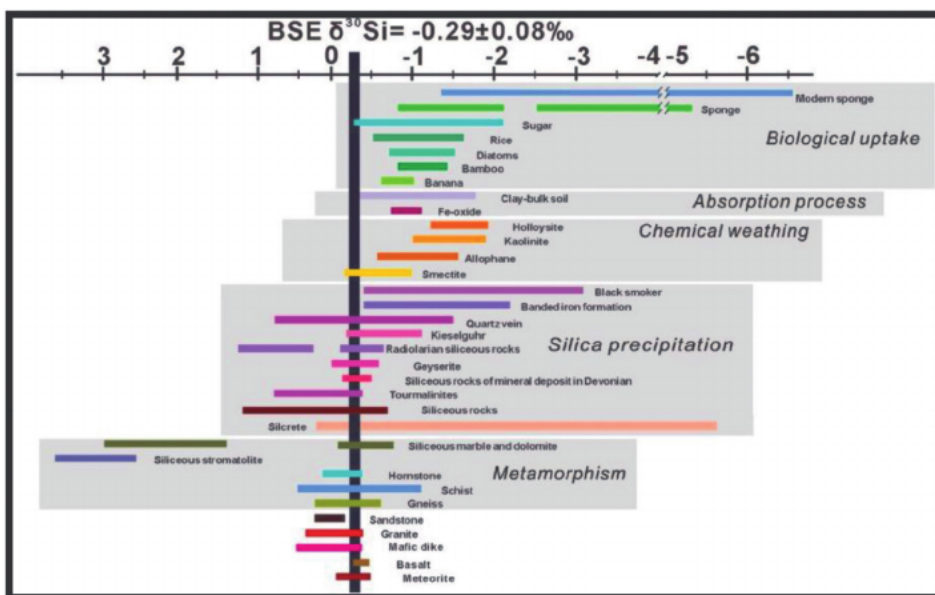


Figure 3. Variations in silicon isotopes in nature as a consequence of host rocks, animals, and associated processes of geology [67].

the Ca and Mg silicate rocks undergo chemical weathering. Affects atmospheric CO₂ concentrations, thereby controlling climate throughout geological periods [70].

4. Aluminum

The modern-day global Si cycle is represented as just a cartoon schematic (**Figure 3**). The fluxes' magnitudes (in 10¹² mol yr⁻¹) and corresponding ³⁰Si values (in percent) are displayed as the most common fractionations (ε, ‰). Inset panels show the mechanisms involved in the production of biogenic silica (BSi) and clay minerals. Lines represent particle fluxes, while solid lines indicate solute fluxes or transformations. Details can be regarded as primary text [68].

Although the role of acidity in the behavior of Aluminum in the podsolization hypothesis is not novel, it was not highlighted in the TACAD investigation. Soils containing HBEF were assessed using the podsolization theory. The organic carbon to organic A1 ratios (C/A1) decreased as soil depth increased. The O₂-horizon has a C/A1 of 228 while the Bhs3-horizon has a C/A1 of 14. Because the solubility of organic A1 complexes decreases as the C/A1 decreases, the lower C/A1 in B-horizon soils was interpreted as evidence of A1 retention, as predicted by the podsolization theory. In the Bhs 1- horizon, however, there was a small but significant loss of inorganic A1. This mobilized A1 was exported from the watershed rather than being kept in the lower B-horizons. Significant deviations from the podsolization theory were found in alkaline European locales. Dissolved A1 concentrations increased with soil type in the Netherlands. The depth (upper 40 cm) and inorganic A1 species accounted for more than 80% of dissolved A1 in B-horizon soil solutions [71].

A common mineralogical characteristic of massif-type anorthosite complexes is high-aluminum orthopyroxene megacrysts (HAOMs). Their primitive geochemical characteristics (high Mg and juvenile isotope signature), high aluminum content

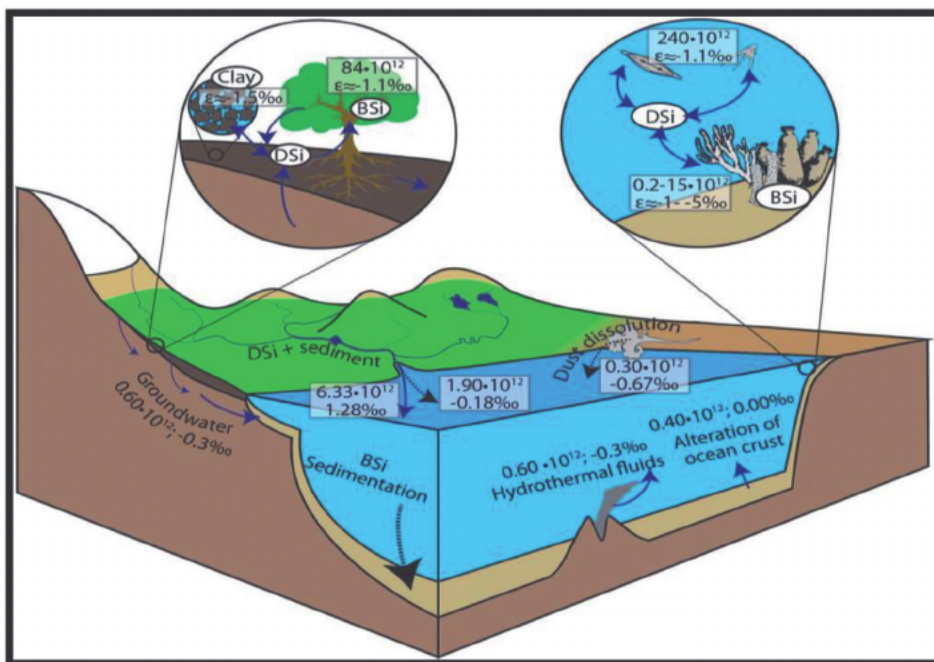


Figure 4.
 The modern-day global Si cycle is represented as just a cartoon schematic [68].

(up to 13 wt.% Al_2O_3), and plagioclase (ilmenite, rutile, and garnet) re-equilibration lamellae due to low-pressure re-equilibration have all been interpreted as evidence of polybasic crystallization history of their parent magmas. They also invented a widely used Alin-Opx geobarometer to analyze the weather [72]. Despite the increasingly technical and commercial importance, understanding of Ga's geochemical behavior in the environment has still been limited. As a result, there is an urgent need to research identified Ga's geochemical cycle, especially in comparison to its geochemical companion aluminum (Al). Gallium and aluminum are "geochemical partners" or "pseudo isotopes" because they are both elements in Periodic Table Group 13. In this case, the term "geochemical twins" is inappropriate because it relates to the geochemical interaction of two trace elements (whereas Al, unlike Ga, is frequently a substantial element). Due to their equal charge and ionic radius, Ga and Al demonstrate related geochemical activity in most natural systems. Surprisingly, there have been few comprehensive investigations of the Ga-Al combination's geochemical behavior. The Ga/Al mass ratios (measured in g Gaper kilogram Al; g/kg) derived from published concentration data appear to be comparable for igneous rocks, sediments, and sedimentary rocks (basalts, granites, shales, loess, deep-sea clay, typical upper continental crust) and cover a small range of 0.19 g/kg to 0.41 g/kg [73].

7. Human health and medical geochemistry

Medicinal chemistry is the study of the dialectical interaction between chemical components, human health, and the biosphere (geochemistry). In the important tissues and bodily fluids, trace elements are found in trace levels [74]. The gut absorbs

only extremely little amounts of vanadium that enter the body [75]. As a result, a liter of water is insufficient to fulfill vanadium's daily requirements. Vanadium is used in the digestion and breakdown of carbohydrates, as well as the proper functioning of the circulatory system. It controls how potassium, sodium triphosphate, and other enzymes act [22]. Furthermore, receiving oxygen stimulates the hepatocytes. It also has activities in the eyes, liver, kidneys, heart, neurological system, and blood insulin management. As a result, vanadium is compared to insulin in terms of its ability to digest blood sugar. Low amounts of this element in the body cause arteriosclerosis, diabetes, sagging muscles, stunted growth, and a range of other pathological signs [76].

In a variety of ways, cobalt is needed for the health and safety of the human body's effective functioning. It is found in vitamin B12, and it's considered a catalyst in this vitamin because it's linked to proteins in the body. This vitamin is involved in several processes, including ribose to deoxyribose conversion and methyl group translocation. Cobalt assists in carbohydrate and protein digestion [77]. The need for cobalt in the diet is about 0.11-ppm (mg/kg) of dry matter, while recent recommendations advocate boosting the diet up to 0.20 mg of Cobalt/kg dry matter, which appears to improve animal productivity, particularly in dairy cattle [78]. It is also responsible for monitoring the work of cells, growth, and the activity of red blood cells and bone marrow, as well as the generation of amino acids, the formation of DNA, and the important activities of the immune system, and neurological system, and digestive system. Cobalt is largely found in bones and muscles, and vitamin B12 is a rich supplier of it. Because 3 mg of this element is consumed daily and 85% of it is excreted in the urine, the heart stores the majority of it [78]. As a result, it has become clear that the chemical balance of living beings' health is exceedingly sensitive, as minor alterations in trace components can have huge implications for public health and safety [79].

8. Conclusion

Metal biogeochemical cycling is frequently accompanied by stable isotope fractionation in natural systems, which can now be quantified thanks to recent analytical breakthroughs. As a result, over the last two decades, a new research field called environmental isotope geochemistry has emerged, complementing traditional stable isotope systems (H, C, O, N, and S) with many more elements from across the periodic table.

The most significant principles of mass-dependent and mass-independent metal stable isotope fractionation are discussed, as well as the magnitude of natural isotopic variations for various elements. Redox transformations, complexation, sorption, precipitation, dissolution, evaporation, diffusion, and biological cycling are all discussed as mechanisms that might cause metal stable isotope fractionation in environmental systems. The utility and limitations of metal stable isotope signatures as tracers in environmental geochemistry are also examined, as well as future directions. As Supporting Information, a summary of analytical methodologies for metal stable isotopes is provided, as well as an overview of the present state of research on various elements. Incorporating the results of all experimental, theoretical, and field study methods will enable the environmental geochemistry community to develop a new tool for mineral isotope analysis to address important scientific questions.

References

- [1] Ekoko Eric B, Emile E, Isaac Konfor N, Fralick P, Salomon Betrant B, Cathryn Ntoboh T. Inorganic geochemistry and petroleum source evaluation of organic black shale in the Mamfe Basin (West Africa). *Solid Earth Sciences*. 2019;**4**(4):166-177. DOI: 10.1016/j.sesci.2019.11.005
- [2] Trueman CN, Rodgers KJ, McLellan IS, Hursthouse AS. *Geochemistry | Inorganic*. 3rd ed. Vol. December 2017. Amsterdam: Elsevier Inc.; 2019
- [3] Corecco L, Pereira VP, Soares MB, Schultz CL. Geochemical study of the vertebrate assemblage zones of the Santa Maria supersequence (middle to late triassic), Paraná Basin, Brazil, South America, and Antarctica. *Brazilian Journal of Geology*. 2020;**50**(4):1-11. DOI: 10.1590/2317-4889202020200014
- [4] Henderson P. *Inorganic Geochemistry*. New York: Oxford [Oxfordshire], Pergamon Press; 1982. pp. 149-160
- [5] Zheng YF. Calculation of oxygen isotope fractionation in anhydrous silicate minerals. *Geochimica et Cosmochimica Acta*. 1993;**57**:1079-1091
- [6] Badawy WM, Duluu OG, El H, El-taher A, Frontasyeva MV. A review of major and trace elements in Nile River and Western Red Sea sediments: An approach of geochemistry, pollution, and associated hazards. *Applied Radiation and Isotopes*. 2021;**170**(January):109595. DOI: 10.1016/j.apradiso.2021.109595
- [7] Hwang H, Nyamgerel Y, Lee J. Distribution of rare earth elements and their applications as tracers for groundwater geochemistry-a Review. *Journal of the Korean Earth Science Society*. 2021;**6692**(4):383-389
- [8] Zuo R, Wang J, Xiong Y, Wang Z. Applied geochemistry the processing methods of geochemical exploration data: Past , present, and future. *Applied Geochemistry*. 2021;**132**(August):105072. DOI: 10.1016/j.apgeochem.2021.105072
- [9] Balaram V. Rare earth elements: A review of applications, occurrence, exploration, analysis, recycling, and environmental impact. *Geoscience Frontiers*. 2019;**10**(4):1285-1303
- [10] Velasco-Tapia F, Verma SP. First partial melting inversion model for a rift-related origin of the sierra de Chichinautzin volcanic field, central Mexican Volcanic Belt. *International Geology Review*. 2001;**43**(9):788-817
- [11] Gómez C, Larsen T, Popp B, Hobson KA, Cadena CD. Assessing seasonal changes in animal diets with stable-isotope analysis of amino acids: A migratory boreal songbird switches diet over its annual cycle. *Oecologia*. 2018;**187**(1):1-13. DOI: 10.1007/s00442-018-4113-7
- [12] D'amore JJ, Al-Abed SR, Scheckel KG, Ryan JA. Methods for speciation of metals in soils. *Journal of Environmental Quality*. 2005;**34**(5):1707-1745
- [13] Godfrey LV et al. Hafnium and neodymium isotope variations in NE Atlantic seawater. *Geochemistry, Geophysics and Geosystems*. 2009;**10**(8):1-13
- [14] Chakrabarti R, Jacobsen SB. The isotopic composition of magnesium in the inner solar system. *Earth and Planetary Science Letters*. 2010;**293**(3-4):349-358

- [15] Ramos SS, Cubillos MDJ, Adelantado JVG, Marco DJY. Quantitative analysis of chromite ores using glass discs in moderate dilutions of lithium tetraborate by x-ray fluorescence spectrometry. *X-Ray Spectrometry: An International Journal*. 2006;**35**(4):243-248
- [16] Breitenlechner E, Hilber M, Lutz J, Kathrein Y, Unterkircher A, Oegg K. Reconstructing the history of copper and silver mining in Schwaz, Tirol. *RCC Perspectives*. 2012;**10**:7-20. Available from: <https://www.jstor.org/stable/>. DOI: 10.2307/26240468
- [17] Mochalov II. Vladimir Vernadsky: Cosmos, earth, life, man, reason— From biosphere to noosphere. *Earth system: History and Natural Variability*. 2009;**4**:384-434
- [18] Moya J-F, Laurent O. Archaean tectonic systems: A view from igneous rocks. *Lithos*. 2018;**302**:99-125
- [19] Dick JM. CHNOSZ: Thermodynamic calculations and diagrams for geochemistry. *Frontiers in Earth Science*. 2019;**7**:180
- [20] Bowie SH, Thornton I. *Environmental Geochemistry and Health: Report to the Royal Society's British National Committee for Problems of the Environment*. Vol. 2. Germany: Springer Science & Business Media; 2012
- [21] Romankevich EA. *Geochemistry of Organic Matter in the Ocean*. Germany: Springer Science & Business Media; 2013
- [22] Saleh HM, Hassan AI. *Medical geochemistry*. Geochemistry. United States: Wiley Online Library; 2021. pp. 127-147. DOI: 10.1002/9781119710134.ch8
- [23] Porcelli DP, Ballentine CJ, Wieler R. Noble Gases: In *Geochemistry and Cosmochemistry*. Vol. 47. Berlin: Walter de Gruyter GmbH & Co KG; 2018
- [24] Wiederhold JG. Metal stable isotope signatures as tracers in environmental geochemistry. *Environmental Science & Technology*. 2015;**49**(5):2606-2624
- [25] Wang L, Jin Y, Weiss DJ, Schleicher NJ, Wilcke W, Wu L, et al. Possible application of stable isotope compositions for the identification of metal sources in soil. *Journal of Hazardous Materials*. 2021;**407**:124812. DOI: 10.1016/j.jhazmat.2020.124812
- [26] Le Roux G, Sonke JE, Cloquet C, Aubert D, De Vleeschouwer F. Comment on "the biosphere: A homogeniser of Pb-isotope signals" by C. Reimann, B. Flem, A. Arnoldussen, P. Englmaier, TE Finne, F. Koller and Ø. Nordgulen. *Applied Geochemistry*. 2008;**23**:2789
- [27] Croteau M-N, Cain DJ, Fuller CC. Novel and nontraditional use of stable isotope tracers to study metal bioavailability from natural particles. *Environmental Science & Technology*. 2013;**47**(7):3424-3431
- [28] Baskaran M. Environmental isotope geochemistry: Past, present and future. In: *Handbook of Environmental Isotope Geochemistry*. Berlin: Springer; 2012. pp. 3-10
- [29] Close HG. Compound-specific isotope geochemistry in the ocean. *Annual Review of Marine Science*. 2019;**11**:27-56
- [30] Charlier BLA, Tissot FLH, Dauphas N, Wilson CJN. Nucleosynthetic, radiogenic and stable strontium isotopic variations in fine-and coarse-grained refractory inclusions from Allende. *Geochimica et Cosmochimica Acta*. 2019;**265**:413-430

- [31] Mattinson JM. Revolution and evolution: 100 years of U–Pb geochronology. *Elements*. 2013;**9**(1): 53-57
- [32] Thurber DL. Anomalous U 234 U 238 in nature. *Journal of Geophysical Research*. 1962;**67**(11):4518-4520
- [33] Yang D, Bayazitoglu Y. Polymer composites as radiation shield against galactic cosmic rays. *Journal of Thermophysics and Heat Transfer*. 2020;**34**(2):457-464
- [34] Proskurowski G, Lilley MD, Kelley DS, Olson EJ. Low temperature volatile production at the lost City hydrothermal field, evidence from a hydrogen stable isotope geothermometer. *Chemical Geology*. 2006;**229**(4):331-343
- [35] Ashraf MA, Khan AM, Ahmad M, Akib S, Balkhair KS, Bakar NKA. RETRACTED ARTICLE: Release, deposition and elimination of radiocesium (¹³⁷Cs) in the terrestrial environment. *Environmental Geochemistry and Health*. 2014;**36**(6):1165-1190
- [36] Wang H, Zhang Z, Liang J, Liu H, Shi S. Application of elemental geochemistry in high-frequency sequence—Stratigraphic analysis of lacustrine shale. *Minerals*. 2021;**11**(6):657
- [37] Sanchez-Hernandez Y, Florentin J-MM. The influence of regional factors in the expression of oceanic anoxic event 1a (OAE1a) in the semi-restricted Organyà Basin, south-Central Pyrenees, Spain. *Palaeogeography Palaeoclimatology Palaeoecology*. 2016;**441**:582-598
- [38] Claes H et al. Elemental geochemistry to complement stable isotope data of fossil travertine: Importance of digestion method and statistics. *Sedimentary Geology*. 2019;**386**:118-131
- [39] Jung S, Pfänder JA. Source composition and melting temperatures of orogenic granitoids: Constraints from CaO/Na₂O, Al₂O₃/TiO₂ and accessory mineral saturation thermometry. *European Journal of Mineralogy*. 2007;**19**(6):859-870
- [40] Fedo CM, Wayne Nesbitt H, Young GM. Unraveling the effects of potassium metasomatism in sedimentary rocks and paleosols, with implications for paleoweathering conditions and provenance. *Geology*. 1995;**23**(10):921-924
- [41] Ramachandran A et al. Geochemistry of Proterozoic clastic rocks of the Kerur formation of Kaladgi-Badami Basin, North Karnataka, South India: Implications for paleoweathering and provenance. *Turkish Journal of Earth Sciences*. 2016;**25**(2):126-144
- [42] Nesbitt HW, Fedo CM, Young GM. Quartz and feldspar stability, steady and non-steady-state weathering, and petrogenesis of siliciclastic sands and muds. *Journal of Geology*. 1997;**105**(2):173-192
- [43] Li Q et al. Geochemical characteristics and organic matter accumulation of argillaceous dolomite in a saline lacustrine basin: A case study from the paleogene xingouzui formation, Jianghan Basin, China. *Marine and Petroleum Geology*. 2021;**128**:105041
- [44] Xiugang PU et al. Geologic features of fine-grained facies sedimentation and tight oil exploration: A case from the second member of Paleogene Kongdian formation of Cangdong sag, Bohai Bay basin. *Petroleum Exploration and Development*. 2016;**43**(1):26-35

- [45] Xu G, Haq BU. Seismic facies analysis: Past, present and future. *Earth-Science Review*. 2022;**224**:103876
- [46] Gogoi M, Mathur N, Kumar TS, Walling T, Phukan S. Geochemical characterization of shales of the Eocene Disang group, Kohima syncline, India: Inferences to hydrocarbon potential and depositional environment. *Petroleum Research*. 2021;**6**(1):42-56
- [47] Jin F, Han C, Wang J, Guo Y, Gao Z. Application of organic geochemical parameters in sequence classification and correlation: A case study from lower Es~3 in Shulu sag Jizhong depression. *Acta Sedimentologica Sinica*. 2008;**26**(1):86
- [48] Hirose K et al. Hydrogen limits carbon in liquid iron. *Geophysical Research Letters*. 2019;**46**(10):5190-5197. DOI: 10.1029/2019GL082591
- [49] Nakajima Y et al. Silicon-depleted present-day Earth's outer Core revealed by sound velocity measurements of liquid Fe-Si alloy. *Journal of Geophysical Research - Solid Earth*. 2020;**125**(6):1-14. DOI: 10.1029/2020JB019399
- [50] Young G, Fan L, Zhao B, Chen X, Liu X, Huang H. Equation of state for Fe-9.0 wt% O up to 246 GPa: Implications for oxygen in the Earth's outer Core. *Journal of Geophysical Research - Solid Earth*. 2021;**126**(2):1-9. DOI: 10.1029/2020JB021056
- [51] Poirier JP. Light elements in the Earth's outer core: A critical review. *Physics of the Earth and Planetary Interiors*. 1994;**85**(3-4):319-337. DOI: 10.1016/0031-9201(94)90120-1
- [52] Hirose K, Wood B, Vočadlo L. Light elements in the Earth's core. *National Review Earth Environment*. 2021;**2**(9):645-658. DOI: 10.1038/s43017-021-00203-6
- [53] Doyle AE, Young ED, Klein B, Zuckerman B, Schlichting HE. Oxygen fugacities of extrasolar rocks: Evidence for an earth-like geochemistry of exoplanets. *Science* (80-.). 2019;**366**(6463):356-359. DOI: 10.1126/science.aax3901
- [54] Noël J et al. Evidence of polygenetic carbon trapping in the Oman ophiolite: Petro-structural, geochemical, and carbon and oxygen isotope study of the Wadi Dima harzburgite-hosted carbonates (Wadi Tayin massif, Sultanate of Oman). *Lithos*. 2018;**323**:218-237. DOI: 10.1016/j.lithos.2018.08.020
- [55] Williams HM, Prytulak J, Woodhead JD, Kelley KA, Brounce M, Plank T. Interplay of crystal fractionation, sulfide saturation and oxygen fugacity on the iron isotope composition of arc lavas: An example from the Marianas. *Geochimica et Cosmochimica Acta*. 2018;**226**:224-243. DOI: 10.1016/j.gca.2018.02.008
- [56] Valley JW et al. 4.4 billion years of crustal maturation: Oxygen isotope ratios of magmatic zircon. *Contributions to Mineralogy and Petrology*. 2005;**150**(6):561-580
- [57] Byerly BL, Kareem K, Bao H, Byerly GR. Early earth mantle heterogeneity revealed by light oxygen isotopes of Archaean komatiites. *Nature Geoscience*. 2017;**10**(11):871-875. DOI: 10.1038/NNGEO3054
- [58] Wang Q, Hao F, Xu C, Zou H. Paleolimnological environments and the formation of high quality source rocks in the Bohai Bay basin: An integrated geochemical study of biomarkers, stable carbon and oxygen isotopes, and trace elements. *Journal of Petroleum Science and Engineering*. 2020;**195**(November 2019):107753. DOI: 10.1016/j.petrol.2020.107753

- [59] Wang W, Li Y, Brodholt JP, Vočadlo L, Walter MJ, Wu Z. Strong shear softening induced by superionic hydrogen in Earth's inner core. *Earth and Planetary Science Letters*. 2021;**568**:1-7. DOI: 10.1016/j.epsl.2021.117014
- [60] Xiao W, Cao J, Liao Z, Hu G, Zuo Z, Hu K. Elemental geochemistry proxies recover original hydrogen index values and total organic carbon contents of over-mature shales: Lower Cambrian South China. *Chemical Geology*. 2021;**562**(August 2020):120049. DOI: 10.1016/j.chemgeo.2020.120049
- [61] Demouchy S, Alard O. Hydrogen, trace, and ultra-trace element distribution in natural olivines. *Contributions to Mineralogy and Petrology*. 2021;**176**(4):1-25. DOI: 10.1007/s00410-021-01778-5
- [62] Savage PS, Armytage RMG, Georg RB, Halliday AN. High temperature silicon isotope geochemistry. *Lithos*. 2014;**190-191**:500-519. DOI: 10.1016/j.lithos.2014.01.003
- [63] Ozawa H, Hirose K, Yonemitsu K, Ohishi Y. High-pressure melting experiments on Fe–Si alloys and implications for silicon as a light element in the core. *Earth and Planetary Science Letters*. 2016;**456**:47-54. DOI: 10.1016/j.epsl.2016.08.042
- [64] Poitrasson F. Silicon isotope geochemistry. *Non-Traditional Stable Isotope*. 2017;**82**:289-344. DOI: 10.2138/rmg.2017.82.8
- [65] Lin J-F et al. Solid earth-SDE 11. Sound velocities of iron-nickel and iron-silicon alloys at high pressures. *Geophysical Research Letters*. 2003;**30**(21):SDE 11-1-11-4. DOI: 10.1029/2003GL018405
- [66] Lin JF et al. Sound velocities of iron- nickel and iron- silicon alloys at high pressures. *Geophysical Research Letters*. 2003;**30**(21):1-4. DOI: 10.1029/2003GL018405
- [67] Wang W, Wei HZ, Jiang SY, Eastoe CJ, Guo Q, Lin YB. Adsorption behavior of Metasilicate on N-methyl d -Glucamine functional groups and associated silicon isotope fractionation. *Langmuir*. 2016;**32**(35):8872-8881. DOI: 10.1021/acs.langmuir.6b02388
- [68] Wang W et al. Silicon isotope geochemistry: Fractionation linked to silicon complexations and its geological applications. *Molecules*. 2019;**24**(7):1-31. DOI: 10.3390/molecules24071415
- [69] Savage PS, Georg RB, Williams HM, Halliday AN. Silicon isotopes in granulite xenoliths: Insights into isotopic fractionation during igneous processes and the composition of the deep continental crust. *Earth and Planetary Science Letters*. 2013;**365**:221-231. DOI: 10.1016/j.epsl.2013.01.019
- [70] Opfergelt S, Delmelle P. Silicon isotopes and continental weathering processes: Assessing controls on Si transfer to the ocean. *Comptes Rendus - Geoscience*. 2012;**344**(11-12):723-738. DOI: 10.1016/j.crte.2012.09.006
- [71] Nelson WO, Campbell PGC. The effects of acidification on the geochemistry of Al, Cd, Pb and Hg in freshwater environments: A literature review. *Environmental Pollution*. 1991;**71**(2-4):91-130. DOI: 10.1016/0269-7491(91)90030-Z
- [72] Heinonen A, Kivisaari H, Michallik RM. High-aluminum orthopyroxene megacrysts (HAOM) in the Ahvenisto complex, SE Finland, and the polybaric crystallization of massif-type anorthosites. *Contributions to Mineralogy and Petrology*. 2020;**175**(1): 1-25. DOI: 10.1007/s00410-019-1648-5

[73] Schier K et al. Gallium-aluminum systematics of marine hydrogenetic ferromanganese crusts: Inter-oceanic differences and fractionation during scavenging. *Geochimica et Cosmochimica Acta*. 2021;**310**:187-204. DOI: 10.1016/j.gca.2021.05.019

[74] Blennerhassett R. The vital question. *Frontier Review*. 1907;**82**:1-11

[75] Lewicka E, Guzik K, Galos K. On the possibilities of critical raw materials production from the EU's primary sources. *Resources*. 2021;**10**(5):50

[76] Jiang P et al. Effect of vanadyl rosiglitazone, a new insulin-mimetic vanadium complexes, on glucose homeostasis of diabetic mice. *Applied Biochemistry and Biotechnology*. 2016;**180**(5):841-851

[77] Okoro HK, Fatoki OS. A Review of sequential extraction procedures for heavy metals speciation in soil and sediments. *Journal of Environmental & Analytical Toxicology*. 2012;**01**(S1):1-9. DOI: 10.4172/scientificreports.181

[78] González-Montaña J-R, Escalera-Valente F, Alonso AJ, Lomillos JM, Robles R, Alonso ME. Relationship between vitamin B12 and cobalt metabolism in domestic ruminant: An update. *Animals*. 2020;**10**(10):1855

[79] Dutta SK and Lodhari DR. Topics in Mining, Metallurgy and Materials Engineering: Extraction of Nuclear and Non-ferrous Metals. Uranium. Singapore: Springer Nature; 2018. p. 27. DOI: 10.1007/978-981-10-5172-2

Geochemistry Applied to the Exploration of Mineral Deposits

John Luis Manrique Carreño

Abstract

Geochemistry can be applied to the exploration of mineral deposits, for which it is necessary to understand the fundamentals of geochemical prospecting, the geochemical dispersion of elements based on their chemical properties. This chapter presents the basics of geochemical prospecting including: element mobility depending on ionic potential, pH, and Eh, with examples of Cu mobility during supergenic alteration of a primary sulfide deposit, a brief overview of sampling/geochemical prospecting methods, as well as a case study of the geochemical prospecting study carried out in the vanadium (V), uranium (U), and zinc (Zn) sedimentary mineral deposit of Puyango, Ecuador, in which anomalous and subanomalous values were detected in rock samples of various pathfinder elements of V and U.

Keywords: geochemical prospecting, mineral deposits, ionic potential, mobility, redox

1. Introduction

Geochemical prospecting is the earth science that applies the theoretical knowledge of geochemistry with the aim of being able to locate mineral deposits, through the study of the primary and secondary dispersion of the elements, performing studies of litho-geochemistry, stream sediments, surface water, soil, and other methods [1, 2].

This chapter shows a review of the basic concepts of geochemical prospecting, taking as an example the mobility of copper (Cu) in during supergenic alteration of a primary sulfide deposit, depending on the ionic potential (charge/radius ratio of the ion), the hydrogen potential (pH), and the redox potential (Eh) [1, 2]. It also includes a brief description of methods (soils, litho-geochemistry, stream sediments, hydro-geochemistry), as well as the case study of geochemical prospecting carried out, in a sedimentary mineral deposit, in Puyango, Ecuador. In this study, anomalous and subanomalous values of several pathfinder elements of vanadium (V) and uranium (U) mineral deposits were detected, among which the following stand out: phosphorus ($P_2O_5 > 5.12$ wt.%), nickel ($Ni > 1824$ ppm) and, yttrium ($Y > 219$ ppm), among the most important and subanomalies of barium ($Ba > 1459$ ppm) and lead ($Pb > 32$ ppm).

2. Mineral deposits

Mineral deposit is a mineralization (referring to an area of the crust where ores were deposited) of sufficient size and grade (concentration), which under favorable circumstances could be exploited with economic benefits, which has sufficient reserves [3].

The concentration of the metals in the deposits varies widely in a range of few parts per million (1–100 g/t or ppm) in noble metals such as platinum (Pt), palladium (Pd), gold (Au), silver (Ag), at a low percentage (1–10 wt.%) for Cu, zinc (Zn), lead (Pb), and higher grade or tenor (40–60 wt.%) for aluminum (Al), chromium (Cr), iron (Fe), and aggregates.

Mineral deposits can be classified from the genetic point of view into five main types: 1) deposits of magmatic segregation ((chromites, iron-titanium-vanadium (Fe-Ti-V), nickel-copper (Ni-Cu) sulfides, platinum group elements (PGEs), diamonds, carbonatites)), 2) pegmatite deposits ((tin-niobium-tantalum (Sn-Nb-Ta), uranium-thorium (U-Th), lithium (Li), rare earth elements (REE)), 3) hydrothermal deposits (volcanogenic massive sulfurs Cu-Zn-Pb, SEDEX Ag-Pb-Zn, Mississippi Valley type (MVT) Ag-Pb-Zn, epithermal Au-Ag, copper-molybdenum-gold (Cu-Mo-Au) porphyry, 4) metamorphic deposits (polymetallic Skarn, graphite), 5) sedimentary deposits ((placers, laterites, Banded Iron Formations (BIFs), Li brines, U in sandstones, among others)) [3, 4].

3. Geochemical prospecting fundamentals

It is mainly concerned with studying the enrichment or impoverishment of certain chemical elements in the vicinity of mineral deposits [5]. Geochemical prospecting is done by systematic measurements of one or more chemical parameters, usually at trace concentrations, of naturally occurring materials in the Earth's crust. The types of samples that are collected include rocks, soils, gossan, river or lake sediments, groundwater, surface water, steam or gases, and vegetation [5] (**Figure 1**).

Primary geochemical dispersion mainly affects the migration of elements of economic interest due to processes, such as the formation and crystallization of magmas and hydrothermal activity. At the local level, these processes can lead to an enrichment or impoverishment of the elements, generating geochemical anomalies [1, 5].

Halos are enriched or depleted in various elements as a result of introduction or redistribution related to mineralization formation phenomena. The shape and size of the halo are exceptionally variable due to the various mobility characteristics of the elements in solution and microstructures in the rocks [1, 2].

The redistribution of chemical elements on or near the Earth's surface due to weathering, transport, sedimentation, and/or biological activity is classified as secondary geochemical dispersion. The secondary geochemical dispersion halo comprises the dispersed remnants of mineralization, caused by surface processes of chemical and physical weathering and the redistribution of the primary patterns. The halo can be recognized in samples taken from soil, rocks, sediments, vegetation, groundwater, and volatiles, at a distance of meters to tens of kilometers [2].

“Pathfinder” or “indicator or tracer” elements (**Table 1**) are characteristic parameters in geochemical prospecting. These are relatively mobile elements due to the physical-chemical conditions of the solutions in which they are found [1].

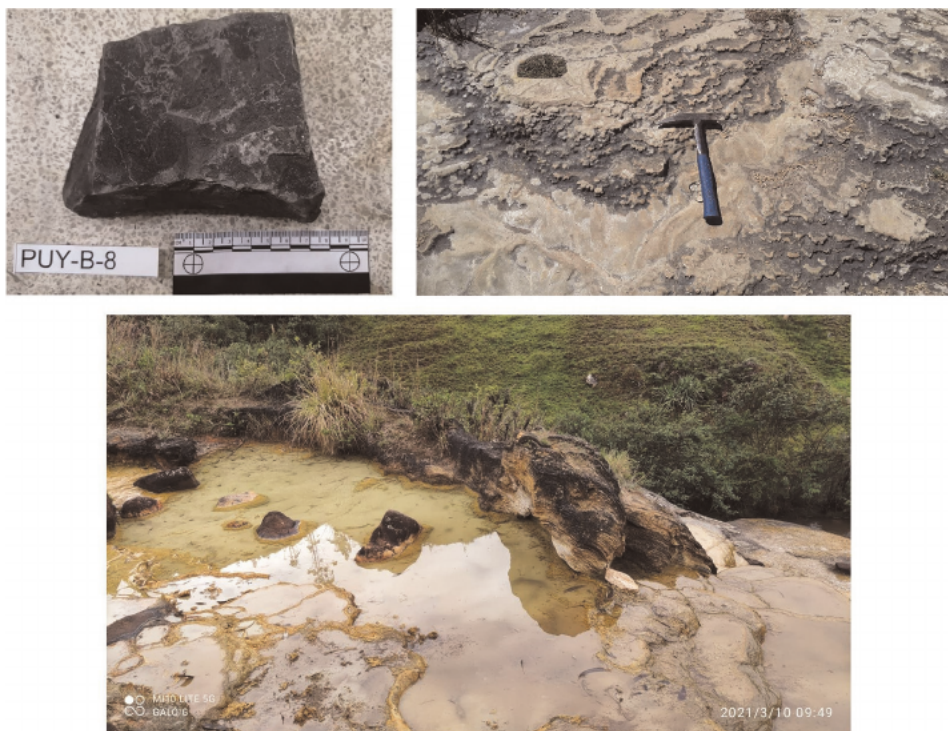


Figure 1.
 Types of samples collected: rock, soil, and surface water (source: author).

Mineral deposit	Metals/elements of economic interest	Pathfinders
Chromium Orthomagmatic (stratiform)	Cr	Cr, PGE, High Mg
PGE Orthomagmatic (stratiform mafic-ultramafic)	PGE (Pt, Pd, Ru, Re, Os)	PGE, Cu, Ni, Cr, Ti, High Mg
REE in Carbonatite	REE, Nb,	Th, U, Ti, Zn, Nb, Y, Ce, Mo, Cu, V, P, Mn, S, La, Pb, Zr, Ba
Porphyry Copper	Cu, Mo, Au	Cu, Mo, Au, Ag, W, B, Sr, High S
VMS	Cu, Zn, Pb	Cu, Zn, Co, Ag, Ni, Cr,
Epithermal Gold	Au, Ag, Cu	Au, As, Sb, Hg, Ag, Pb, Zn
SEDEX Zn-Pb	Zn, Pb	Cu, Pb, Zn, Ba
Sandstones Uranium	U	U, V, Mo, Se
Phosphates	P, REE (by-product)	P, N, F, C, U
Lateritic Nickel	Ni, Sc or Co (by-product)	Ni, Co, Cr

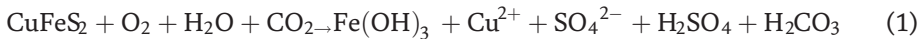
Table 1.
 Examples of pathfinders in some types of mineral deposits.

The ionic potential is the charge/radius ionic ratio, which together with the pH and Eh allows us to understand the mobility of chemical elements during geochemical dispersion, being important parameters for geochemical prospecting [1, 2]. Ions with

ionic potential less than 3 can be soluble in water, for example: alkaline cations (Li^+ , Na^+ , K^+), alkaline earth cations (Ca^{2+} , Mg^{2+}), transition metal cations (Fe^{2+} , Cu^{2+} , Cd^{2+} , Zn^{2+} , Pb^{2+}). Ions with an ionic potential between 3 and 12 will be insoluble under certain pH conditions, examples: Fe^{3+} , Al^{3+} , Si^{4+} , Zr^{4+} , Pb^{4+} , REE^{3+} , Th^{4+} , Nb^{5+} .

Ions with ionic potential greater than 12 will form soluble cations or anions, examples: P^{5+} (phosphate), As^{5+} , S^{6+} (sulfate), Se^{6+} , U^{6+} (uranyl), Mo^{6+} .

An example of secondary geochemical dispersion can occur due to Cu sulfide weathering and erosion, in which surface waters percolate to primary sulfide deposits, oxidizing many ores and producing solvents that dissolve other minerals. The chemical reaction observed below describes the oxidation process of chalcopyrite (Cu ore) in waters rich in oxygen and carbon dioxide, producing goethite (gossan), Cu^{2+} (in solution), sulfate, sulfuric acid, and carbonic acid [3, 5]:



Cu^{2+} in oxidizing environments and with acidic pH (<4) is a soluble cation; therefore, it can be leached from the mineral deposit in surface waters and underground waters. If the pH is higher, various secondary minerals can be formed such as: chalcantite (CuSO_4), azurite ($\text{Cu}_3(\text{CO}_3)_2(\text{OH})_2$), malachite ($\text{Cu}_2(\text{CO}_3)(\text{OH})_2$), including tenorite (CuO) at alkaline pH. This process is known as supergenic sulfide alteration and may be useful in geochemical prospecting for Cu sulfide mineral deposits [3, 4].

3.1 Geochemical anomalies

The purpose of geochemical prospecting studies is to find geochemical anomalies, which are abnormal chemical patterns in a region. For this, the background values, threshold, subanomalies, and anomalies must be established, which are statistically calculated from the data. The “background” values are characterized by the normal range of concentration of elements in regional perspective rather than localized mineral occurrences. It is significant to establish the background value of the area against anomalies due to the accumulation of economic minerals, if any, they can be identified [1, 5].

The arithmetic mean (average) is obviously skewed by some high scattered values. The most frequent value (median) tends to be within the relatively narrow range and is considered to represent the normal or background abundance for that particular element in that area.

The “threshold” (Eq. (2)) value is defined as the probable upper limit or lower limit of the background value, at some statistically precise confidence level. Any sample that exceeds this threshold is considered possibly abnormal and belongs to a separate population. The following equation is usually used to calculate it:

$$\text{Threshold} = \text{Background (median)} + \text{standard deviation} \quad (2)$$

The subanomaly is calculated using the background + twice the standard deviation, while the anomalies are calculated with the background plus three times the standard deviation.

4. Geochemical prospecting methods

In general terms, they can be classified into the following types depending on the sampling stages, the nature of the terrain, the signal associated with the

mineralization, the type of analytical instrumentation available, and finally, the time and cost allowable for the program [5]:

- Pedogeochemistry (soil sampling).
- Lithogeochemistry (rock sampling).
- Sampling of fluvial sediments.
- Sampling of heavy minerals.
- Hydrogeochemical sampling.
- Geochemistry of radiogenic isotopes.
- Geochemical sampling of glacial sediments.
- Vegetation sampling.
- Gas sampling.

Some of the afore mentioned methods are described below:

4.1 Soil sampling

Soil is the unconsolidated product of weathering. It is usually found at or near its source of formation such as residual soils. It can be transported over long distances, forming alluvial soils. It is widely used in geochemical prospecting and often produces successful results.

Anomalous element enrichment from underlying mineralization may occur due to secondary dispersion in overlying soil, weathered product, and groundwater during weathering and leaching processes. The dispersion of the elements can be large, forming an exploration target larger than the actual size of the deposit.

4.2 Lithogeochemistry

Rock sampling is useful during regional work to recognize favorable geochemical provinces and favorable host rocks to host mineral deposits. Most of the epigenetic and syngenetic mineral deposits show primary dispersion around the mineralization, due to the presence of abnormally high values of the trace elements.

Lithogeochemistry aims to identify primary dispersion, diagnosis of other geochemical characteristics, and association of trace elements, which are different in sterile rocks.

Rock outcrop can be sampled directly by breaking up a small hand sample using a geological hammer or hammer and chisel. Generally, 1–3 kg is a suitable sample size (mass). Sampling is based on the analysis of fresh rocks or individual minerals. Sampling is conducted on a uniform grid across a geologic terrain that includes various rock types from fresh outcrops, wall rocks, and core samples.

4.3 Sampling of fluvial sediments

River sediment sampling is the most widely used in all reconnaissance and detailed study of watersheds. Many minerals, particularly sulfide minerals, are unstable in the weathering environment, breaking down as a result of oxidation and other chemical reactions. The process will produce secondary dispersion of both minerals and trace elements. Elements will move in solid form and in solution greater relative distances within the basin drainage.

The mobility of different elements will vary significantly, between fine-grained particles and, eventually, in detrital rock fragments, clay minerals, organic and inorganic colloids enriched in ore minerals, and in pathfinders, which are deposited downstream.

The optimum size fraction varies in different environments, and generally 80 mesh size is recommended. Samples are generally collected in natural sediment traps along streams.

4.4 Hydrogeochemical sampling

There are two types of water sources, i.e., groundwater and surface water; they have very different chemical and physical properties. Groundwater is produced in springs and wells. It has a better potential in geochemical prospecting especially if it is acidic (low pH) by dissolving and transporting metallic elements such as Cu, Pb, Zn, Mo, Sn, S, U, Ni, and Co more than in surface waters, due to chemical weathering and oxidation followed by leaching.

Surface water from streams, rivers, and oceans has less dissolving power, and fine-grained sediments absorb much of the metals carried by the water. River water samples and sediment samples are collected simultaneously for analysis.

Water samples are easy to obtain. About a liter of water is collected and stored in a special container. Metal solubility decreases with increasing pH 4–7. Therefore, the pH is recorded at the time of sampling and other physicochemical parameters (Eh, temperature, salinity, total dissolved solids, among others). Suspended solids are filtered before analysis.

5. Case of study: U, V, Zn sedimentary mineral deposit of Puyango, Ecuador

Here, the outcome of a preliminary study on the geochemical prospecting of a set of rock samples of the Puyango sedimentary deposit in Ecuador is presented, focusing on the quantification of certain trace elements in whole rock samples. Analytical techniques such as X-ray fluorescence and inductively coupled plasma mass spectrometry were used. The chemical obtained data were used to determinate and quantify the concentrations for the majority and some particularly economic trace chemical elements such as U, V, and Zn.

5.1 Geology of Puyango sedimentary deposit

The study area is a part of the Alamor—Lancones basin [6] and is located between the Amotape Tahuín Block of Paleozoic age to the west and the Celica continental volcanic arc to the east [7]. This Late Cretaceous basin is of marine origin, composed of a turbiditic sequence, whose siliciclastic sediments were supplied from the west, and the vulcanoclastic sediments were supplied from the east [8]. The Chirimoyo and Guineo micro-watersheds are geologically located in the Early Cretaceous Ciano, Zapotillo, and Cazaderos (**Figure 2**) sedimentary formations initially identified as belonging to the Alamor group [9], but later detailed studies in the Cazaderos Formation have differentiated the sequences from various sedimentary environments, identified informally, such as Bosque de Piedra and Puyango Formations [8]. At present, they are identified according to the outcropping site as Quebrada Los Zabalos Unit

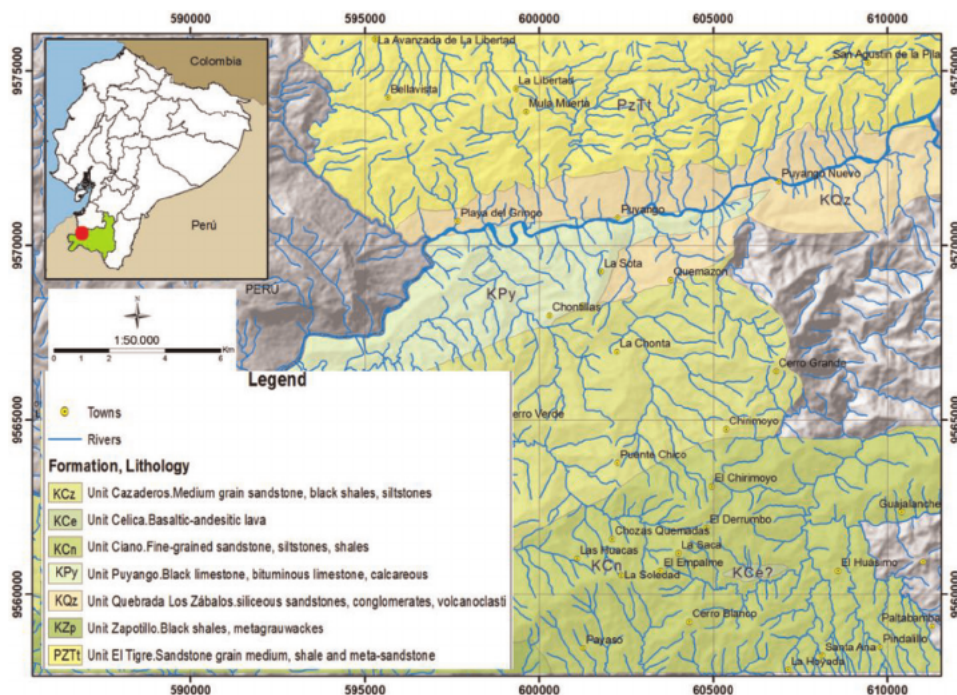


Figure 2.
 Geological map of Puyango sector (source: author).

and Puyango Unit (**Figure 2**), maintaining the Zapotillo and Ciano Formations identified in the first instance [10].

Rocks of Paleozoic age initially identified as Metamorphic Series Tahuín by Kennerley (1973) [9], now defined as Amotape—Tahuín Block, within which the Tahuín Semipelitic Division [11] comprises the informal units, El Tigre and La Victoria. The El Tigre unit is exposed to the north of the study area characterized by sedimentary rocks and low-grade metamorphic sequences, with immature medium-grain sandstones (La Victoria unit) interbedded with fissile shales of brown color and meta-sandstone from fine-grained.

The Early Cretaceous sedimentary rocks are formed by the Quebrada los Zabalos unit that lies to the north, overlying discordant contact with the El Tigre unit. It is constituted by basal layers of silicified fine-grained sandstones, thick conglomerates with subangular clasts of metamorphic composition and volcanic, coarse volcanic sandstones, very compact fine sandstones containing incrustated fossil trunks, and volcanoclastic middle sandstones containing outcrop fossil trunks [10]. The Puyango Unit occupies a strip of E-W direction. The rocks of this unit are chemical sediments made of black limestones and bituminous limestones interspersed with calcareous sandstones. The Puyango Unit (**Figure 2**) through paleontological interpretations is attributed to early to late Albian age [12, 13]. It is considered that the Puyango unit is of a platform environment below the wave train allowing the deposition of calcium carbonate in an anoxic environment, the sandstones are interpreted as distal turbidites. The Unit is found discordantly to the Quebrada Los Zabalos Unit. The unit is strongly deformed, and the erosion of the Pre-Campanian makes it difficult to determine its thickness (approximately 300 m) [10].

Late Cretaceous rocks are attributed to the Ciano Units made up of fine-grained sandstones, limonites, and shales. The Zapotillo Unit that overlies the Ciano Unit is made up of black shales and grawacas, flysh type. The Cazaderos Unit is found out discordantly to the calcareous rocks of the Puyango unit to the north and south to the rocks of the Ciano and Zapotillo units, while in the eastern part, they discordantly cover the metamorphic rocks of the El Tigre unit. The unit consists of brown, medium-grained sandstones, black shales interspersed with siltstones, and is attributed to an environment of turbiditic forearc sequences due to its fossiliferous content [8], indicating this faunal association of a late Campanian to Maastrichtian age.

5.2 Method

Rock samples were collected in outcrops, approximately 1 kg of fresh material per sample, 30 samples in were taken in Puyango sector, Ecuador, some rock replicas were taken for internal verification. The samples were dried at 105 °C for 24 hours in the oven, then they were cut, crushed, and pulverized. The chemical analyses were made in Actlabs, Canada, carried out using the analytical package: Code 4LITHO, Major Elements Fusion ICP(WRA)/Trace Elements Fusion ICP/MS(WRA4B2), detecting the following elements (with its detection limits or lower limits): Si (0.01 wt.%), Al (0.01 wt.%), Fe (0.01 wt.%), Mn (0.01 wt.%), Mg (0.01 wt.%), Ca (0.01 wt.%), Na (0.01 wt.%), K (0.01 wt.%), Ti (0.01 wt.%), P (0.01 wt.%), Zr (2 ppm), Sr (2 ppm), Cr (20 ppm), Ba (2 ppm), Y (1 ppm), Rb (2 ppm), Ni (20 ppm), Zn (30 ppm), Pb (5 ppm), V (5 ppm), U (1 ppm), and Th (1 ppm). XRF was used for internal verification of samples, using the USGS reference material code SGR-1b (Green River Shale), in the Laboratory of Analytical Geochemistry of the Department of Geosciences of the Universidad Técnica Particular de Loja, Ecuador.

5.3 Results

The statistical parameters were calculated: minimum, maximum, mean, median, and standard deviation (**Table 2**), according to which black bituminous limestones have the mean U content of 27 ppm, reaching the maximum value of 266 ppm (**Figure 3b**), while the mean content of Ni is 331 ppm, reaching the maximum value of 2937 ppm. As for V and Zn, the mean values are 1897 ppm V and 1048 ppm Zn, with maximum values of 6837 and 4704 ppm, respectively (**Figure 3a**). The content of another element of economic interest, yttrium (Y), widely ranges, reaching the maximum value of 257 ppm (**Figure 3b**).

To calculate the background value, the median of the values was used, for the threshold the median + standard deviation was used, for the values of subanomalies the median + twice the standard deviation was used and, finally, to calculate the anomalies, the median + three times the standard deviation (**Table 3**).

5.4 Final considerations

The calculations in the dataset in rock samples of Puyango sector, Ecuador, identify anomalies of U (>158 ppm), V (>6440 ppm), Zn (>3959 ppm), P₂O₅ (>5.12 wt.%), Ni (>1824 ppm), and Y (>219 ppm), among the most important and subanomalies of Ba (>1459 ppm) and Pb (>32 ppm). All of these elements are pathfinders for U in sedimentary mineral deposits.

Element	Min [*]	Max	Mean	Median	Stand Deviation
SiO ₂ (wt.%)	7.27	60.19	20.75	15.97	13.72
Al ₂ O ₃	0.69	21.13	4.65	2.95	5.30
Fe ₂ O ₃	0.23	9.23	2.03	1.22	2.48
MnO	0.01	0.09	0.02	0.01	0.02
MgO	0.38	1.51	0.69	0.63	0.27
CaO	0.76	49.77	37.38	41.53	12.98
Na ₂ O	0.04	1.05	0.24	0.21	0.21
K ₂ O	0.17	3.05	0.84	0.57	0.75
TiO ₂	0.07	0.95	0.27	0.22	0.23
P ₂ O ₅	0.07	5.92	1.23	0.43	1.56
LOI ^{**}	6.05	40.62	31.23	32.82	9.11
Zr (ppm)	3	234	59	40	62
Sr	121	1528	877	963	377
Cr	20	586	184	174	125
Ba	4	1612	670	620	420
Y	14	257	63	51	56
Rb	7	152	38	25	37
Ni	29	2937	331	229	532
Zn	58	4704	1048	713	1082
Pb	5	40	17	15	9
V	123	6837	1897	1538	1634
U	1	266	27	8	50
Th	1	17	4	2	6

^{*}Min: minimum; Max: maximum; Mean; Median; Standard Deviation in wt.% (SiO₂ to LOI) and in ppm (trace elements).
^{**}% Loss on ignition at 1000°C.

Table 2.
 Statistical parameters of the chemical composition of the Puyango deposit rocks.

	Background	Threshold	Subanomalies	Anomalies
SiO ₂ (wt.%)	15.97	29.69	43.41	57.13
Al ₂ O ₃	2.95	8.25	13.54	18.84
Fe ₂ O ₃	1.22	3.70	6.18	8.66
MnO	0.01	0.03	0.05	0.07
MgO	0.63	0.90	1.16	1.43
CaO	41.53	not apply	not apply	not apply
Na ₂ O	0.21	0.42	0.63	0.83
K ₂ O	0.57	1.32	2.08	2.83
TiO ₂	0.22	0.45	0.68	0.91

	Background	Threshold	Subanomalies	Anomalies
P ₂ O ₅	0.43	1.99	3.55	5.12
LOI	32.82	not apply	not apply	not apply
Zr (ppm)	40	102	164	225
Sr	963	1340	not apply	not apply
Cr	174	299	424	550
Ba	620	1040	1459	not apply
Y	51	107	163	219
Rb	25	62	99	135
Ni	229	761	1293	1824
Zn	713	1795	2877	3959
Pb	15	24	32	not apply
V	1538	3172	4806	6440
U	8.1	58	108	158

Table 3.
Geochemical anomalies in the data set.

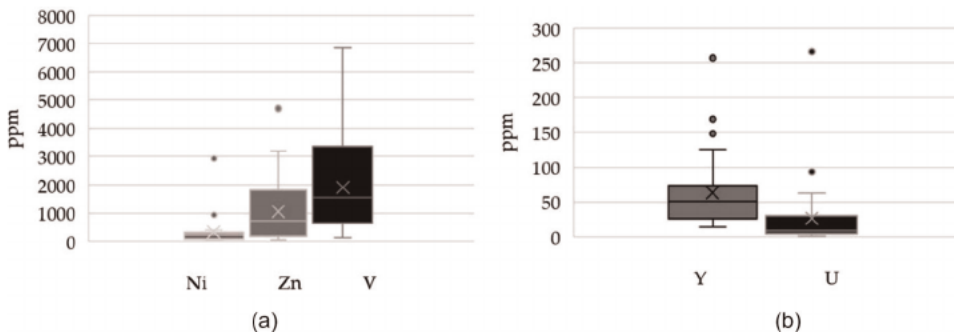


Figure 3.
(a) Box plot of trace elements contents (Ni, Zn, and V); and (b) Box plot of trace elements contents (Y and U) in Puyango deposit.

6. Conclusions

Geochemical prospecting is an important tool in the early stages of exploration of mineral deposits, since it allows delimiting anomalous areas that could be favorable for the discovery of a mineral deposit of economic interest.

To carry out a geochemical prospecting study, it is necessary to know the geochemical fundamentals that control the mobility of the different elements: ionic potential (charge/radius ratio of the ions, physicochemical parameters such as Eh and pH, among others).

When a mineral deposit is formed, some elements (pathfinders) will be dispersed to a greater extent, which can be used as tracers of the deposit.

Data from a case study of geochemical prospecting of the sedimentary mineral deposit of V, U, and Zn from Puyango, Ecuador, in which anomalous and

subanomalous values of several pathfinder elements associated with elements of economic interest were detected, among which stand out: P_2O_5 (>5.12 wt.%), Ni (>1824 ppm), and Y (>219 ppm), among the most important and subanomalies of Ba (>1459 ppm) and Pb (>32 ppm).

Acknowledgements

I thank the department of Geosciences and the Research Vice-rectorate of the Universidad Técnica Particular de Loja, Ecuador, for their support in this research.

References

- [1] Hawkes HE. Principles of geochemical prospecting. Geological Survey Bulletin 1000-F: USGS. 1957;1:355. DOI: 10.3133/b1000F
- [2] Kyser K, Barr J, Ihlenfeld C. Applied geochemistry in mineral exploration and mining. *Elements*. 2015; **11**(4):241-246. DOI: 10.2113/gselements.11.4.241
- [3] Pohl WL. Economic Geology Principles and Practice. Metals, Minerals, Coal and Hydrocarbons—Introduction to Formation and Sustainable Exploitation of Mineral Deposits. West Sussex, UK: Wiley—Blackwell; 2011. p. 699
- [4] Neukirchen F, Ries G. The World of Mineral Deposits. Switzerland: Springer; 2020. p. 378. DOI: org/10.1007/978-3-030-34346-0
- [5] Haldar SK. Mineral Exploration. Principles and Applications. Oxford, UK: Elsevier; 2013. p. 333
- [6] Eguez A, Poma O. The Alamor-Lancones Basin in the Geodynamic Context of the Andes of Huancabamba, SW Ecuador. In: Fourth Conferences in Earth Sciences, National Polytechnic School. Ecuador: Quito; 2001. (In Spanish)
- [7] Jaillard H, Bengtson P, Bulot L, Dhont A, Laubacher G, Robert E. Stratigraphy of the western Celica basin (SW Ecuador). In: Third ISAG. France: St. Malo; 1996. p. 17
- [8] Jaillard H, Laubache G, Bengtson P, Dhondt A, Bulot L. Stratigraphy and evolution of the cretaceous fore arc celica-lancones basin of southwestern Ecuador. *Journal of South American Earth Sciences*. 1999;**12**:51-68
- [9] Kenerley J. Geology of the Loja Province, Southern Ecuador. London Institute of Geological Sciences; 1973 Report 23
- [10] National Institute of Geological Metallurgical Mining Research (INIGEMM). Technical Report, Puyango Geological Sheet. Scale. 2013;**1**:50000. (In Spanish)
- [11] Aspden J, Bonilla W, Duque P. The el Oro Metamorphic complex, Ecuador: Geology and Economic Mineral Deposits. Overseas Geology and Mineral Resources. Vol. 67. Keyworth, Nottingham: British Geological Survey; 1995
- [12] Bristow C, Hoffstetter R. International Stratigraphic Lexicon. Vol. 51977. Fascicle 5. Ecuador
- [13] Shoemaker R. The Geology and Paleontology of the Cretaceous Sediments of the Puyango River Valley, Provinces of Loja and El Oro, Ecuador. Ecuadorian Subcommittee PREDESUR—Towson State University—PREDESUR. Quito, Ecuador; 1982. Publication No. 64 (in Spanish)

Mineralogy and Geochemistry of Shales of Mamu Formation in Nigeria: Effects of Deposition, Source Rock, and Tectonic Background

Segun A. Akinyemi, Olajide F. Adebayo, Henry Y. Madukwe, Adeyinka O. Aturamu and Olusola A. OlaOlorun

Abstract

Study of lithofacies identification, geochemical characterization of shales is vital to the provenance, paleoweathering, and tectonic setting reconstruction. The combination of morphological analysis, bulk chemical analysis and in-situ multi-element analysis was used to investigate the provenance, source area weathering, and depositional setting of outcropped Maastrichtian shale sequence of the Mamu Formation, Anambra Basin in Nigeria. Ten representative shale samples were examined by scanning electron microscopy/energy dispersive spectroscopy (SEM/EDS). Geochemical analysis was performed by X-ray fluorescence (XRF) Spectroscopy and Laser Ablation-Induced Coupled Plasma Mass Spectrometry (LA-ICPMS) techniques. The structural and morphological development of kaolinite in the outcropped shale samples of Mamu Formation is due to mechanical disintegration during transportation and re-deposition. Major oxides such as SiO_2 , Al_2O_3 and Fe_2O_3 constitute greater than 86% of the bulk composition. The weathering indices suggest highly weathered source materials. The plot of Cr versus Ni indicated the studied samples are Late Archean shale. Binary plots of trace elements suggest derivation from acidic or felsic sources rather than intermediate or basic source rocks. Ternary plot of $\text{Na}_2\text{O} + \text{K}_2\text{O}$, $\text{SiO}_2/10$ and $\text{CaO} + \text{MgO}$ indicated multiple sources such as felsic igneous rocks or recycled residues of quartz-rich. Tectonic discrimination diagram depict a typical Passive Margin field.

Keywords: mineralogy, geochemistry, provenance, tectonic-setting, depositional history, formation

1. Introduction

The Mamu Formation (Middle-Upper Maastrichtian) in the Anambra Basin is categorized by fossiliferous dark gray, indurated, and fissile shale. In addition, it is typically overlain by the intercalation of sand and shale facies sequence with coal inter-beds previously deposited under surface marine settings [1]. Selected studies have examined the Mamu Formation, Anambra Basin based on the following; stratigraphic/biostratigraphy [2–5], sedimentology and depositional environments [6], sequence stratigraphy [7, 8], palynology [1, 9–11], coal characterization [12–14], petroleum potential [15–17], palynofacies and kerogen analysis [18], geochemical indicator [19–21] and ichnology and lithofacies [22].

Some authors have indicated that analysis of the major elemental geochemistry of sedimentary rocks is useful in discerning its tectonic background [23, 24]. However, trace elements such as; La, Y, Sc, Cr, Th, Zr, Hf and Nb, mostly combined with TiO₂ are suitable for determining the provenance and tectonic settings. This is attributed to the comparatively poor mobility throughout sedimentary deposition and short habitation periods in seawater [25, 26]. The study by Armstrong-Altrin et al. [25] reported that all sedimentary rocks principally derived from Precambrian terrains could be predisposed to variations from the source materials. The comparative distribution of immobile elements showed diverse concentrations in felsic and basic rocks. For example, the immobile elements La and Th (enriched in felsic rocks) and Sc, Cr, and Co (basic rock compared to felsic rock enriched) are employed to understand the relative contributions of felsic and basic origins in shales derived from diverse tectonic locations [27, 28]. Akinyemi et al. [19] reported the paleoenvironment reconstruction of the outcropped Maastrichtian shale along Auchi-Igarra road using redox sensitive inorganic elements and mineralogical approach. However, the provenance, tectonic setting and paleoweathering of the Maastrichtian Mamu Shale Formation exposed at Auchi-Igarra Road, Edo State in Nigeria is hitherto not documented in the literature. Therefore, the main objective of the present study is to identify the source rock characteristics (i.e. provenance), source area weathering, and tectonic background through primary and immobile trace elements.

2. Geological setting

The Anambra Basin is located from longitudes 6.30 E to 8.00 E and from the latitudes 5.00 N to 8.00 N. It is a syncline that trends from NE to SW as part of Central African Rift System. The basin was established in reaction to the widening and settling of major crustal blocks through the Early Cretaceous plate partitioning of South America and Africa [29]. The movements were restarted through additional activity on the Lower Tertiary plate subsequent to the alternation in the Upper Cretaceous rift. The proposed rift model was based on the evidence gathered by geomorphic, stratigraphic, structural, and paleontological research in literature [30–32]. The development of the basin denotes the third evolutionary sequence of the Benue Trough and its related basins when the Abakaliki Trough was elevated to the Abakaliki Anticlinorium whereas the Anambra Platform was transformed into the Anambra Basin [33, 34]. This transformation gave way to the westward transposition of the depositional axis of the troughs.

The sedimentation trend of the Anambra Basin is categorized by unstable depocentres. The basin consists of nearly 6 km of dense Cretaceous/Tertiary sediments

and is the structural connection from the Cretaceous Benue Trough to the Tertiary Niger Delta [35]. The basin is a portion of the lower Benue Trough comprising the post-deformational Campanian—Maastrichtian to the Eocene sedimentary strata. Sedimentation in the basin started with the Campano—Maastrichtian marine and paralic shales of the Enugu and Nkporo formations superimposed by the coal seams of the Mamu Formation. The fluivo-deltaic sandstones of the Ajali and Owelli sandstones are located in the Mamu Formation, which mostly comprises of its equivalents. The marine shales of the Imo and Nsukka formations were deposited in the Paleocene; superimposed by the tidal Nanka sandstones of the Eocene age. The down-dip towards the Niger Delta, Akata Shale and Agbada Formation account for the Paleogene equivalents of the Anambra Basin [1].

3. Materials and method

3.1 Sampling method

The outcrop of the Maastrichtian shale is located at coordinates 07°05'.071" N and 06°14'.826" E at 162.72 m above sea level (**Figure 1**). About 500 g of each sample was obtained at a sequence interval of 0.2 m from the shale. After collection, the samples directly stored in zipped lock polyethene bags for preservation at ambient temperatures. Next, the shales were oven dried at 60°C for 12 h. On cooling, the each sample was milled into a homogeneous powder using an agate ball mill. Next, the crushed shales characterized by scanning electron microscopy/energy dispersive spectroscopy (SEM/EDS) technique. Geochemical analysis was performed by X-ray fluorescence (XRF) Spectroscopy and Laser Ablation-Induced Coupled Plasma Mass Spectrometry (LA-ICPMS).

3.2 X-ray diffraction analysis

The nine representative samples collected from the Maastrichtian shale of Mamu Formation were characterized to determine bulk mineralogy by X-ray diffraction (XRD). A detailed analytical procedure is reported in Akinyemi et al. [19].

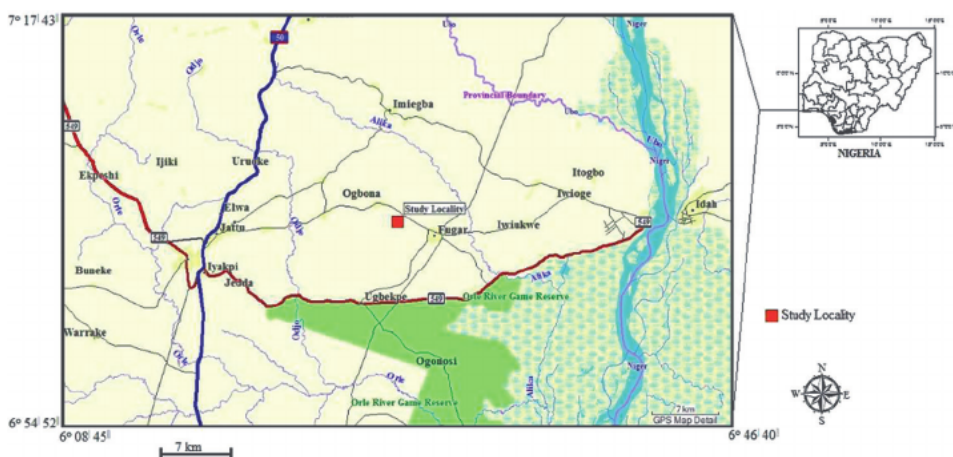


Figure 1.
Map showing the location of the study area.

3.3 SEM/EDS analysis

The surface morphology of the nine samples was determined by scanning electron microscopy (SEM). The SEM is an FEI Nova NanoSEM (Model: Nova NanoSEM 230). The EDS analyses were determined at 20 kV and 5 mm working distance. The EDS detector is an Oxford X-Max (large area silicon drift detector) operated with the INCA- (INCAmicaF+ electronics and INCA Feature particle) analysis software.

3.4 XRF and LA-ICPMS analyses

The composition of the metal oxides in the nine samples acquired at various heights in the Formation was determined by X-ray fluorescence (XRF) spectroscopy. The major oxides detected during XRF were; SiO₂, TiO₂, Al₂O₃, Fe₂O₃, MgO, MnO, CaO, Na₂O, K₂O, Cr₂O₃ and P₂O₅. However, the composition of the trace elements in the samples was examined by LA-ICP-MS. The trace elements determined include; Ni, Cu, Zn, Ga, Rb, Sr, Y, Zr, Nb, Co, V, Pb, Th, U, Ti, Cr, Ba, La, Ce, Nd and P). The XRF and LA-ICP-MS tests were performed at the elemental analysis laboratories of the Stellenbosch University in South Africa. The techniques for sample preparation and ICP-MS analyses are as described in Akinyemi et al. [19]. The precision of the findings is presented as comparative standard deviation (in %) which is 5% for most of the elements analyzed with the LA-ICP-MS technique. The geochemical results from XRF were regularized to 100% volatile-free before plotting the data.

3.5 Loss on ignition determination

The loss of ignition (LOI) was examined through the experimental techniques reported in Ojo [36]. The LOI was determined by first weighing an empty porcelain crucible, before adding 1 g of the dry mass of each sample to the crucible. Next, each sample was oven dried at 120°C for half an hour (30 min). The crucible and the sample were subsequently transferred to a furnace pre-heated to 1000°C for about 45 min. On completion, the samples were cooled in desiccators and weighed repeated until a constant weight was reached.

4. Results and discussion

4.1 Mineralogy and surface morphology

The base of the Mamu Formation is mainly dominated by quartz and kaolinite with minor traces of hematite, as described in literature [19]. The hematite in the base of the shale profile shows the oxidizing diagenetic setting for deposition. However, the upper portion of the profile is characterized by quartz and kaolinite with minor quantities of halloysite and grossite. **Figures 2 and 3** present the results of the SEM micrographs of the samples taken at the basal and upper part of the lithosection of the outcropped Mamu Shale.

The SEM investigation of samples taken at the basal and the upper part of the outcropped shale section show a mixture of sizes and morphologies of kaolinite in all the samples. As shown in **Figure 2a**, the quartz particles are spherical to rounded and exfoliated. The kaolinic particles are rolled with rough edges and some individual particles have lamellar shape indicating a terrigenous origin (**Figure 2b and c**).

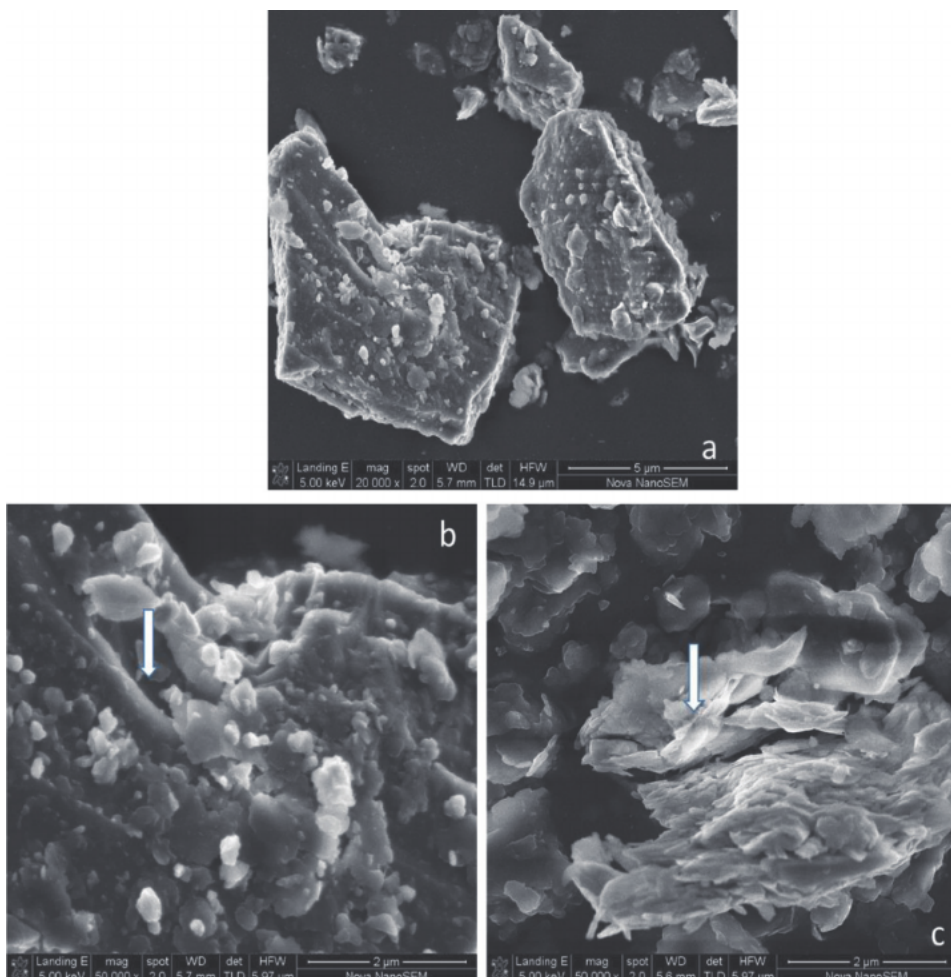


Figure 2. SEM photomicrographs of samples taken at basal part of outcropped shale of Mamu Formation. (a) Spherical quartz particle, rounded corners, and exfoliation, (b) rolled and rough edged kaolinite particles and (c) lamellar kaolinitic crystals.

Bortnikov et al. [37], reported that terrigenous kaolinite consists of lamellar particles and remains of differently preserved vermicular crystals. Kaolinite particles are arranged face to face and individuals show well defined crystalline pseudo-hexagonal and rough edges indicating detrital origin (**Figure 3b** and **c**). **Figure 3c** shows the face to face arrangement patterns of kaolinite particles in which larger platelets are surrounded by smaller ones suggesting bimodal origin (i.e. both terrigenous and authigenic varieties). Therefore, structural, and morphological growth of kaolinite in the outcropped shale samples of Mamu Formation is attributed to mechanical disintegration during transportation and redeposition.

4.2 Bulk composition and geochemical classification

The chemical composition and ratios of selected major oxides of the studied samples are shown in **Tables 1** and **2**, respectively. The major oxide components are SiO_2 ,

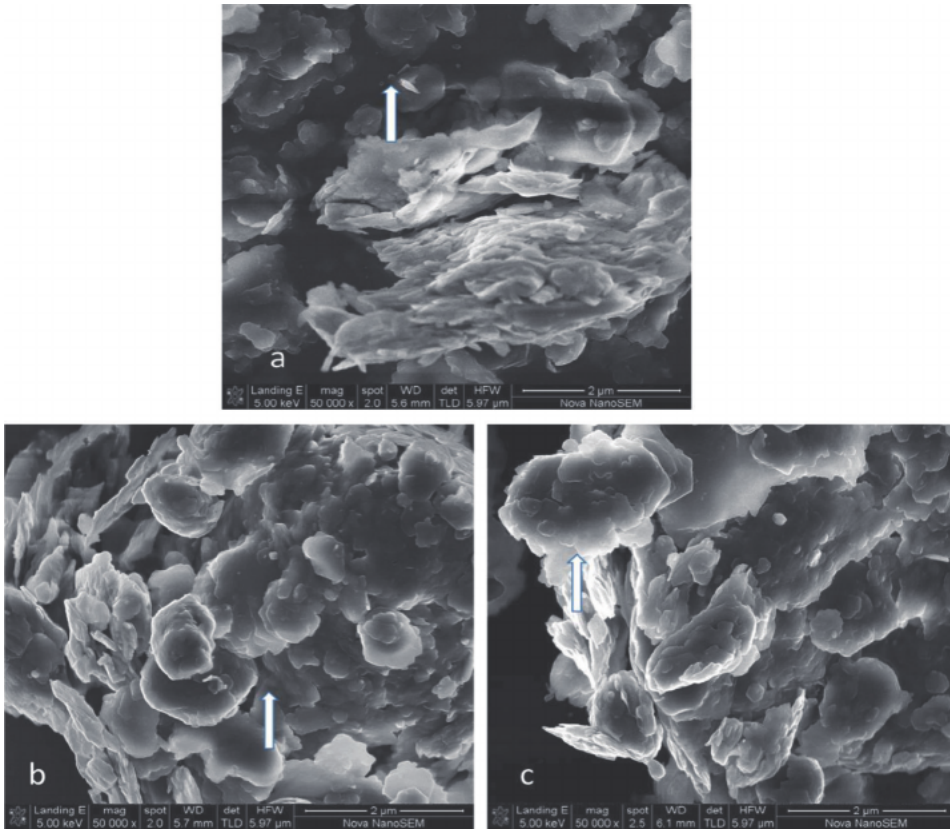


Figure 3. SEM photomicrographs of samples taken at upper part of outcropped shale of Mamu Formation. (a) Authigenic quartz particle and face to face arrangement of kaolinite particles, (b) face to face arrangement patterns of larger platelets of kaolinite surrounded by smaller ones and (c) pseudo hexagonal and rough edges kaolinite particles.

Al₂O₃ and Fe₂O₃ while other oxides occurred in minor quantities. The average contents of SiO₂, Al₂O₃ and Fe₂O₃ are 64.84 wt%, 19.79 wt% and 2.22 wt%, respectively (Table 1). The ratios of SiO₂ to Al₂O₃ ranged between 1.96 wt.% and 26.95 wt.% with an average value of 5.29 wt.%. The TiO₂/Al₂O₃ ratios varied between 0.04 and 0.08 with an average value of 0.07. The K₂O/Na₂O ratios ranged from 1.96 to 24.67 with an average value of 16.50 (Table 2). The ratios of Fe₂O₃ + MgO to K₂O + Na₂O ranged from 1.57 to 14.31 with an average value of 3.31. The plot of log (SiO₂/Al₂O₃) versus log (Fe₂O₃/K₂O), based on Herron [42], clearly shows the studied samples majorly fall within the shale field with one sample within the greywacke field and another in the Fe-sand field (Figure 4). This exceptional trend of the two samples is attributed to the relatively high Fe₂O₃ contents in samples taken at 0.0 m and 0.2 m depths.

The major oxides were compared with the average values of shales worldwide [43], Average North American Shale [44, 45], Average Post-Archaean Australian Shale, and Upper Crust (data from Taylor and McLennan [46]). As observed, the average SiO₂, Al₂O₃, and TiO₂ in the studied samples is higher than Average World Shale, PAAS, NASC, Upper Crust [45]. Conversely, the average Fe₂O₃, CaO, MgO, MnO, Na₂O, P₂O₅ and K₂O contents in the studied samples is below the Average World Shale, PAAS, NASC, Upper Crust (Table 3) [45]. The average trace element such as Ba, Cu, Ni, Zn, and U in the studied samples is lower than shales from various regions of the globe

Sample ID	SiO ₂	Al ₂ O ₃	CaO	Cr ₂ O ₃	Fe ₂ O ₃	K ₂ O	MgO	MnO	Na ₂ O	P ₂ O ₅	TiO ₂	LOI	Total
0.0 m	92.20	3.42	0.08	0.00	3.15	0.15	0.10	0.00	0.08	0.10	0.29	1.81	101.37
0.2 m	63.62	19.56	0.02	0.02	3.56	1.00	0.25	0.01	0.10	0.11	1.42	10.79	100.45
0.4 m	62.48	21.49	0.02	0.02	1.56	1.07	0.27	0.01	0.06	0.09	1.57	11.15	99.77
0.6 m	72.77	14.83	0.04	0.01	2.75	0.74	0.21	0.01	0.08	0.10	1.09	7.917	100.53
0.8 m	51.83	26.46	0.06	0.03	2.26	1.41	0.35	0.01	0.07	0.17	1.10	16.16	99.9
1.0 m	61.22	23.25	0.02	0.02	1.62	1.00	0.22	0.01	0.06	0.07	1.55	11.52	100.56
1.4 m	56.52	24.86	0.04	0.02	1.94	1.20	0.29	0.01	0.06	0.12	1.33	13.84	100.23
1.6 m	64.49	20.01	0.04	0.02	1.46	0.97	0.22	0.00	0.05	0.08	1.61	10.45	99.39
1.8 m	58.30	24.20	0.06	0.02	1.66	1.19	0.29	0.00	0.05	0.06	1.40	12.68	99.39
2.0 m	58.27	24.22	0.07	0.02	1.67	1.20	0.30	0.00	0.05	0.07	1.41	12.7	99.97
Aver.	64.82	19.79	0.04	0.02	2.22	0.97	0.24	0.01	0.07	0.10	1.26	10.704	100.24

Table 1.
 Bulk chemical composition of Maastrichtian Mamu shale sequence.

Sample ID	$\text{SiO}_2/\text{Al}_2\text{O}_3$	$\text{TiO}_2/\text{Al}_2\text{O}_3$	$\text{K}_2\text{O}/\text{Na}_2\text{O}$	$\text{Fe}_2\text{O}_3 + \text{MgO}/\text{K}_2\text{O} + \text{Na}_2\text{O}$	CIA	CIW	PIA	MIA
0.0 m	26.95	0.08	1.96	14.31	91.75	95.60	95.40	91.19
0.2 m	3.25	0.07	10.05	3.47	94.60	99.40	99.37	98.80
0.4 m	2.91	0.07	17.97	1.62	94.95	99.64	99.62	99.28
0.6 m	4.91	0.07	9.41	3.62	94.54	99.21	99.17	98.42
0.8 m	1.96	0.04	21.53	1.78	94.53	99.53	99.50	99.06
1.0 m	2.63	0.07	16.90	1.74	95.57	99.67	99.65	99.34
1.4 m	2.27	0.05	19.33	1.76	95.01	99.59	99.57	99.19
1.6 m	3.22	0.08	19.37	1.66	95.01	99.57	99.55	99.14
1.8 m	2.41	0.06	23.80	1.57	94.90	99.55	99.52	99.10
2.0 m	2.41	0.06	24.67	1.58	94.84	99.51	99.48	99.01
Aver.	5.29	0.07	16.50	3.31	94.57	99.13	99.08	98.25

$\text{CIA} = 100 * \text{Al}_2\text{O}_3 / (\text{Al}_2\text{O}_3 + \text{CaO} + \text{Na}_2\text{O} + \text{K}_2\text{O})$ [38].
 $\text{CIW} = (\text{Al}_2\text{O}_3 / (\text{Al}_2\text{O}_3 + \text{CaO} + \text{Na}_2\text{O}) * 100$ [39].
 $\text{PIA} = (\text{Al}_2\text{O}_3 - \text{K}_2\text{O}) / (\text{Al}_2\text{O}_3 + \text{CaO} + \text{Na}_2\text{O} - \text{K}_2\text{O}) * 100$ [40].
 $\text{MIA} = 2 * (\text{CIA} - 50)$ [41].

Table 2.
Ratios of major oxides in the Maastrichtian Mamu shale sequence.

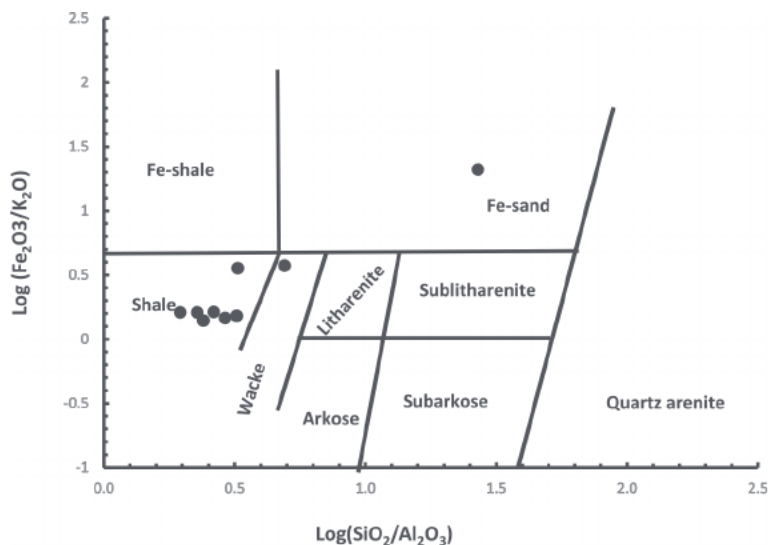


Figure 4. Chemical classification of the Mamu shale sequence based on $\log(\text{SiO}_2/\text{Al}_2\text{O}_3)$ vs. $\log(\text{Fe}_2\text{O}_3/\text{K}_2\text{O})$ diagram of Herron [42].

Oxides	Present study	AWS	PAAS	NASC	UC	Turekan and Wedephol [47]
SiO ₂	64.17	58.90	62.80	64.80	66.00	58.5
Al ₂ O ₃	20.23	16.70	18.90	16.90	15.20	15
Fe ₂ O ₃	2.16	6.90	7.22	5.65	5.00	4.72
TiO ₂	1.28	0.78	1.00	0.70	0.50	0.77
CaO	0.04	2.20	1.30	3.63	4.20	3.1
Cr ₂ O ₃	0.02	—	—	—	—	—
K ₂ O	0.99	3.600	3.700	3.970	3.400	3.1
MgO	0.24	2.60	2.20	2.86	2.20	2.5
MnO	0.01	—	0.11	0.06	0.08	—
Na ₂ O	0.07	1.60	1.20	1.14	3.90	1.3
P ₂ O ₅	0.10	—	0.16	0.13	—	0.16
LOI	10.90	—	6.00	—	—	—
H ₂ O	—	—	—	—	—	—
Total	100.16	93.28	104.59	99.84	100.48	89.15

Average Shale Worldwide [43]; Average Post-Archaean Australian Shale [48]; NASC = Average North American Shale (data from [44]); UC = Upper Crust (data from [48]); Turekan and Wedephol [47].

Table 3. Major oxides of Maastrichtian Mamu shale sequence compared with worldwide shales.

(Table 4). On the other hand, the average concentrations of Ce, Co, Nb, Rb, Sr, V, Y, Zr, Th, Cr, La and Nd in the studied samples is higher than shales from various areas of the globe (Table 4).

Trace elements	Present study	ASW	*PAAS	*NASC	UC	Turekan and Wedephol [47]
As	—	—	—	28.4	1.50	—
Ba	245.8	580	650	636		580
Ce	183.0	—	80	66.7	64	—
Co	54.3	19	23	25.7	10	—
Cu	11.0	45	50	—	25	45
Nb	26.7	—	19	13	25	—
Ni	16.2	68	55	58	20	68
Pb	150.9	22	20	—	—	—
Rb	52.4	140	160	125	112	—
Sr	95.7	300	200	142	350	300
V	212.7	130	150	130	60	130
Y	47.8	—	25	35	22	—
Zn	27.4	95	85	—	71	95
Zr	328.9	160	210	200	190	160
Ga	25.0	—	—	—		—
Th	15.1	—	14.6	12.3	10.7	—
U	0.7	3.7	3.1	2.66	2.8	—
Ti	9475.0	—	—	—	—	—
Cr	138.8	90	110	125	35.0	—
La	72.0	—	38	31.1	30	—
Nd	77.8	—	32	27.4	26	—
P	450.4	—	—	—	—	—

Average Shale Worldwide [43]; Average Post-Archaean Australian Shale [48]; NASC = Average North American Shale (data from [44]); UC = Upper Crust (data from [48]); Turekan and Wedephol [47].

Table 4.
Comparison of average trace element contents with other worldwide shales.

4.3 Source area weathering

Several authors have recommended that the chemical composition of clastic sedimentary rocks is mainly reliant on the composition and weathering settings in the area of the source rock [49, 50]. The study by Nesbitt and Young [50] examined the extent of weathering of a clastic sedimentary rock by computing the chemical index alteration (CIA) which is defined as:

$$CIA = 100 \times \left(\frac{Al_2O_3}{Al_2O_3 + CaO^* + Na_2O + K_2O} \right) \quad (1)$$

This weathering index is mostly valid when Ca, Na, and K declines with increasing weathering intensity [51]. In Eq. (1), CaO* is the concentration of CaO fused in the silicate portion of the shales examined [40]. However, the CaO correction from

the carbonate influence was not performed for the samples examined in this study due to lack of CO₂ data. Therefore, the computation for CaO* from the silicate portion requires adopting Bock et al. [52] hypothesis. Based on the assumption, the CaO values are only valid when CaO ≤ Na₂O. However, if CaO > Na₂O, it is probable that the CaO concentration is equivalent to Na₂O [52]. The outlined technique is the basis for the measure of the weathering intensity and the ratio of the lesser aluminous compound to feldspar [53]. The Chemical Index of Weathering (CIW) proposed by Harnois [39] is similar to the CIA except for the exclusion of K₂O in the equation:

$$CIW = \text{molar} \times \left(\frac{Al_2O_3}{Al_2O_3 + CaO + Na_2O} \right) \quad (2)$$

For CIA and CIW, the values are deduced in the similar to the unweathered upper continental crust (~50) and for greatly weathered constituents (~100) with comprehensive elimination of the alkali and alkaline-earth metals [26, 54, 55]. Typically, small values of CIA (50 or less) may reflect cool and/or dry conditions [40]. In this study, the values of CIA for shale samples ranged from 91.75% to 95.57%, or 94.57% on average. Similarly, the values of CIW varied between 95.60% and 99.67%, or 99.13% on average. The CIA and CIW standards for the examined shale sequence indicate highly weathered source constituents. This observation is corroborated by the previous study by Ejeh [20].

The chemical weathering intensity is typically computed according to the Plagioclase Index of Alteration [40] in molecular proportions:

$$PIA = \text{molar} \times \left(\frac{Al_2O_3 + K_2O}{Al_2O_3 + CaO^* + Na_2O - K_2O} \right) \times 100 \quad (3)$$

The term CaO* represents the CaO residing exclusively in the silicate portion. The unweathered plagioclase typically has a PIA value of 50. In this study, the PIA for the shale samples ranged from 95.40% to 99.67% with an average value of 99.08%, which indicates highly weathered source constituents.

The Mineralogical Index of Alteration (MIA) is a weathering index computed from the equation [41];

$$PIA = 2 \times (CIA - 50) \quad (4)$$

The MIA values from 0 to 20% are designated as incipient i.e. just starting, 20–40% (weak), 40–60% (moderate), and 60–100% as strong to a great degree of weathering. The MIA values for shale samples examined ranged from 91.19% to 99.34%, with an average value of 98.25%. Therefore, the MIA for shales showed a great amount of source weathering constituents.

Figure 5 shows that the studied samples plots are near the “A” vertex above the upper continental crust (UCC) line, which indicates a high extent of weathering. Nesbitt et al. [49] used the ternary diagrams of Al₂O₃-(CaO + Na₂O)-K₂O (the A-CN-K), and Fe₂O₃ + MgO-(CaO + Na₂O + K₂O)-Al₂O₃ (the A-CNK-FM) to deduce weathering trends. On both the A-CN-K and the A-CNK-FM diagrams in **Figures 6** and **7** respectively, all the sediments indicated an extreme weathering history. The studied samples plot evidently suggest different contents of Al₂O₃, CaO, Na₂O, and K₂O in a region examined compared to the Average World Shale, PAAS, NASC, and UC indices. The studied samples plot near the high contents of Al₂O₃ suggests a relatively high intensity of

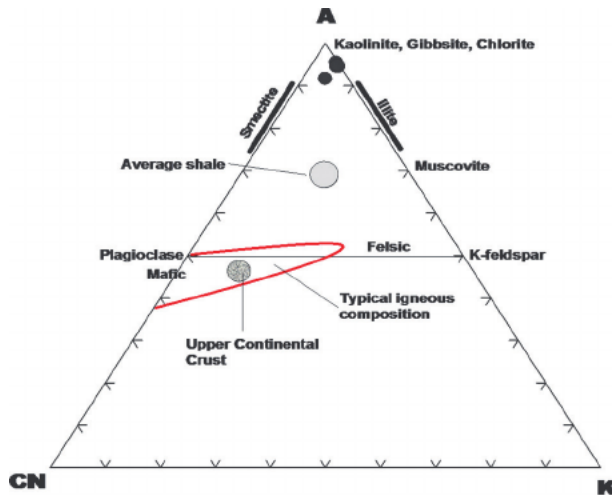


Figure 5. Ternary diagram showing the weathering trend of the studied samples (all in molar proportions); Al_2O_3 - $CaO + Na_2O$ - K_2O (A-CN-K). Fields from Gu et al. [56].

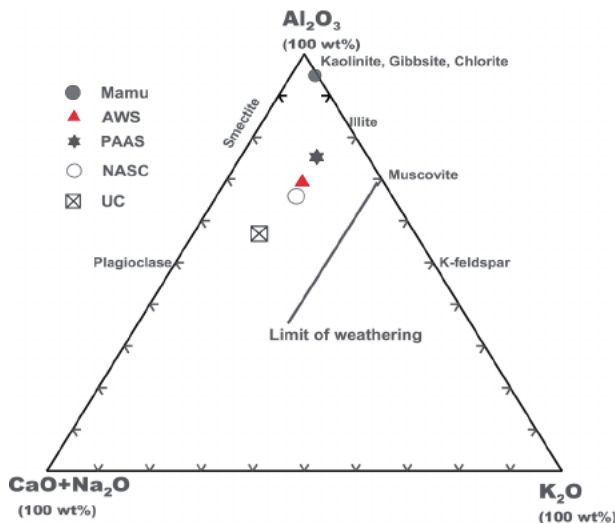


Figure 6. Al_2O_3 -($CaO + Na_2O$)- K_2O plot of sediment samples (after [49, 50]), compared to data for post-Archean average shale (PAAS) and upper crust (UC) given by Taylor and McLennan [48]; and north American shale composite (NASC) given by Gromet et al. [44].

weathering. This implies that substantial content of the alkali and alkaline earth elements were detached from the shales in this study [57].

4.4 Chemical maturity and paleoclimatic condition

Suttner and Dutta [58], suggested the plot of SiO_2 versus $Al_2O_3 + K_2O + Na_2O$ to infer the paleoclimatic condition of the source region. The studied samples mainly fall within the semi-arid condition at the source area (**Figure 8**). Therefore, the prevalent dry settings of the source region will slow down the weathering process and thereby impede chemical maturity.

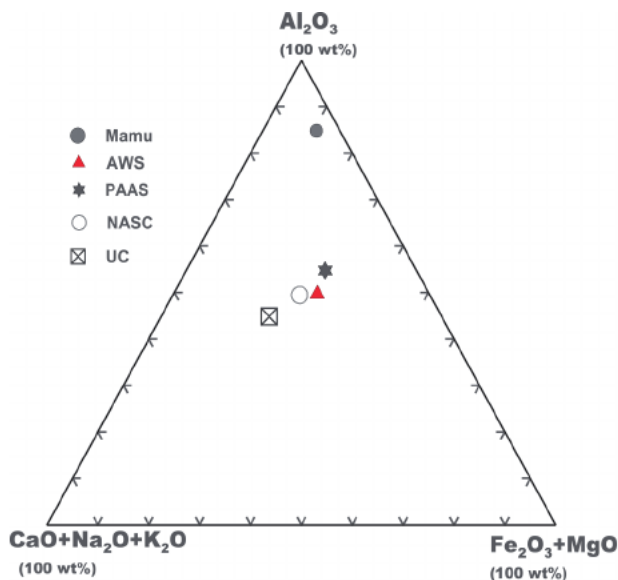


Figure 7. Triangular Al_2O_3 - $(CaO + Na_2O + K_2O)$ - $Fe_2O_3 + MgO$ plot of the current sediment data (after [49, 50]) in comparison with post-Archean average shale and upper crust (data from [48]) and north American shale composite (data from [44]).

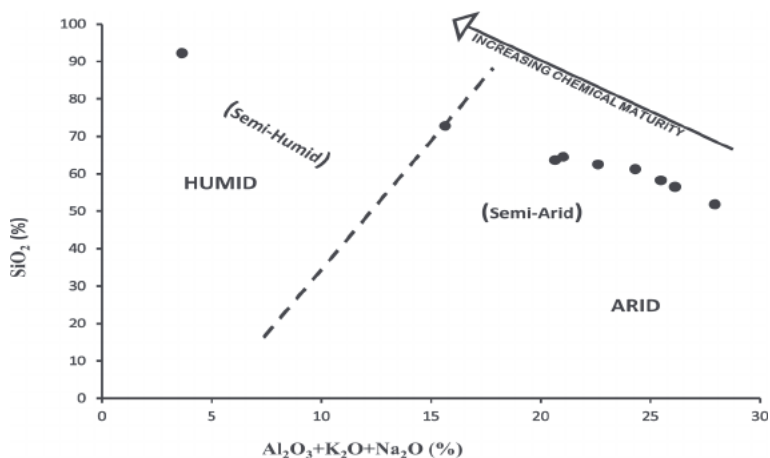


Figure 8. Chemical maturity and paleoclimate of the Mamu shale sequence expressed by bivariate plot of SiO_2 versus $Al_2O_3 + K_2O + Na_2O$ (after [58]).

4.5 Provenance

Major element geochemistry could offer empirical evidence on the rock composition, source rock, along with the outcome of sedimentary techniques like sorting and weathering [26]. The outlined properties provide evidence of the source rock attributes and definite patterns of historical sediments [59, 60]. Therefore, it is a common practice to infer the origin of deposits and sedimentary rocks [61–66]. The two variable plots of Na_2O versus K_2O reveals the studied samples are rich in quartz, which shows felsic sources (**Figure 9**). The ternary diagram shows the plots of the

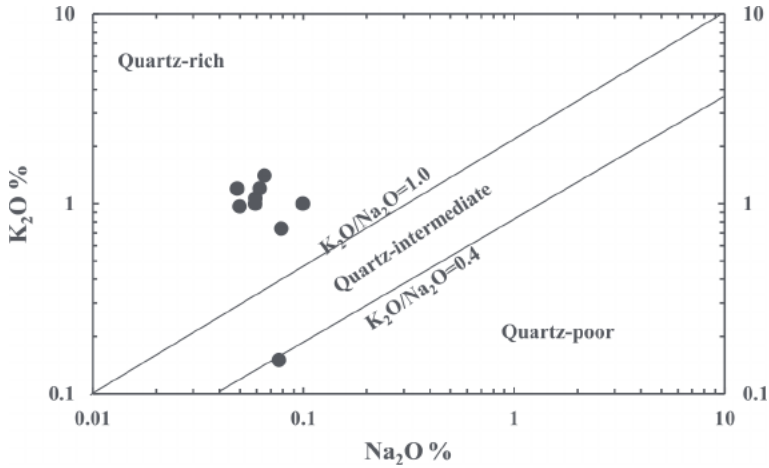


Figure 9. Bivariate plot of Na_2O versus K_2O of the Mamu shale sequence showing quartz content, after Crook [67].

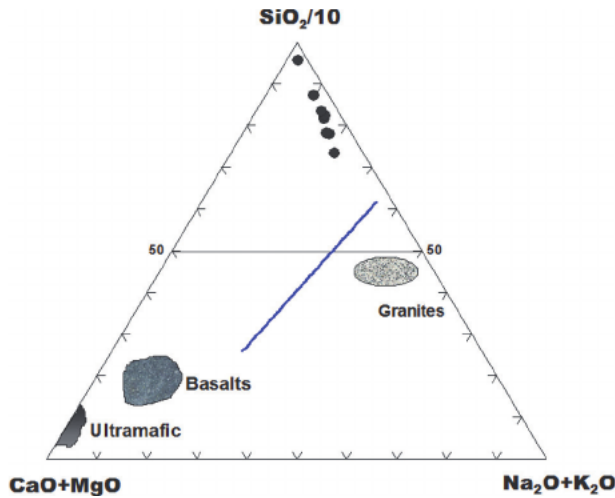


Figure 10. Plot of $\text{Na}_2\text{O} + \text{K}_2\text{O}$, $\text{SiO}_2/10$ and $\text{CaO} + \text{MgO}$ to illustrate possible affinities of the samples to felsic, mafic, and ultramafic rocks (after [48]).

studied samples in the SiO_2 are distant from the basalts, ultramafic, and granitic regions (**Figure 10**). This submits that the felsic igneous or metamorphic or recycled rocks rich in quartz deposits derivation are evident.

Similarly, the composition of zircon is used to describe the nature and content of source rock [68, 69]. The study by Hayashi et al. [68] recommended that TiO_2/Zr ratios can distinguish the three different felsic, intermediate, and mafic types of source rock. The TiO_2 versus Zr plot (**Figure 11**) indicates that the samples examined are mostly plotted in the intermediate field although few lie within the felsic and mafic zones. The origins of a sedimentary rock suite can be computed through the K_2O versus Rb ratios, which are mostly identical to the standard Upper Continental Crust values [70]. The Cr/V–Y/Ni ratios could also provide estimations of the specific composition of chromium over other ferromagnesian elements [26, 71].

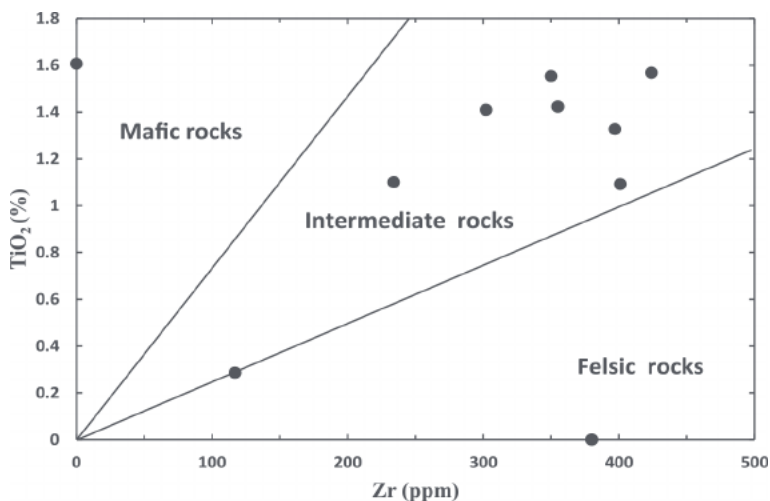


Figure 11.
TiO₂-Zr plot for the Mamu shale sequence [68].

Figure 12 shows the plots of studied samples in the acidic/intermediate composition zone with one sample located in the basic composition zone. The Cr/V ratio describes the enrichment of Cr regarding additional ferromagnesian elements. However, the Y/Ni ratio appraises the connection amongst the ferromagnesian minor elements (denoted by Ni) and the HREE using Y as a substitute [26]. The Y/Ni ratios typically range across values from midway to the felsic calc-alkaline rocks (**Figure 13**). The sediments resulting from ultrabasic origins typically have high Cr/V ratios above 1 and low Y/Ni ratios below 1 [71]. The Cr/V ratio ranged from 0.52 to 0.99, or 0.66 on average. However, the Y/Ni ratio was from 1.1 to 9.6 with an average value of 4.79, which suggests felsic compositions in the source materials.

Figure 14 reveals that the source rocks for shales examined are Late-Archean. The residues reveal minimal scatter along with trace Cr constituents, which indicates

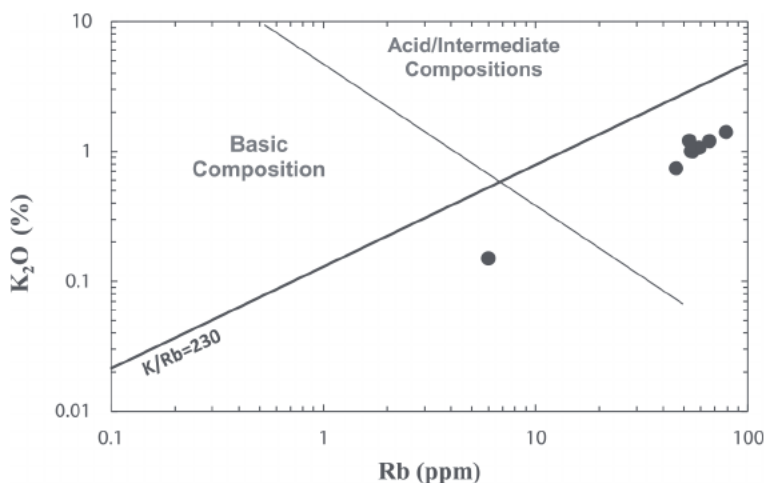


Figure 12.
K₂O versus Rb plot. Fields after Floyd and Leveridge [72].

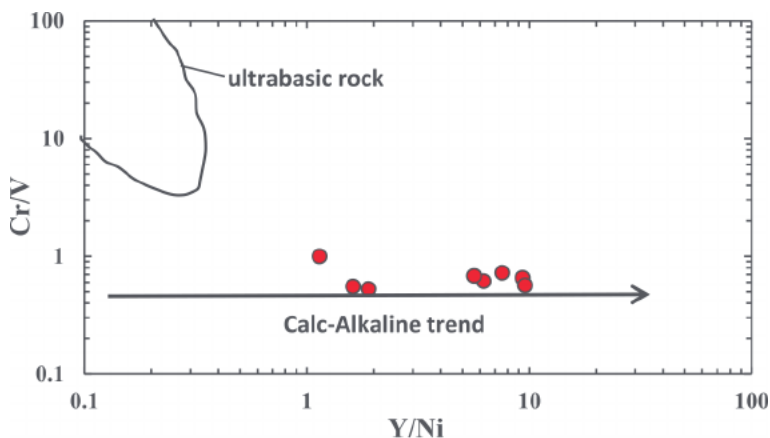


Figure 13. *Cr/V–Y/Ni plots for the sediments showing the lack of ultrabasic sources (after [26]). Ultrabasic field of sands derived from ultrabasic rocks, after Ortiz and Roser [73].*

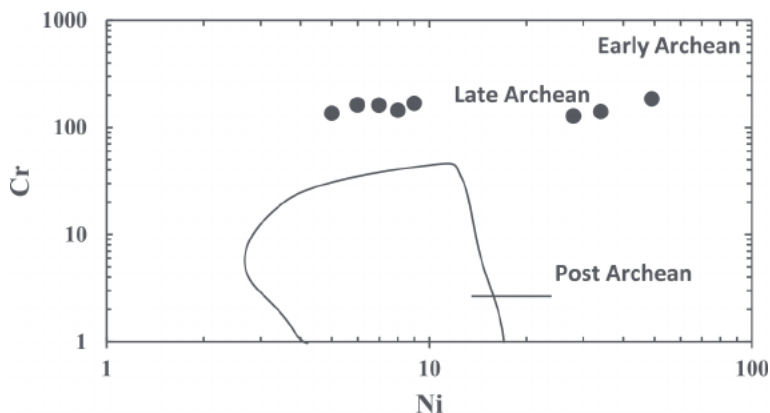


Figure 14. *Cr–Ni plot for the studied samples showing the plots in the late-Archean field [48] and fractionation from source rocks to the sediments.*

depletion and homogenization could have occurred in the course of transportation or weathering. Floyd et al. [70], applied immobile elements such as TiO_2 and Ni to deduce the original lithological structure of rocks. The technique was also employed to separate unformed residues of magmatic origins from standard mature sediments. The studied samples are plotted within the zone of an acidic or felsic source (**Figure 15**). According to Cullers and Berendsen [74], the Th/Co versus La/Co ratios are used to distinguish the source materials of sedimentary rocks. The shale samples examined in this study are plotted mainly in the upper continental crust and one sample each show close proximity to basaltic and granodioritic zone respectively (**Figure 16**). This observation agreed with the previous study conducted by Ogbahon and Olujinmi [76].

4.6 Tectonic evolution

The discrimination diagrams of major elements can be used to describe or distinguish rocks based on the tectonic setting was suggested by several authors [23, 24, 77].

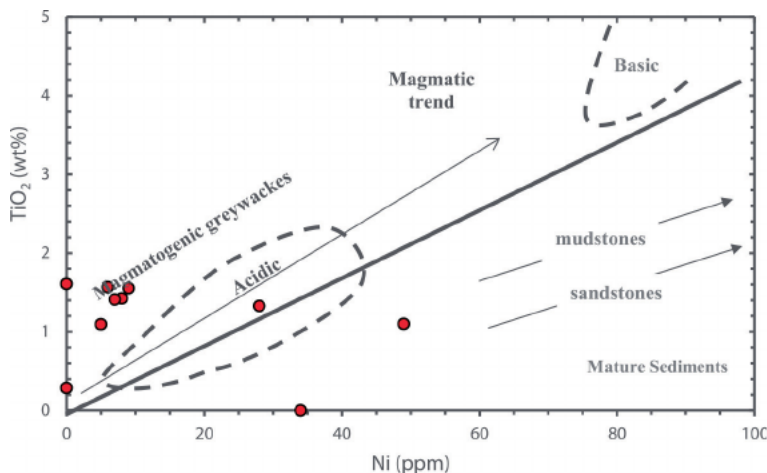


Figure 15. TiO_2 vs. Ni plot. Fields and trends fashioned after Gu et al. [56] and Floyd et al. [70].

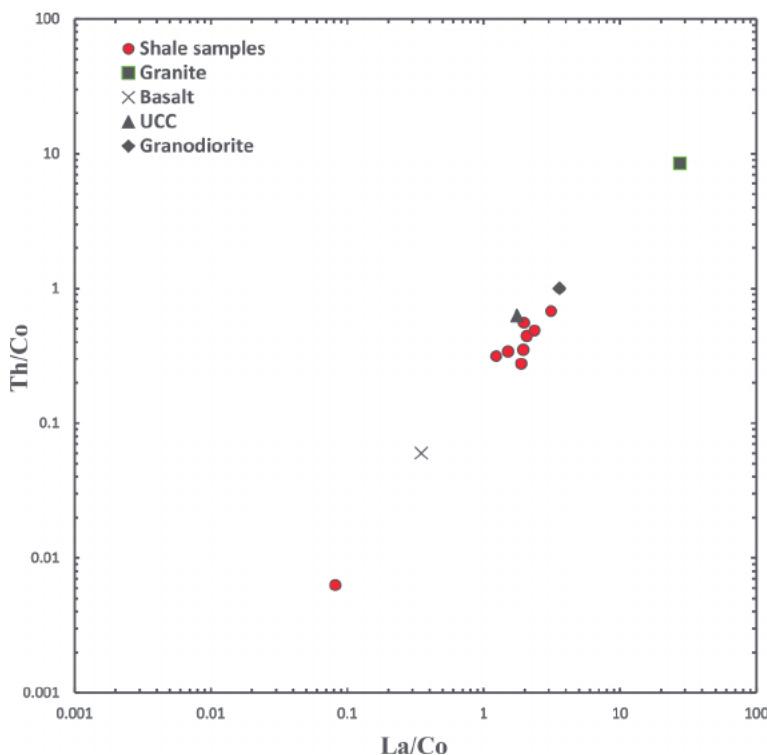


Figure 16. Source rock discrimination diagram for Mamu shale sequence (after [74]), in relation to average values of granites, basalts, granodiorite [75] and upper continental crust [46, 48].

Roser and Korsch [24] suggested four tectonic discrimination diagrams based on the SiO_2 as the x-axis and K_2O/Na_2O as the y-axis. As shown in **Figure 17**, the studied samples indicated Passive Margins tectonic field. Furthermore, the tectonic discrimination

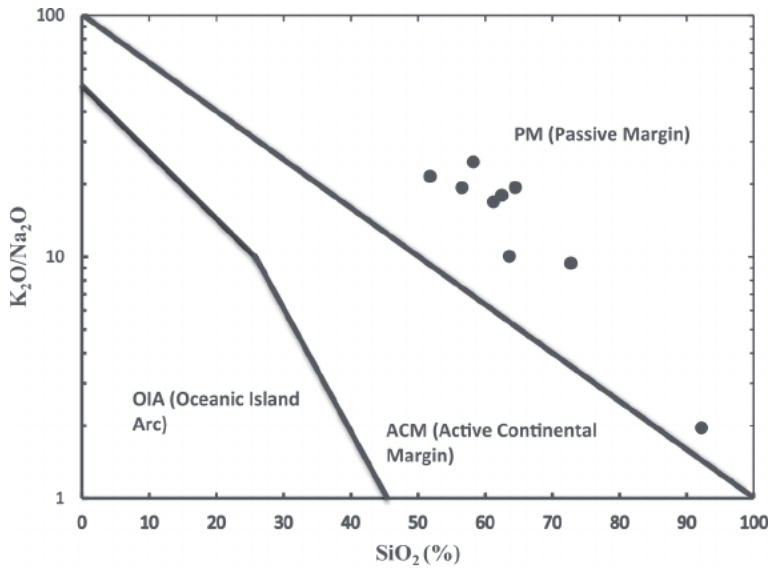


Figure 17.
Tectonic discrimination plot for the Mamu shale sequence (after [24]).

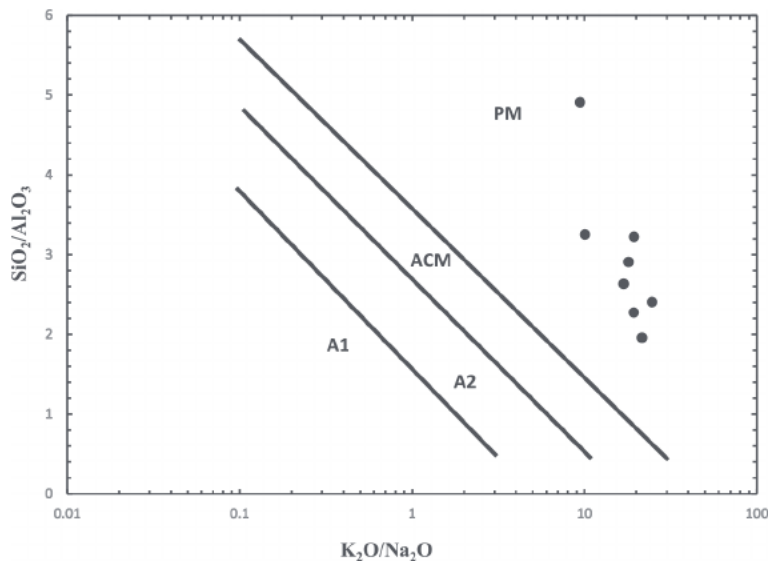


Figure 18.
 SiO_2/Al_2O_3 ratio versus K_2O/Na_2O ratio plot for Mamu shale sequence. Fields and boundary lines (after Maynard et al. [78]; Roser and Korsch [24]). A1 = arc setting, basaltic and andesitic detritus; A2 = evolved arc setting; ACM = active continental margin; PM = passive margins.

diagram of K_2O/Na_2O as the x-axis and SiO_2/Al_2O_3 as the y-axis similarly depicted studied samples in the Passive Margins zone (**Figure 18**). This trend is supported by the previous study done by Ogbahon and Olujinmi [76]. The residues from the passive margin are fundamentally rich in quartz and derived from established continental regions, placed in intracratonic basins or on passive continental boundaries [24].

5. Summary and conclusion

In this study, the structural and morphological evolution of kaolinite in the samples is attributed to mechanical disintegration during sediment transportation and redeposition. The shales of the Mamu Formation show considerable variation with regards to major oxides, trace, and rare earth elements. The abundant major oxides showed that SiO_2 , Al_2O_3 and Fe_2O_3 constitute more than 86% of the bulk chemical composition. The plot of $\log (\text{SiO}_2/\text{Al}_2\text{O}_3)$ versus $\log (\text{Fe}_2\text{O}_3/\text{K}_2\text{O})$ indicated that the samples examined are majorly within the shale field. The weathering indices such as CIA, CIW, PIA and MIA indicated highly weathered source materials. Provenance indicated heterogeneous sources for the studied clastic sediments. The examination of geochemical parameters such as Th/Co versus La/Co, TiO_2 versus Ni, Cr/V versus Y/Ni and TiO_2 versus Zr suggest the samples could be the result of acidic or felsic sources and not intermediate or basic source rocks. The Cr versus Ni plots indicated the studied samples are Late Archean shales. In the provenance discrimination diagrams based on major and immobile elements, the outcropped shale samples show geochemical markers in agreement with the source rocks of intermediate structure, whereas the tectonic discrimination diagrams indicate Passive Continental Margin field.

References

- [1] Ogala J, Ola-Buraimo A, Akaegbobi I. Palynological and palaeoenvironmental study of the middle-upper Maastrichtian Mamu coal facies in Anambra Basin, Nigeria. *World Applied Sciences Journal*. 2009;7(12):1566-1575
- [2] Adeniran B. Maastrichtian tidal flat sequences from the northern Anambra Basin, southern Nigeria. *Nigerian Association of Petroleum Exploration Bulletin*. 1991;6:56-66
- [3] Gebhardt H. Benthic Foraminifera from the Maastrichtian lower Mamu Formation near Leru (southern Nigeria); paleoecology and paleogeographic significance. *The Journal of Foraminiferal Research*. 1998;28(1):76-89
- [4] Ladipo KO. Paleogeography, sedimentation and tectonics of the upper cretaceous Anambra Basin, southeastern Nigeria. *Journal of African Earth Sciences (and the Middle East)*. 1988;7(5-6):865-871
- [5] Petters S. Stratigraphic evolution of the Benue trough and its implications for the upper cretaceous paleogeography of West Africa. *The Journal of Geology*. 1978;86(3):311-322
- [6] Lukman A, Ayuba R, Alege T. Sedimentology and depositional environments of the Maastrichtian Mamu formation, northern Anambra Basin, Nigeria. *Advances in Applied Science Research*. 2020;9(2):53-68
- [7] Nwajide CS, Reijers TJ. Sequence architecture in outcrops: examples from the Anambra Basin, Nigeria. *NAPE Bulletin*. 1996;11(01):23-32
- [8] Onyekuru S, Iwuagwu C. Depositional environments and sequence stratigraphic interpretation of the Campano-Maastrichtian Nkporo shale group and Mamu formation exposures at Leru-Okigwe axis, Anambra Basin, Southeastern Nigeria. *Australian Journal of Basic Applied Sciences*. 2010;4(12):6623-6640
- [9] Mebradu S. Palynofacies of Enugu/Iva valley shales, Enugu State, Nigeria. *Journal of Mining & Geology*. 1982;26(1):5-11
- [10] Onuigbo E, JO, E.-E., & Okoro, A. Palynology, paleoenvironment and sequence stratigraphy of the Campanian-Maastrichtian deposits in the Anambra Basin, Southeastern Nigeria. *European Journal of Scientific Research*. 2012;78(3):333-348
- [11] Onyeachonam N, Fregene TJ. Palynological studies of upper Cretaceous-Paleocene rocks in Auchi sheet 266, Benin flank, Western extension of the Anambra Basin, southwestern Nigeria. *Journal of Geosciences and Geomatics*. 2021;9(3):145-159. DOI: 10.12691/jgg-9-3-5
- [12] Akande SO, Hoffknecht A, Erdtmann BD. Rank and petrographic composition of selected upper cretaceous and tertiary coals of southern Nigeria. *International Journal of Coal Geology*. 1992;20(3-4):209-224
- [13] Akinyemi SA, Adebayo OF, Madukwe HY, Kayode AT, Aturamu AO, OlaOlorun OA, et al. Elemental geochemistry and organic facies of selected cretaceous coals from the Benue trough basin in Nigeria: Implication for paleodepositional environments. *Marine and Petroleum Geology*. 2022;137:105490

- [14] Akinyemi SA, Adebayo OF, Nyakuma BB, Adegoke AK, Aturamu OA, OlaOlorun OA, et al. Petrology, physicochemical and thermal analyses of selected cretaceous coals from the Benue Trough Basin in Nigeria. *International Journal of Coal Science & Technology*. 2020;7(1):26-42
- [15] Maju-Oyovwikowhe GE, Malomi BP. Evaluation of hydrocarbon potential, quality of source rock facies, and delineating of their depositional environment in Mamu formation of Anambra Basin, Nigeria. *Journal of Applied Sciences & Environmental Management*. 2019;23(3):383-388
- [16] Ogala JE. Hydrocarbon potential of the upper cretaceous coal and shale units in the Anambra Basin, Southeastern Nigeria. *Petroleum & Coal*. 2011;53(1):35-44
- [17] Ogungbesan GO, Adedosu TA. Geochemical record for the depositional condition and petroleum potential of the late cretaceous Mamu formation in the western flank of Anambra Basin, Nigeria. *Green Energy & Environment*. 2020;5(1):83-96
- [18] Chiaghanam O, Chiadikobi K, Ikegwuonu O, Omoboriowo A, Onyemesili O, Acra E. Palynofacies and kerogen analysis of upper cretaceous (early Campanian to Maastrichtian) Enugu shale and Mamu formation in Anambra Basin, south-eastern Nigeria. *International Journal of Scientific & Technology Research*. 2013;2(8): 87-97
- [19] Akinyemi S, Adebayo O, Ojo O, Fadipe O, Gitari W. Mineralogy and geochemical appraisal of paleo-redox indicators in Maastrichtian outcrop shales of Mamu formation, Anambra Basin, Nigeria. *Journal of Natural Science Research*. 2013;3:48-64
- [20] Ejeh OI. Geochemistry of rocks (late cretaceous) in the Anambra Basin, SE Nigeria: Insights into provenance, tectonic setting, and other palaeo-conditions. *Heliyon*. 2021;7(10):e08110
- [21] Okiotor ME, Ighodaro EJ. Geochemical appraisal of the Mamu shales exposed around Igodor in the Benin flank of the Anambra Basin, Nigeria. *Journal of Applied Sciences & Environmental Management*. 2020;24(3):489-493
- [22] Odumodu CF. Ichnology and lithofacies analysis of the Campano-Maastrichtian Mamu formation in the northern parts of the Anambra Basin, Nigeria. *International Journal of Geology. Earth Environmental Sciences*. 2014;4:3
- [23] Bhatia MR. Plate tectonics and geochemical composition of sandstones. *The Journal of Geology*. 1983;91(6):611-627
- [24] Roser B, Korsch R. Determination of tectonic setting of sandstone-mudstone suites using content and ratio. *The Journal of Geology*. 1986;94(5):635-650
- [25] Armstrong-Altrin J, Lee YI, Verma SP, Ramasamy S. Geochemistry of sandstones from the upper Miocene Kudankulam Formation, southern India: Implications for provenance, weathering, and tectonic setting. *Journal of Sedimentary Research*. 2004;74(2):285-297
- [26] McLennan S, Hemming S, McDaniel D, Hanson G. Geochemical approaches to sedimentation, provenance, and tectonics. *Special Papers-Geological Society of America*. 1993:21-21. DOI: 10.1130/SPE284-p21
- [27] Condie KC, Wronkiewicz DJ. A new look at the Archaean-Proterozoic boundary sediments and the tectonic

setting constraint. *Developments in Precambrian Geology*. 1990;**8**:61-83

[28] Okunlola OA, Idowu O. The geochemistry of claystone-shale deposits from the Maastrichtian Patti formation, Southern Bida basin, Nigeria. *Earth Sciences Research Journal*. 2012;**16**(2):139-150

[29] Burke K. The African plate. *South African Journal of Geology*. 1996;**99**:339-409

[30] Benkhelil J. The origin and evolution of the cretaceous Benue trough (Nigeria). *Journal of African Earth Sciences (and the Middle East)*. 1989;**8**(2-4):251-282

[31] Guiraud R, Bellion Y. Late carboniferous to recent, geodynamic evolution of the west Gondwanian, cratonic, Tethyan margins. *The Tethys Ocean*. 1995;**1**(1):101-124

[32] Reymont R. Ammonite biostratigraphy, continental drift and oscillatory transgressions. *Nature*. 1969;**224**(5215):137

[33] Murat RC. Stratigraphy and paleogeography of the cretaceous and lower tertiary in Southern Nigeria. In: Dessauvage TFJ, Whiteman AJ, editors. *African Geology*. Ibadan: Ibadan University Press; 1972. pp. 251-266

[34] Weber K, Daukoru E. Petroleum geological aspects of the Niger Delta. *Journal of Mining and Geology*. 1975;**12**(1/2):1-22

[35] Mebradu S. Palynofacies of Enugu/ Iva valley shales Anambra State, Nigeria. *Journal of Mining and Geology*. 1990;**26**(1):13-20

[36] Ojo O. Mineralogy and Chemical Mobility in some Weathered Ash Dump Sites. South Africa: University of the Western Cape, South Africa; 2010

[37] Bortnikov N, Novikov V, Savko A, Boeva N, Zhegallo E, Bushueva E, et al. Structural-morphological features of kaolinite from clayey rocks subjected to different stages of lithogenesis: Evidence from the Voronezh anticline. *Lithology and Mineral Resources*. 2013;**48**(5):384-397

[38] Nesbitt HW, Young GM. Early Proterozoic climates and plate motions inferred from major element chemistry of lutites. *Nature*. 1982;**299**:715-717

[39] Harnois L. The CIW index: A new chemical index of weathering. *Sedimentary Geology*. 1988;**55**: 319-322

[40] Fedo CM, Wayne Nesbitt H, Young GM. Unraveling the effects of potassium metasomatism in sedimentary rocks and paleosols, with implications for paleoweathering conditions and provenance. *Geology*. 1995;**23**(10):921-924

[41] Voicu G, Bardoux M, Harnois L, Crepeau R. Lithological and geochemical features of igneous and sedimentary rocks at the Omai gold mine, Guyana, South America. *Exploration and Mining Geology*. 1997;**2**(6):153-170

[42] Herron MM. Geochemical classification of terrigenous sands and shales from core or log data. *Journal of Sedimentary Research*. 1988;**58**(5):820-829

[43] Pettijohn FJ. *Sedimentary Rocks*. Vol. 2. New York: Harper & Brothers; 1957

[44] Gromet LP, Haskin LA, Korotev RL, Dymek RF. The "North American shale composite": Its compilation, major and trace element characteristics. *Geochimica et Cosmochimica Acta*. 1984;**48**(12):2469-2482

- [45] Turekian KK, Wedepohl KH. Distribution of the elements in some major units of the earth's crust. *Geological Society of America Bulletin*. 1961;72(2):175-192
- [46] Taylor SR, McLennan SM. The geochemical evolution of the continental crust. *Reviews of Geophysics*. 1995;33(2):241-265
- [47] Turekian KK, Wedepohl KH. Distribution of the elements in some major units of the Earth's crust. *Geological Society of America Bulletin*. 1961;72:175-192. DOI: 10.1130/0016-7606(1961)72[175:DOTAIS]2.0.CO;2
- [48] Taylor SR, McLennan SM. *The Continental Crust: Its Composition and Evolution: An Examination of the Geological Record Preserved in Sedimentary Rocks*. Oxford, UK: Blackwell; 1985. 328 pp
- [49] Nesbitt H, Young G, McLennan S, Keays R. Effects of chemical weathering and sorting on the petrogenesis of siliciclastic sediments, with implications for provenance studies. *The Journal of Geology*. 1996;104(5):525-542
- [50] Nesbitt H, Young GM. Formation and diagenesis of weathering profiles. *The Journal of Geology*. 1989;97(2):129-147
- [51] Duzgoren-Aydin N, Aydin A, Malpas J. Re-assessment of chemical weathering indices: Case study on pyroclastic rocks of Hong Kong. *Engineering Geology*. 2002;63(1-2):99-119
- [52] Bock B, McLennan S, Hanson G. Geochemistry and provenance of the middle Ordovician Austin Glen member (Normanskill formation) and the Taconian orogeny in New England. *Sedimentology*. 1998;45(4):635-655
- [53] Elzien S, Farah A, Alhaj A, Mohamed A, Al-Imam O, Hussein A, et al. Geochemistry of Merkhayat Sandstones, Omdurman Formation, Sudan: Implication of depositional environment, provenance and tectonic setting. *International Journal of Geology, Agriculture and Environmental Sciences*. 2014;2(3):10-15
- [54] McLennan SM, Taylor S, Eriksson K. Geochemistry of Archean shales from the Pilbara Supergroup, western Australia. *Geochimica et Cosmochimica Acta*. 1983;47(7):1211-1222
- [55] Mongelli G. Trace elements distribution and mineralogical composition in the < 2- μ m size fraction of shales from the Southern Apennines, Italy. *Mineralogy and Petrology*. 1995;53(1-3):103-114
- [56] Gu XX, Liu JM, Zheng MH, Tang JX, Qi L. Provenance and Tectonic setting of the Proterozoic turbidites in Hunan, South China: Geochemical evidence. *Journal of Sedimentary Research*. 2002;72:393-407
- [57] Nyakairu GW, Koeberl C. Mineralogical and chemical composition and distribution of rare earth elements in clay-rich sediments from Central Uganda. *Geochemical Journal*. 2001;35(1):13-28
- [58] Suttner LJ, Dutta PK. Alluvial sandstone composition and paleoclimate; I, framework mineralogy. *Journal of Sedimentary Research*. 1986;56(3):329-345
- [59] Dickinson WR. Interpreting provenance relations from detrital modes of sandstones. Provenance of Arenites. 1985;148:333-361
- [60] Dickinson WR. Provenance and sediment dispersal in relation to

- paleotectonics and paleogeography of sedimentary basins. In: Kleinspehn KL, Poala C, editors. *New Perspective in Basin Analysis*. New York: Springer; 1988. pp. 3-25
- [61] Etemad-Saeed N, Hosseini-Barzi M, Armstrong-Altrin JS. Petrography and geochemistry of clastic sedimentary rocks as evidences for provenance of the lower Cambrian Lalun formation, Posht-e-badam block, Central Iran. *Journal of African Earth Sciences*. 2011;**61**(2):142-159
- [62] Perri F. Composition, provenance and source weathering of Mesozoic sandstones from Western-Central Mediterranean alpine chains. *Journal of African Earth Sciences*. 2014;**91**:32-43
- [63] Saxena A, Pandit M. Geochemistry of Hindoli group metasediments, SE Aravalli craton, NW India: Implications for palaeoweathering and provenance. *Journal of the Geological Society of India*. 2012;**79**(3):267-278
- [64] Wang B-Q, Wang W, Zhou M-F. Provenance and tectonic setting of the Triassic Yidun group, the Yidun terrane, Tibet. *Geoscience Frontiers*. 2013;**4**(6):765-777
- [65] Xu Y, Du Y, Cawood PA, Yang J. Provenance record of a foreland basin: Detrital zircon U–Pb ages from Devonian strata in the North Qilian Orogenic Belt, China. *Tectonophysics*. 2010;**495**(3-4):337-347
- [66] Zaid SM, Elbadry O, Ramadan F, Mohamed M. Petrography and geochemistry of pharaonic sandstone monuments in Tall San Al Hagr, Al Sharqiya Governorate, Egypt: Implications for provenance and tectonic setting. *Turkish Journal of Earth Sciences*. 2015;**24**(4):344-364
- [67] Crook KAW. Lithogenesis and tectonics: The significance of compositional variation in flysch arenites (greywackes). In: Dott RH, Shaver RH, editors. *Modern and Ancient Geosynclinal Sedimentation*, Special Publication 19. Society of Economic Geologists and Paleontologists; 1974. pp. 304-310
- [68] Hayashi K-I, Fujisawa H, Holland HD, Ohmoto H. Geochemistry of ~ 1.9 Ga sedimentary rocks from northeastern Labrador, Canada. *Geochimica et Cosmochimica Acta*. 1997;**61**(19):4115-4137
- [69] Paikaray S, Banerjee S, Mukherji S. Geochemistry of shales from the Paleoproterozoic to Neoproterozoic Vindhyan Supergroup: Implications on provenance, tectonics and paleoweathering. *Journal of Asian Earth Sciences*. 2008;**32**(1):34-48
- [70] Floyd P, Winchester J, Park R. Geochemistry and tectonic setting of Lewisian clastic metasediments from the early Proterozoic Loch Maree Group of Gairloch, NW Scotland. *Precambrian Research*. 1989;**45**(1-3):203-214
- [71] Hiscott RN. Ophiolitic source rocks for Taconic-age flysch: Trace-element evidence. *Geological Society of America Bulletin*. 1984;**95**(11):1261-1267
- [72] Floyd PA, Leveridge BE. Tectonic environment of the Devonian Gramscatho basin, south Cornwall: Framework mode and geochemical evidence from turbiditic sandstones. *Journal of the Geological Society London*. 1987;**144**:531-542
- [73] Ortiz E, Roser BP. Major and trace element provenance signatures in stream sediments from the Kando river, San'in district, southwest Japan. *Island Arc*. 2006;**15**:223-238

[74] Cullers RL, Berendsen, P. The Provenance and chemical variation of sandstones associated with the mid-continent rift system, USA. *European Journal of Mineralogy*. 1998;**10**:987-1002. DOI: 10.1127/ejm/10/5 /0987

[75] Taylor SR. Geochemistry of Andesites. In: Ahrens LH, editor. *Origin and Distribution of the Elements*. Vol. 30. International Series of Monographs in Natural Philosophy; 2015, 2015. pp. 559-582

[76] Ogbahon O, Olujinmi O. Geochemistry of Maastrichtian clastic sedimentary rocks from Western flank of Anambra Basin, Nigeria: Implications for provenance, tectonic setting, paleoclimate and depositional paleoenvironment. *International Journal of Geosciences*. 2019;**10**:91-118. DOI: 10.4236/ijg.2019.101007

[77] Bhatia MR, Crook KA. Trace element characteristics of graywackes and tectonic setting discrimination of sedimentary basins. *Contributions to Mineralogy and Petrology*. 1986;**92**(2):181-193

[78] Maynard JB, Valloni R, Yu HS. Composition of modern deep-sea sands from arc-related basin. In: Leggett JK, editor. *Trench Forearc Geology: Sedimentation and Tectonics on Modern and Ancient Active Plate Margins*. Vol. 10. Geol.Soc. Lond. Spec. Pub.; 1982. pp. 551-561

Petroleum Geochemistry

Mei Mei and Barry Katz

Abstract

Petroleum geochemistry has entered its second period of growth. The first period, largely associated with conventional oil and gas, occurred in the 70s and 80s when the classic works on source rock characterization, biomarkers, depositional systems, and petroleum generation, including kinetics and basin modeling were the focus. The second period began slightly after the turn of the century as a consequence of the “unconventional resource” revolution and the interest in distressed resources developed, the focus turned to non-hydrocarbon contaminants, new interest in hydrocarbon expulsion and retention, identification of tight rock pay zones, and the development of organic porosity. This chapter will discuss source rock characterization and formation, petroleum generation, expulsion, and retention, correlation among hydrocarbon accumulations and to their source rock(s), and organic porosity.

Keywords: source rock, characterization, deposition, petroleum generation, retention, expulsion, migration, geochemical inversion, correlation, petroleum geochemistry, oil, biomarker, organic porosity

1. Introduction

There are five components to a petroleum system - hydrocarbon charge, reservoir, seal, trap, and overburden [1]. When assessing exploratory risk each of these elements is directly assessed except for overburden, which is incorporated into the different risk elements (e.g., overburden is incorporated into charge through thermal maturity, seal and reservoir through porosity and permeability reduction associated with compaction). The absence of any of these elements brings the chance of exploratory success to zero. Hydrocarbon charge is considered the most important component of any petroleum system evaluation [2] because there is no alternative. In frontier regions and play extensions, post-drill assessments have indicated that the absence of hydrocarbon charge is a disproportionate cause of exploratory failure [3, 4]. Significant improvement in exploration efficiency was reported when geochemistry was taken into consideration as compared to simply assessing opportunities by trap size alone [5]. Fundamental to understanding hydrocarbon charge is clarity on its components which include the source rock presence and quality, generation process (maturation), and alteration (e.g., biodegradation, thermal cracking, phase segregation).

The importance of the organic matter to the formation and accumulation of hydrocarbons was fundamentally established by (1) the identification of porphyrins, a chlorophyll derivative, in shales, coals, and crude oils [6], and (2) the observation

of threshold level of total organic carbon (TOC), approximately 1.5% as a mean of petroliferous basins, rather than the 0.35% of non-petroliferous basins of the Russian Platform [7].

Since these works, and especially over the past five decades, there has been considerable advancement in the foundational understanding of hydrocarbon charge. There have effectively been two major periods of advancement in petroleum geochemistry. The first growth episode occurred, in part, as a result of advances in analytical methods as well as insights into the controls on source rock development and the processes of hydrocarbon generation, expulsion, migration, and alteration. During this period the application of gas chromatography/mass spectrometry (GC/MS) became routine for the assessment of source rock depositional setting and thermal maturity; and basin models became commonplace, requiring an understanding of the kinetics of hydrocarbon generation. The second growth period came with the increase in the importance of self-sourced petroleum systems and tight rock resources. During this recent phase, the focus has been on the identification of landing zones, hydrocarbon expulsion and retention, hydrocarbon cracking, and the development of organic porosity.

This overview discusses the identification, characterization, and formation of hydrocarbon source rocks, the generation process, the characterization of produced fluids including post-accumulation alteration processes, hydrocarbon migration, and establishing genetic relationships among hydrocarbon accumulations, and to their source rock(s), and organic porosity.

2. Source rock identification and characterization

It is important to establish a consistent definition of source rock. A source rock is a rock that contains sufficient quantities of organic matter that after having achieved the appropriate thermal maturity will generate and expel sufficient quantities of hydrocarbons to result in an accumulation. At this point issues of commerciality are not considered because they are dependent on logistics, the presence of prior infrastructure as well as commodity price.

Petroleum source rocks are atypical and are not uniformly distributed either stratigraphically or spatially [8]. The mean value for organic carbon in fine-grain sedimentary is ~0.7 wt.% with a standard deviation of 0.3 wt.% as established using a statistical approach and more than 15,000 fine-grained rock samples worldwide [9]. It was then noted that source rocks should display above-average TOC levels establishing a threshold TOC of 1.00 wt.% (**Figure 1**). However, a review of data from a number of world-class source rocks such as the Kimmeridge Clay (North Sea Basin), Green River Formation (western United States), Pematang Formation (Central Sumatra Basin, Indonesia), Bucomazi Formation (Lower Congo Basin, Angola), Hydria-Hanifa Formation (Saudi Arabia), Maykop Formation (South Caspian Basin, Azerbaijan), Shublik Formation (Alaska) and Kazhdumi Formation (Mesopotamian Foreland Basin, Iran), all contained significant stratigraphic intervals where organic carbon contents exceeded several weight percent organic carbon. This indicates that source rocks, in fact, typically contain TOC levels that significantly exceed the 1.0% wt.% TOC threshold.

It has also been suggested that there is an upper limit for TOC that limits a source rock's effectiveness. It is suggested that at TOC levels of 12 to 15 wt.%, oil is retained within the source rock limiting its effectiveness [10]. This upper limit may also partially explain why most coals do not act as an effective source [11].

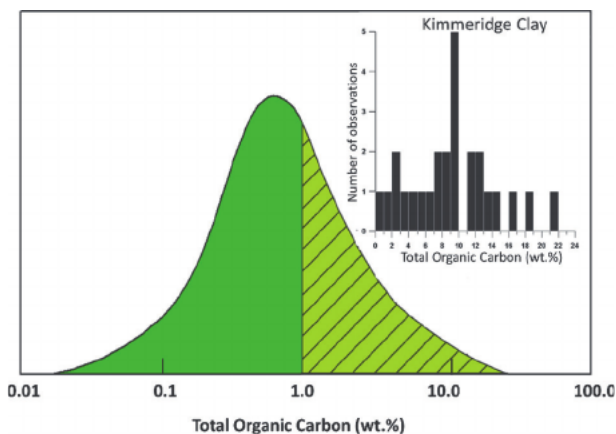


Figure 1. Global distribution of total organic carbon within fine-grain sedimentary rocks. Insert represents the organic carbon measured at the type locality of the Kimmeridge clay (United Kingdom), after Bissada 1982 [9].

It was, however, established early that not all organic matter is the same with respect to hydrocarbon generation and that the assignment of source rock potential based on organic carbon is insufficient. Similar quantities of organic matter can have yields that range over several orders of magnitude depending on the type of organic matter and the thermal maturity (**Figure 2**). This question of yield was approached using the total generation potential (free hydrocarbons + generatable hydrocarbons: S1 + S2) as determined using Rock-Eval pyrolysis. A threshold of 2.5 mg HC/g rock [9] was considered for a possible oil-prone source rock (**Figure 3**). This threshold was established as outlined above for organic carbon. A physical reason for this threshold

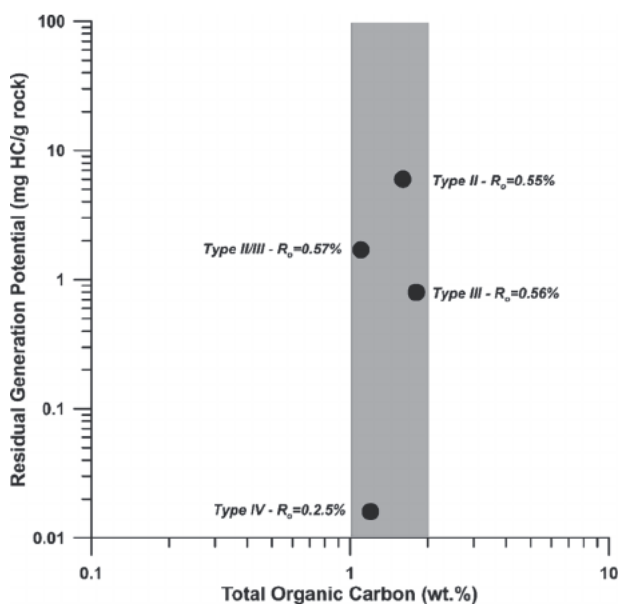


Figure 2. Comparison of residual generation potential (S2) of samples with similar total organic carbon content. Note that for the same TOC, hydrocarbon yield can vary by order of magnitude.

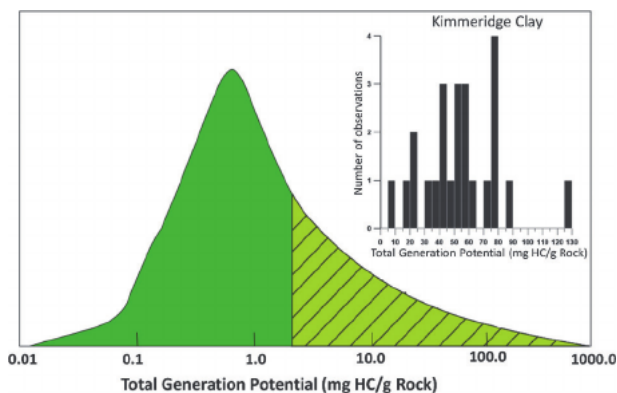


Figure 3. Global distribution of total generation potential of fine-grain samples containing a minimum of 0.5 wt.% TOC. Insert represents the total generation potential measured on samples greater than 0.5 wt.% TOC at the type locality of the Kimmeridge clay (United Kingdom), after [9].

also appears present. This reported threshold is consistent with the previously reported minimum of 825–850 ppm hydrocarbons thought to be required for expulsion to occur [10]. A rock having a total generation potential of ~ 2.5 mg HC/g rock as it approaches the main stage of hydrocarbon generation approaches a free hydrocarbon content consistent with this threshold. Thresholds for possible gas-prone source rocks are less well-defined, in part, because of their different expulsion mechanisms [12]. Oil expulsion requires that the pore network becomes saturated, and the rock becomes over-pressured. In contrast, gas expulsion can occur through diffusion which simply requires a concentration gradient once the sorption capacity of the source is achieved [13] or in solution within a liquid hydrocarbon phase.

The atomic H/C and O/C ratios were used to define three primary kerogen types as an explanation for the observed differences in hydrocarbon yield and product character [14]. This van Krevelen diagram has been modified to provide more specific guidance on product characterization (i.e., oil yield) [15] and visualized here in **Figure 4**.

Type I kerogen was defined using the Green River Formation and algal kerogens and has the greatest hydrocarbon yield for a given mass resulting from the abundance of hydrogen. When mature type I kerogen will yield principally oil with a lesser amount of gas. The kerogen structure contains abundant long-chain hydrocarbons [16]. This type of kerogen is principally derived from algal material and often appears associated with marine and lacustrine carbonate depositional systems.

Type II kerogen displays lower atomic H/C and higher atomic O/C ratios than Type I organic matter. It produces both oil and gas upon maturation and was defined using the Schistes Carton Formation (lower Toarcian, Paris Basin, France) and Silurian shales of North Africa. The kerogen structure is much more diverse than Type I kerogen due to the diversity of the organic material that led to its development, which includes algal material, plant cuticle, spores, pollen, and resin, which may be microbially reworked. Although often considered to represent a marine depositional system, such kerogen was found to also dominate in siliciclastic-dominated lacustrine systems, such as the Pematang Formation of Central Sumatra.

As implied, the difference in organic matter type between a clay-rich mudstone and a carbonate source rock rest with one of the foundational differences in the development of these two rock types. Carbonate rocks are generally considered to be autochthonous with both the mineral and organic matter forming at or very near to

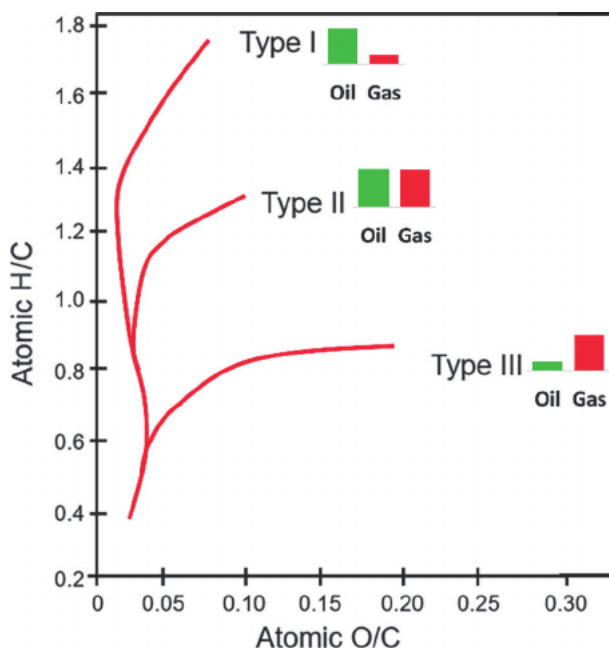


Figure 4. Conventional van Krevelen diagram based on the atomic H/C and O/C ratios. Relative oil and gas yields have been added.

the depositional site. In contrast, clay-rich mudstones are derived from both inorganic and organic material that is transported to their depositional site, reflecting the provenance of the drainage basin, with the lesser autochthonous contribution.

A subset of Type II kerogen is Type II-S, which contains greater than 6% organic sulfur [17]. This differentiation is important because the C-S bond is weaker than the C-C bond and generation proceeds at lower levels of thermal maturity, producing products with greater amounts of asphaltenes and resins.

Type III kerogen was defined using Cretaceous shales from the Douala and Western Canadian Sedimentary basins. It has lower H/C and more elevated O/C ratios than Type II kerogen. It produces the lowest amounts of hydrocarbons per unit mass and yields principally gas. The kerogen structure is envisioned to be dominated by interconnected aromatic rings, with shorter chain hydrocarbon elements. Although this type of organic matter is often associated with vitrinite (a wood derivative) it may also be derived through the poor preservation (oxidation) of marine organic matter.

As a consequence of thermal maturation and the generation of products including organic acids and hydrocarbons both the atomic H/C and O/C ratios decrease. In the case of Type I kerogen, there is a rapid decrease in the atomic H/C ratio and a modest decrease in O/C ratio with increasing thermal maturation. In contrast, there is a rapid decrease in the atomic O/C ratio and a modest decrease in the atomic H/C ratio for Type III kerogen. These changes result in an inability to differentiate among the different kerogen types using their elemental composition at more advanced levels of thermal maturity and alternative means are required for such kerogens.

Subsequently, a fourth kerogen type has been defined, which represents residual organic matter [18]. It displays very low atomic H/C ratios and highly varied atomic O/C ratios. This material is largely inert and incapable of yielding any significant

amount of hydrocarbons. It is dominated by inertinite. This material commonly forms through prolonged transport, very slow sedimentation rates leading to long exposure times, or forest fires.

The aforementioned approach to organic matter characterization requires the isolation of kerogen from the rock matrix. This is a time-consuming process that utilizes hydrochloric and hydrofluoric acids as well as requiring relatively large sample volumes. An alternative was proposed that was rapid and required only grinding as sample preparation and did not require large sample volumes. This method was Rock-Eval pyrolysis, where the sample was heated in an inert atmosphere. Two of the measured parameters are used to calculate the hydrogen index ($S_2 \cdot 100 / \text{TOC}$) and the oxygen index ($S_3 \cdot 100 / \text{TOC}$, where S_3 represents the CO_2 yield) are substituted for the atomic H/C and O/C ratios, respectively (Figure 5).

Although these indices have become routinely accepted for kerogen characterization there are some limitations that are known to exist and should be considered when interpreting the data. For samples with very high generation potentials, the use of the standard sample size may result in the saturation of the flame ionization detector, which produces an apparent reduction in S_2 yield and consequently the hydrogen index making the sample appear more gas-prone than would be implied if elemental analysis on isolated kerogen was used. In addition, several studies have shown that there are mineral matrix effects. These effects are especially notable for samples with lower organic carbon contents. It is suggested that for samples with less than 2 wt.% TOC hydrocarbons are retained by the rock matrix, especially in clay-rich samples. This retention reduces the apparent generation potential and the derived hydrogen index [19]. It was also observed that the oxygen index was sensitive to the presence of carbonate minerals, especially siderite. These effects cause the organic matter to appear more gas-prone than in kerogen isolates. Alternative means of correcting the oxygen index for the presence of siderite-derived CO_2 have been proposed [20, 21], however, these approaches alter the value proposition, which was a rapid and simple means to assess generation potential, organic matter type, and thermal maturity.

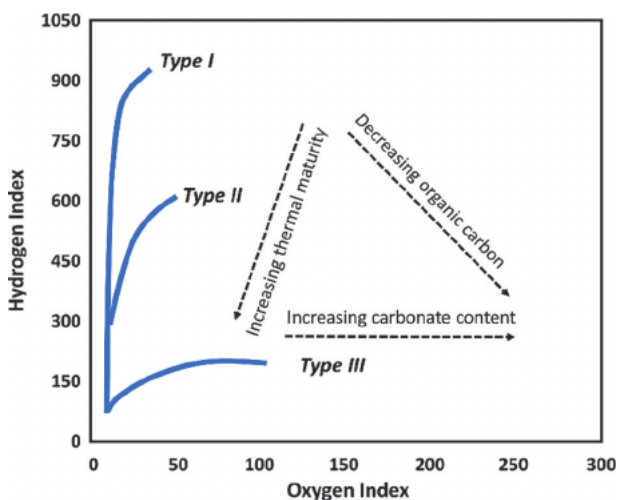


Figure 5. Modified van Krevelen diagram based on the rock-Eval parameters the hydrogen and oxygen indices. Arrows represent changes in parameters as a function of increasing thermal maturity, increasing carbonate (especially siderite) content, and decreasing organic carbon.

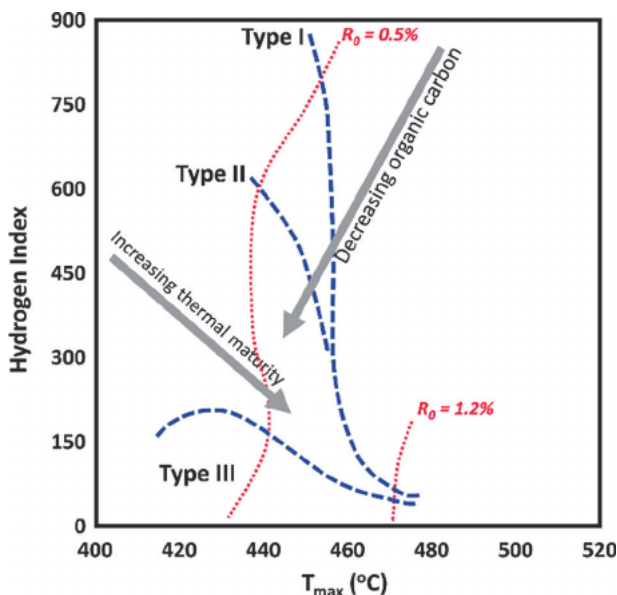


Figure 6. Alternate means of characterizing organic matter utilizing the hydrogen index and T_{max} . Arrows represent changes in parameters as a function of increasing thermal maturity and decreasing organic carbon.

An alternative approach to organic matter characterization without the possible oxygen index complication relies on the relationship between the hydrogen index and T_{max} (Figure 6). This approach is still limited at lower TOC values.

Alternative pyrolysis approaches have been developed that provide additional information. The first adds gas chromatography to the pyrolysis unit and is known as Py-GC. This analytical approach provides a more detailed understanding of the products generated beyond a simple assessment of oil- and gas-proneness [22, 23]. A chromatogram of isolated kerogen through Py-GC with vented free hydrocarbons below 320°C (equivalent to Rock-Eval S1 peak) and then pyrolyzed up to 600°C is produced from what essentially was the Rock-Eval S2 peak (Figure 7). These chromatograms provide information on such geochemical properties as waxiness, relative abundance of naphthenes, and aromatic compounds. The relative abundance of C_1 - C_5 , C_6 - C_{14} , and C_{15}^+ in the Py-GC was used to assess the oil and gas-proneness of different types of kerogens [23].

Another thermal extraction-pyrolysis innovation has been developed, which has a more complex temperature ramp and is designed to better characterize the free hydrocarbons present in the rock, where the free hydrocarbons are broken down into four fractions (thermal extraction <350°C), representing C_4 - C_5 , C_6 - C_{10} , C_{11} - C_{19} , and C_{20} - C_{36} (the four oil fractions in Figure 8). The K-1 peak in Figure 8 represents pyrolysis of kerogen at 350–600°C. The Petroleum Assessment Method (PAM) was developed to better assess the nature of the hydrocarbons present in self-sourced petroleum systems [24].

Part of the assessment of the validity of a geochemical assessment is a determination as to whether a sample has been stained (natural processes) or contaminated (anthropogenic processes). This assessment is based on the relationships between the abundance of free hydrocarbons (S1) and the total organic carbon content (Figure 9), and the relationship between T_{max} (temperature of maximum hydrocarbon yield)

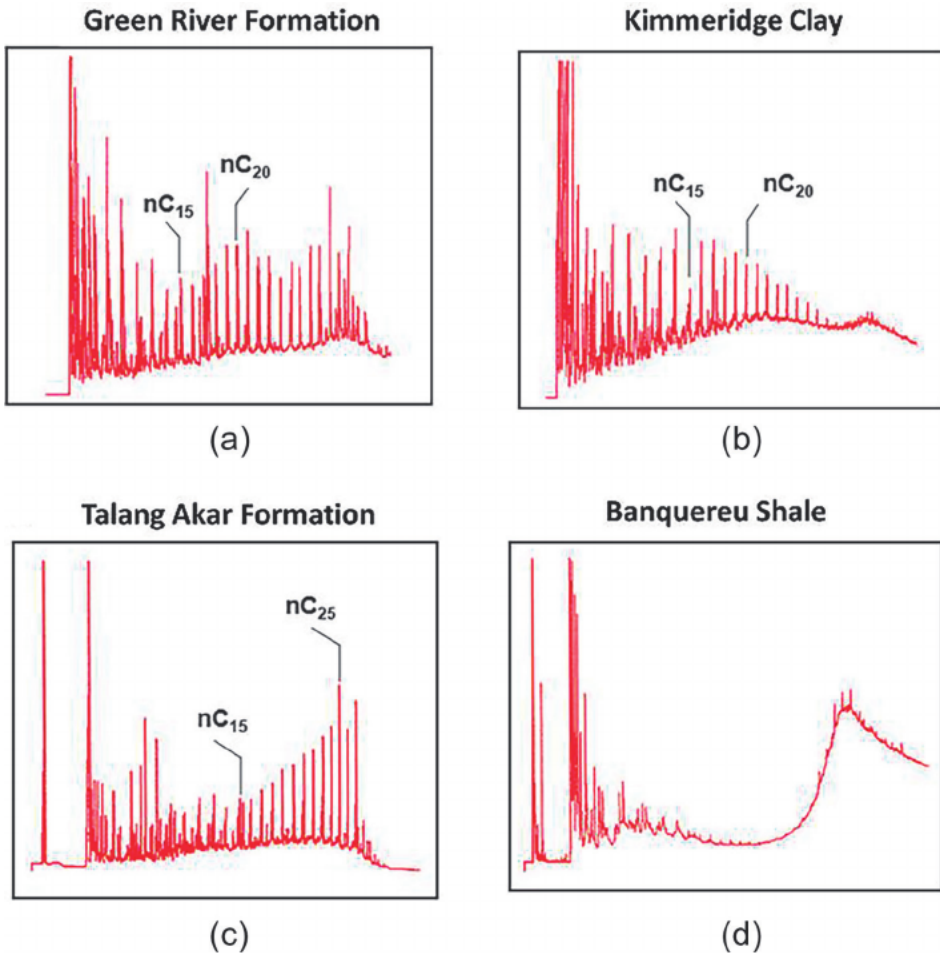


Figure 7. Pyrolysis-gas chromatograms of A - Green River Formation (Utah, United States); B - Kimmeridge Clay (United Kingdom); C - Talang Akar Formation (Indonesia); D - Banquereu Shale (Atlantic Canada).

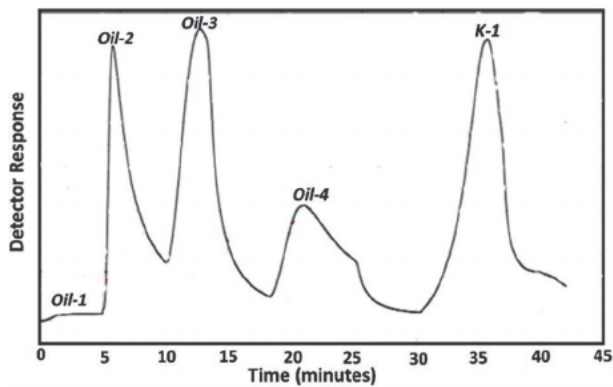


Figure 8. Representative PAM pyrolysis of Devonian Shale (Western Canadian Basin).

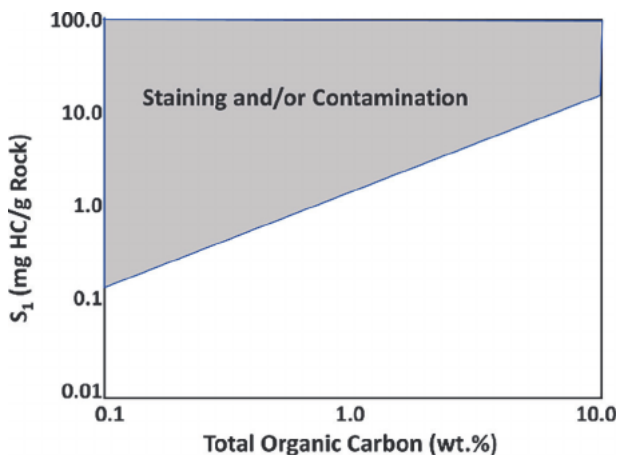


Figure 9.
 The relationship between total organic carbon and S_1 yield is used to define the presence of staining or contamination.

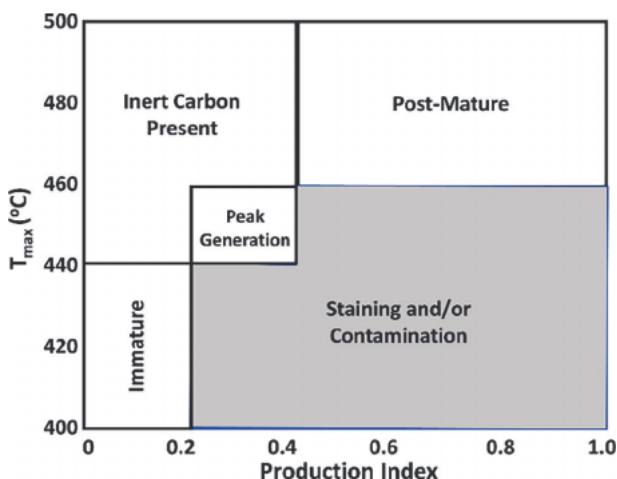


Figure 10.
 The relationship between T_{max} and the production index is used to define the presence of staining or contamination.

and the transformation ratio ($S_1/(S_1 + S_2)$); **Figure 10**). These assessments do not differentiate between natural and anthropogenic hydrocarbons additional analyses would be needed for this differentiation.

The $S_1 \cdot 100 / \text{TOC}$ (OSI; oil saturation index) ratio was proposed for identifying potentially productive zones, with values greater than 100 mg HC/g TOC being zones of interest [25]. This approach is essentially limited, however, to wells not drilled with an oil-based drilling fluid system.

There has been some recent work that has also led to questions on the validity of source rock assessment and characterization when organic-based drilling fluids are used. Organic-based drilling fluids are becoming more commonly used because of their greater stability at higher temperatures and improved hole stability when shales are water-sensitive [26]. It was reported that the often-used solvent pretreatment of

contaminated samples does not permit an assessment of the original *in situ* characters of the rock [27]. The reported organic carbon, generation potential, hydrogen, and oxygen indices were all impacted by the contamination by the drilling fluid and the solvent extraction of the contaminated samples.

3. Source rock depositional controls

As a consequence of the uniqueness of petroleum source rocks, it has been generally accepted that they form under somewhat distinct sedimentary conditions. It was suggested that nearly half of the known source rock systems lack modern analogs (e.g., anoxic epeiric seaways and anoxic oceans [28]). In general, there have been three principal schools of thought on source rock deposition: 1) enhanced organic preservation, often associated with anoxia; 2) enhanced primary productivity, often associated with oceanic upwelling or riverine transport of nutrients; and 3) sedimentation rate, often associated with either rapid removal of the sediment from the various microbial zones or through the concentration of organic matter through a lack of dilution by sediment (i.e., a condensed section). Arguments have been presented to support each as a stand-alone model.

The enhanced preservation model is largely based on the argument that anoxic environments, where oxygen consumption exceeds supply, favored preservation [29]. Such settings are associated with stratification, reduced circulation, water body isolation, or estuarine flow. The primary argument for this was the presumed relative inefficiency of anaerobic processes, which slows decomposition [30]. However, activity levels of anoxic and oxic microbial communities have been shown to display similarities [31]. It appears that the absence of meiobenthos and macrobenthos may be more important than microbial rates because they are more efficient consumers of organic matter compared to microbes [32] and also provide a means to irrigate the sediment through bioturbation [33]. Similarly, the absence of alternative oxidizers such as sulfates also leads to more efficient preservation. This limits the source rock potential of evaporitic settings once gypsum precipitation is initiated, and sulfate reduction may occur. Another argument for enhanced preservation was associated with settling or exposure time within the oxic portion of the water column. It was observed that there were order of magnitude reduction in organic matter preservation efficiency from the shelf to the central ocean basin as a result of exposure time [34]. Further reports suggest that settling time could be reduced through the pelletization process, where the increase in particle size and the incorporation of mineral matter increased the settling rate with added protection coming from the mucilaginous cover that the pellets have after passing through the digestive system [35]. It should be noted, however, that stratification may limit nutrient renewal and lead to oligotrophic conditions, suggesting limited autochthonous input and that under such circumstances terrestrial input may be favored.

The primary productivity model was based on the general concept that elevated amounts of organic matter would be incorporated into the sedimentary record if productivity was high [36]. Higher levels of productivity are associated with regions of nutrient renewal such as coastal upwelling, seasonal water body turnover (which is especially common in lake systems and temperate water bodies), as well as riverine input. Numerous publications attempted to highlight areas of high productivity through time through paleoclimate and paleocirculation modeling (e.g., see [37]). In the modern ocean, there are numerous regions of high productivity, however, that

lack significant organic carbon in the sediment. This is clearly documented in the Southern Ocean where an intense upwelling system has been established but is also a region where freshly-oxygenated bottom waters are present. Here the sediment appears dominated by siliceous tests and TOC is minimal, (typically below 1.0 wt.%) as a result of organic carbon's brief residence time of 15 to 150 years [38]. Attempts to correlate regions of modeled high productivity have had limited success. In part, this is because of factors beyond nutrient availability that influence productivity such as turbidity. For example, the suspended load of the Mississippi River results in limited light penetration at the river's mouth. The region of elevated productivity is thus shifted further offshore to where the sediment has salted-out.

The discussion on the role of sedimentation rate follows two paths. Early arguments suggested greater potential for organic matter preservation when sedimentation rate was high [39]. It was suggested that rapid sedimentation would reduce the time spent within the various microbial zones ranging from oxidation through sulfate reduction and eventually methanogenesis. This concept appears supported by the positive correlation between sedimentation rate and total organic carbon [40, 41]. The specific relationship appears to differ among lithologies. However, when the sedimentation rate exceeds approximately 20 m/MY, the organic carbon content begins to decrease as a result of dilution by sediment. An increase in carbon content with an elevated sedimentation rate can only occur if the level of primary productivity increases. In contrast, it's suggested that source rocks are associated with condensed sections, where dilution by sedimentary material has been minimized. An often-cited example of a condensed section source rock is the Shublik Formation in Alaska [42], which also appears to be associated with elevated productivity as suggested by the presence of phosphorites [43]. Not all sediment starved areas develop oil-prone source rocks. It was reported that for a condensed section deposited under oxic conditions such as the Upper Jurassic/Lower Cretaceous of SE France the section is bioturbated and TOC values are less than 0.25% [44]. The influence of sedimentation rate was also noted as part of the preservation model, where more oil-prone material was associated with higher sedimentation rates and inert material was preserved with slow sedimentation rates [29].

In addition to the three working models, it is also important to understand that the reactivity of organic matter is not uniform. It was noted that under oxic conditions planktonic material would degrade more rapidly than the remnants of vascular plants because of chemical differences [38]. Algal amorphous material was easier

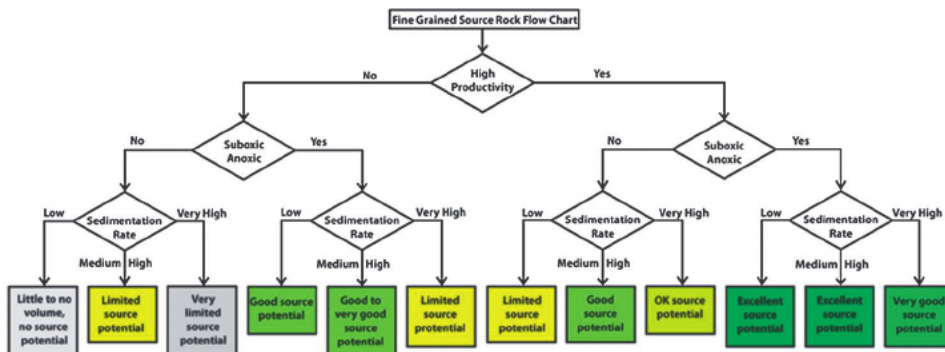


Figure 11. Workflow to assess the probability of source rock presence and quality based on primary productivity, preservation potential, and sedimentation rate [46].

to decompose than structured organic matter [45]. This was, in part, a result of the greater surface area of amorphous organic material.

It was reported that the three single factor models proposed were insufficient and that a more robust model requires the integration of the three taking into consideration the interplay among them (**Figure 11**, [46]).

4. Petroleum generation, retention, and expulsion

Organic matter in source rocks are composed of extractable organic matter (EOM) - bitumen and insoluble organic matter including oil/gas prone kerogen and inert carbon. Under sufficient thermal stress, petroleum is formed incrementally from the decomposition of kerogen and secondary cracking of generated petroleum molecules. This process can be simulated as a series of parallel first-order reactions following the Arrhenius Law. A simple reaction of an initial reactant X with mass x generating a product Y with mass y can be represented by:



$$\frac{\partial y}{\partial t} = -\frac{\partial x}{\partial t} = kx \quad (1)$$

$$k = Ae^{-E/RT} \quad (2)$$

where t is the reaction time, k is the reaction rate, A is the frequency factor, E is the activation energy, and R is the universal gas constant $8.314 \text{ J}\cdot\text{K}^{-1}\cdot\text{mol}^{-1}$.

Laboratory anhydrous and hydrous pyrolysis are used to simulate the processes of natural petroleum generation, retention, and expulsion [23, 47–53]. Burnham systematically documented integration of kinetics and pyrolysis methods to simulate petroleum generation reactions [54]. As shown in **Figure 12**, it is observed that (1) Type I kerogen generates petroleum over a narrower oil window to decompose a more uniform composition; (2) Type II-S kerogen enters oil-window earlier with lower reaction activation energies to breakdown weaker bonds; in contrast to (3) Type II and Type III kerogens that react with an extended and elevated range of reaction activation energies, respectively, to breakdown mixed kerogens with more complex structures.

In most cases, source rocks contain mixed kerogens. Compositional kinetics was developed to simulate a series of reactions from mixed types of kerogens to form complex petroleum compositions and the secondary cracking of products [56–58].

Figure 13 shows an example of petroleum primary generation and secondary cracking reactions. **Figure 14** shows how these reactions work in a closed system through modeling calibrated with Vaca Muerta Formation data [56]. It shows that (1) asphaltenes and NSO-bearing polar components are formed in the early oil window at 0.5–0.7% R_o , (2) followed by secondary cracking of these components and continuous cracking of kerogens forming saturated and aromatic hydrocarbons in the main oil window at 0.7–1.3% R_o , by then, asphaltenes, NSO-bearing polar components, and large (C_{15+}) aromatic compounds are fully cracked; (3) Beyond 1.3% R_o , large (C_{15+}) saturated and small (C_6 - C_{14}) aromatic hydrocarbons start cracking, forming light oils (dominant light saturates) and gas hydrocarbons, (4) until 2% R_o where all liquid components are fully cracked to gas and eventually forming dry gas - methane.

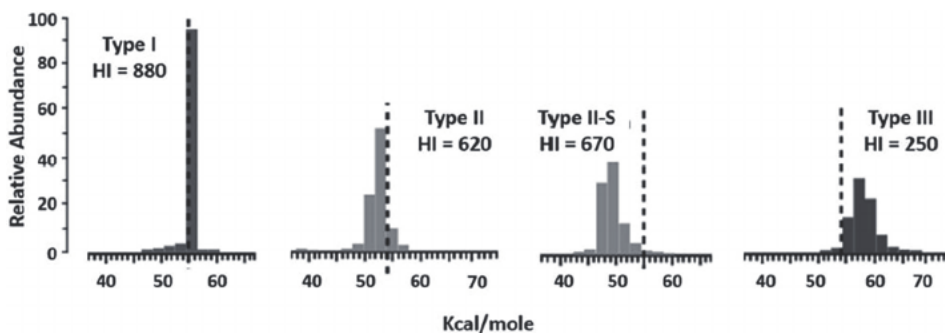


Figure 12.
 Comparison of activation energy distributions for hydrocarbon generation of four representative different kerogen types (modified after [55]).

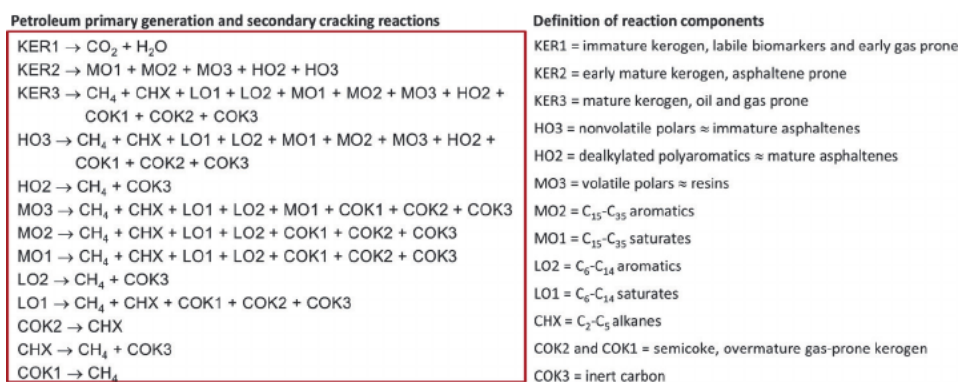


Figure 13.
 Schematic reaction mechanism of petroleum primary generation and secondary cracking with 17 species (modified after [56]).

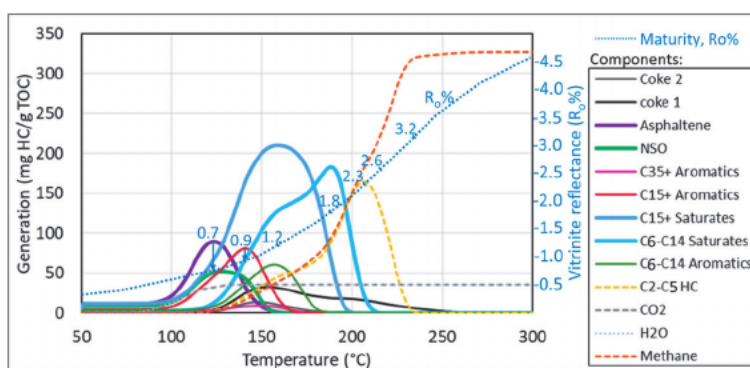


Figure 14.
 Simulation of petroleum primary generation and secondary cracking in a closed system using calibrated compositional kinetics based on Vaca Muerta Formation data (adapted from [56]).

Natural petroleum systems in the subsurface are semi-closed systems with not only petroleum generation/cracking reactions, but also retention and expulsion. Kinetics and retention models are incorporated into basin modeling together with

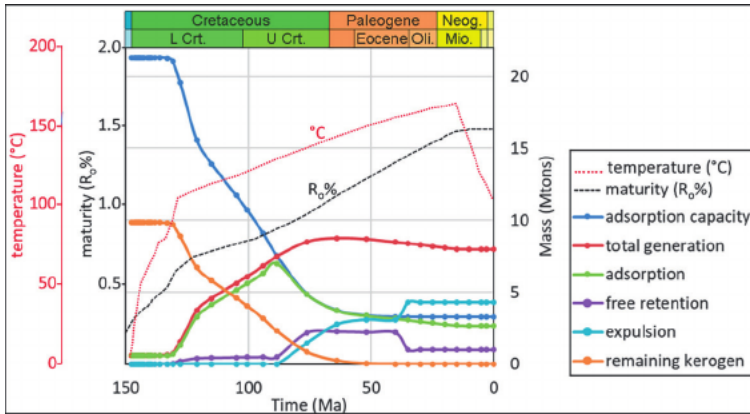


Figure 15. Basin model showing petroleum generation, retention, and expulsion through time and temperature changes, a Vaca Muerta Formation example (adapted from Mei [56]).

other necessary geochemical and geological inputs to simulate and quantify petroleum generation, retention, and expulsion in subsurface [56, 59, 60]. **Figure 15** shows an example of petroleum generation, retention, and expulsion of Vaca Muerta petroleum system through time and temperature.

Organic matter and clay minerals in source rock have a high sorption capacity for petroleum [61–63]. As shown in **Figure 15** using the Vaca Muerta Formation as an example, the initially high sorption capacity decreases through petroleum generation and sorption with increasing time and temperature. Until the quantity of generated petroleum exceeds source rock sorption capacity, major petroleum expulsion occurs at about 0.85–1%R_o and 120–140°C. This process associates with increasing pore pressure, permeability, and organic porosity. The sorbed components can be further cracked with elevated temperature over time. When thermal maturity is increased to above 1.3%R_o and 160°C, intensive petroleum cracking creates volume expansion and excess pore pressure, which in turn induces rock fracturing and the second stage of major expulsion. Tectonic uplift decreases pressure and temperature, which temporarily stops petroleum generation and expulsion. Continuous burial can result in further cracking and expulsion.

5. Petroleum migration

Within this study, migration is considered the movement of hydrocarbons within a carrier system once they have been expelled from the source rock. This includes the initial movement to the trap as well as any remigration that may occur following the initial accumulation as a result of tectonic movements or the subsequent addition of hydrocarbons.

Hydrocarbon migration is considered the least understood aspect of the petroleum system. This, in part, is a result of our limited ability to observe migration and that we typically see only the results of migration (i.e., the position of the accumulations [64]). Migration is driven by buoyancy, which is controlled by density differences between the migrating hydrocarbons and pore fluids, largely controlled by brine salinity and API gravity [65]. Hydrocarbon migration can occur laterally, vertically, or a combination of the two.

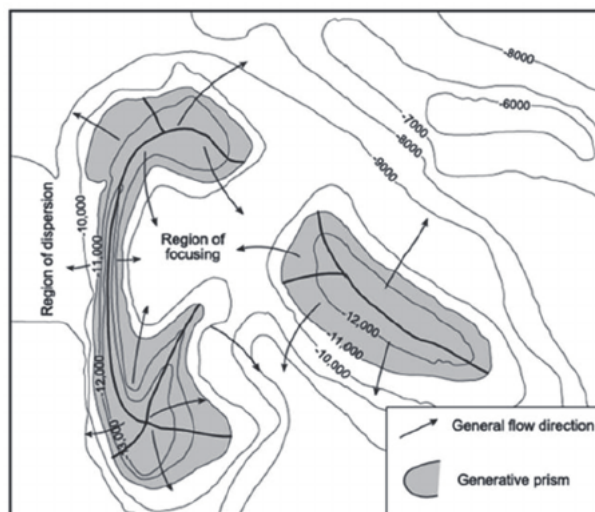


Figure 16. Structural patterns establish general hydrocarbon migration patterns. Regions of focusing and dispersion are identified.

Lateral migration occurs in stratigraphic proximity to the source, but over significant distances potentially exceeding 100 km, with accumulations developing beyond the limits of the generative kitchen. A single stratigraphic unit may contain multiple accumulations. The flow paths or migration patterns are, in general, controlled by structural patterns, where hydrocarbons may be focused or dispersed as shown in **Figure 16**. Regions of focus are preferred sites for exploration, while dispersive regions are to be avoided [66]. Flow paths are established at the base of low permeability layers. These flow patterns may change through time as a consequence of structural evolution. Carriers may include permeable beds, fracture networks, and certain unconformity surfaces. Depending on the availability of hydrocarbons an examination of structural patterns may also aid in the identification of migration shadows, as well as opportunities for fill and spill establishing up-dip hydrocarbon charge potential. These migration patterns can be altered by strong water movement and the distribution, character (including variability in permeability), and extent of the carrier beds. Sheet sands provide potentially the longest and least controlled migration patterns, whereas isolated reef bodies such as those of the Michigan Basin provide no continuity and are not effective carriers.

Vertical migration provides a means of transferring fluids across stratigraphic horizons. Accumulations develop above or near the active source. Stacked reservoirs with a common source exist. Surface seepage is common. Although the lateral movement in such systems can be limited, vertical fluid movement can be quite significant, on the order of several kilometers [67, 68].

There are examples where multiple generative kitchens can focus on a common trap. In some cases, these oils may remain distinct, and in others where the oils may mix. Situations exist where sealing faults are present within a structure and no mixing occurs. Such is the case in the Minas field (Central Sumatra, Indonesia) where distinct oils are present on the two sides of the Main Minus Fault Zone.

Migration may be episodic, potentially as a result of fault movement as in the case of deep-water Nigeria, where unaltered oil is introduced into a shallow reservoir

where the oil pool has undergone biodegradation [69] or largely continuous and potentially in near real time such as at Eugene 330 Field in Gulf of Mexico [70].

Remigration or dysmigration may result in the loss of hydrocarbons, the repositioning of the remaining hydrocarbons, and changes in oil character (e.g., phase segregation). Remigration may take place as a result of fault movement or structural inversion.

6. Geochemical inversion and correlation

Integrating geochemical inversion, oil to oil and oil to source rock correlations, basin modeling, and regional geology is important to understanding the petroleum system and significantly reducing the risks of petroleum exploration [71, 72]. For clarification, geochemical inversion entails utilizing diagnostic molecular and isotopic characteristics of petroleum collected from seeps, various types of rock samples, and produced fluids to infer (1) the organic-matter type and thermal maturity of the source rock as well as that of the oil or gas at time of generation [72]; (2) the depositional environment (salinity, redox conditions, and lithology) of the source beds [73]; (3) the age of the likely source rocks [74]; (4) accumulation history; and (5) secondary alteration such as biodegradation [75] and migration after expulsion from the source rocks with anomalous or mixing signatures [76–78]. In addition, petroleum to source correlation entails comparison of the geochemical markers in source-rock candidates with equivalent markers in the petroleum to better understand oil origin and migration history. Furthermore, basin modeling entails analyzing the geological and thermal settings for a stratigraphic sequence in a basin to understand the burial and thermal histories of the source bed, and to deduce the probable occurrence of petroleum generation, expulsion, and migration relative to reservoir deposition and trap formation.

To understand whether an oil accumulation is charged from the direct contact source rock or migration from deeper or downdip kitchens, it is critical to understand source rock maturity based on maturity indicators in source rock and calibrated basin modeling. Maturity indicators such as vitrinite reflectance (R_o) and spore-color thermal alteration index (TAI) are commonly measured using microscopic technologies. Uncertainties include (1) indicators that are based on terrigenous organic matter that are commonly deposited in fluvial deltaic environments or transported to marginal marine settings in post-Silurian age. However, oils generated from aquatic kerogen (amorphous alginate and exinite) in marine or lacustrine environments or older source rocks contain limited or no higher plant materials such as vitrinites to measure R_o , or spores and pollen to measure TAI. When bitumen exists, bitumen reflectance can be used to estimate vitrinite reflectance [79, 80], although discrepancies in derived vitrinite reflectance are common using different algorithms. (2) Recycled vitrinite may not experience the same thermal history as the primary kerogen. (3) Even with the same thermal history, different types of kerogen may achieve different extents of maturity via different kinetics. Therefore, it is important to develop direct measurements of thermal maturity for aquatic kerogens and correlate them to the thermal maturity standard R_o [81]. Transmission light spectroscopy and Raman spectroscopy show promising results [82].

In addition, to infer oil origin, identify oil families (oil to oil correlation), and correlate oil with possible source rocks, it is important to analyze and interpret the chemical compositions of oil and bitumen in source rock(s) when available. Crude oil and bitumen are complex mixtures of organic compounds consisting of four major group

types: saturated hydrocarbons, aromatic hydrocarbons, resins, and asphaltenes (SARA). Among these compounds are numerous trace components such as biomarkers that are organic compounds derived from ancient living organisms (algae, bacteria, and plants), that can provide source-diagnostic information and relatively resistant to alteration.

To analyze biomarkers in oil and rock samples, SARA group-type separation is used to prepare saturated and aromatic fractions of oils for GC-MS analysis. This sample preparation is required to avoid coelution interference and enhance the sensitivity and accuracy of the analytical method [83–86]. Recent advancements using modern analytical technologies such as GC tandem triple quadrupole mass spectrometry (GC-QQQ-MS/MS) and 2D-Gas-chromatography/time of flight mass spectrometry (GC × GC-TOF) with enhanced analytical resolution enabled simultaneous analysis of diverse trace components in whole oil and minimized volatile loss during sample preparation [87–89]. Sometimes, many of the biomarkers are absent or occur at much-reduced abundance as a result of alteration. New proxies using alteration-resistant compounds such as diamondoids have been investigated [90–92]. Diamondoids are saturated hydrocarbons with cage-like (bridged cyclohexane) structures. They are derived from the structural rearrangements of saturated hydrocarbons catalyzed by Lewis acids (chemical species with an empty orbital that is capable of accepting an electron pair; commonly associated with clay minerals and thermal cracking). Diamondoids are resistant to many alteration processes, particularly stable at higher maturity, and can be used to indicate advanced thermal maturity and cracking.

The analytical results of relative abundances of chemical compositions such as biomarker ratios are commonly used as geochemical indices. The concept, history, and guidelines for geochemical data interpretations with case studies using global samples were systematically documented in the Biomarker Guide [93]. In brief, alteration, source facies, and maturity are interpreted using multiple intact and diagnostic signatures. These interpretations can then be compared with source rock data in a geologic context. **Figure 17** shows examples of geochemical interpretations using GC-MS m/z 191 traces of intact terpanes. **Figure 17(a)** and **(b)** are two examples of carbonate sourced oil. **Figure 17(a)** is a low maturity oil from the Triassic carbonate platform in Sicily with characteristics of (1) abundant extended homohopane H35 equal to or more than H34 indicating anoxic water bottom, (2) presence of abundant gammacerane (G) indicating stratified water column which is commonly associated with hypersalinity from carbonate or evaporative settings, and (3) abundant C24 tetracyclic terpane relative to C26 tricyclic terpane indicating a carbonate or evaporite depositional environment. **Figure 17(b)** is a high maturity oil from a Late Jurassic to Early Cretaceous carbonate source rock from Guatemala with characteristics of (1) abundant norhopane (H29) relative to hopane (H30) and (2) relatively higher amount of Ts than Ts indicating carbonate depositional environment. In contrast, **Figure 17(c)** shows a Tertiary oil from the Niger Delta (similar examples see [94]). Specifically, the presence of abundant oleanane (O) indicates terrigenous organic matter inputs in post-Jurassic age and is most associated with Tertiary age, and the stair-step pattern of homohopanes with relatively lower abundance of H35 than H34 indicates a suboxic environment commonly associated with clastic facies. The interpretation above is an example of geochemical inversion. In addition, oil-oil and oil-source correlation are to compare the similarities and differences of geochemical characteristics of oil and source rock. To confirm a genetic relationship, multiple available geochemical characteristics (biomarkers such as terpanes, steranes, and isoprenoids, bulk components such as alkanes and aromatics, and others like elements, isotope ratios, and API gravity, etc.) should be interpreted comprehensively in the context of reasonable geological scenarios.

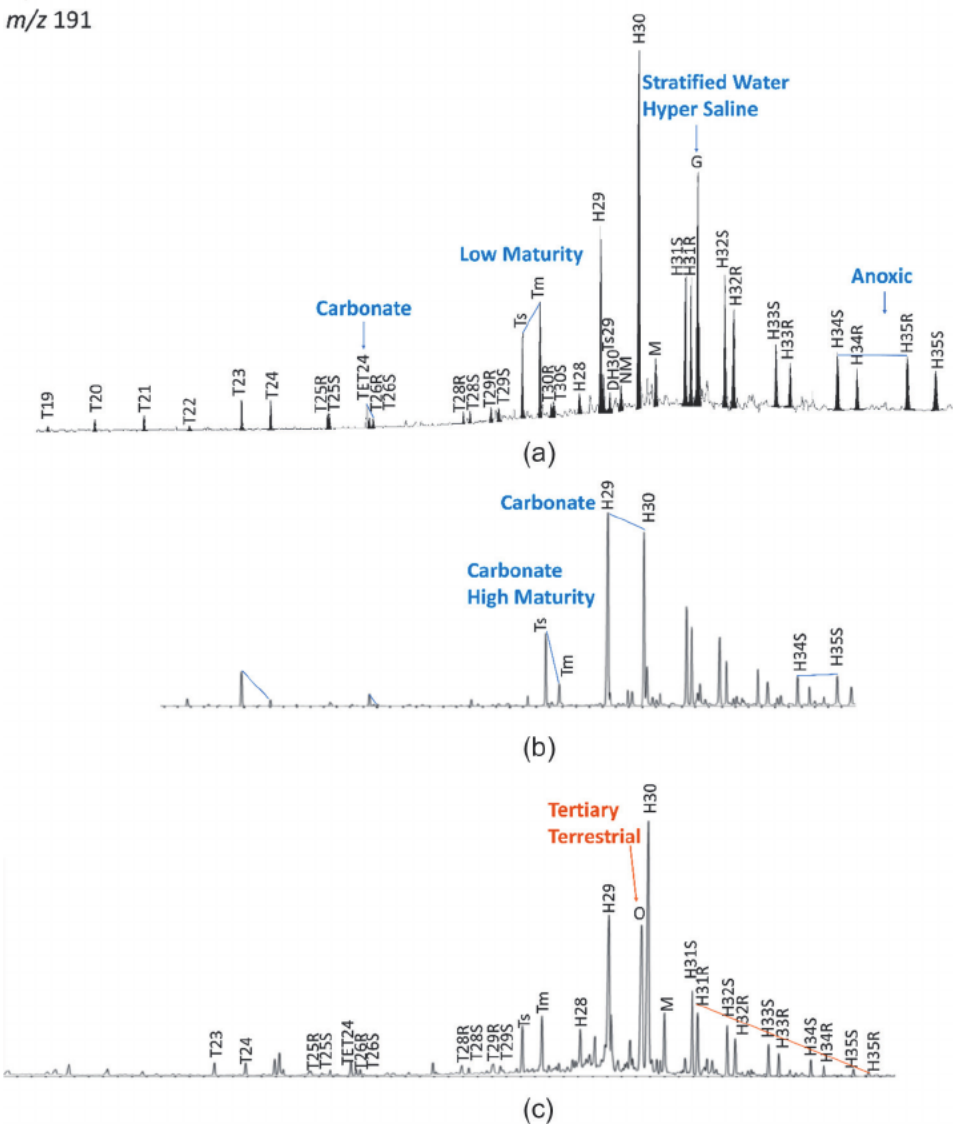


Figure 17. Examples of GC-MS m/z 191 traces show different oil biomarker (terpane) distribution patterns and indications for different sources (Triassic carbonate oil data is from [89], Jurassic-Cretaceous carbonate oil and Tertiary deltaic oil are from Geomark database).

7. Organic porosity

With respect to shale, resource plays geochemistry plays a role in establishing source rock potential as well as reservoir potential. Within unconventional reservoirs three porosity types have been characterized: 1) interparticle pores; 2) intraparticle pores; and 3) organic pores. The importance of pore type varies among the different shale plays [95]. Organic porosity is the porosity that has developed or exists with the kerogen, bitumen, and/or pyrobitumen present within the shale play. Organic porosity within plays such as the Barnett Shale (Forth Worth Basin, Texas) and the Longmaxi

Formation (Sichuan Basin, China) provides important storage capacity. These pores, because of their small size (often less than 1 μm), are potentially more important for gas systems [96] although organic pores may play a limited role in some oil plays.

Organic pores may be primary, associated with the kerogen's initial structure, or secondary, where it is hosted in bitumen or pyrobitumen as a function of generation and alteration. The assignment to primary and secondary pores may be complicated because the visual differentiation between the kerogen and bitumen is not simple. The means to differentiate between kerogen and bitumen pores were proposed in the literature [97, 98].

Organic pores display multiple morphologies, bubbly, spongy, or fracture/crack-based pores as shown in **Figure 18** [99]. These forms have different formation mechanisms and associations. For example, the bubbly pore type seems to be largely associated with the oil window and maybe artifacts of water droplets [100]. While cracks and fractures may form through devolatilization of solid bitumen [101] or volume changes [102]. The distribution of pores further suggests that the nature of the organic matter, as well as the relationship with the mineral matrix, may play a controlling role. Some of the pores may reflect the initial kerogen character.

Thermal maturity is one of the key controls on organic porosity. The specifics remain poorly understood and are evolving. Porosity has been observed in immature kerogen (e.g., Eagle Ford Shale [100]), with amorphous kerogen being inherently porous, while the cell structure of vitrinite may also provide primary pores. There is some evidence that as the shales enter the oil-window there is a reduction in observed porosity. This is thought to be a result of the generation of bitumen and oil, which fills pre-existing pore space [103], although there are contradictory data that indicates that porosity may begin to develop within the oil-window [100], not at the onset of generation but at a slightly higher thermal maturity (R_o between 0.8 and 0.9% [104, 105]). It was suggested that the pore generation begins with the onset of hydrocarbon generation and increases through the oil-window, with a decreasing rate of organic-pore generation in the gas-window and terminating at 3.5% R_o [106]. These changes in porosity reflect the release of volatiles and the restructuring of the organic matter. It was noted that changes in porosity are not monotonic [107]. It was further suggested that there is an evolution of the porosity type as maturity increases [108]. Pores may coalesce with increasing maturity causing an increase in pore size and complexity. At advanced levels of thermal maturity, there is also some evidence that pores size decreases [109].

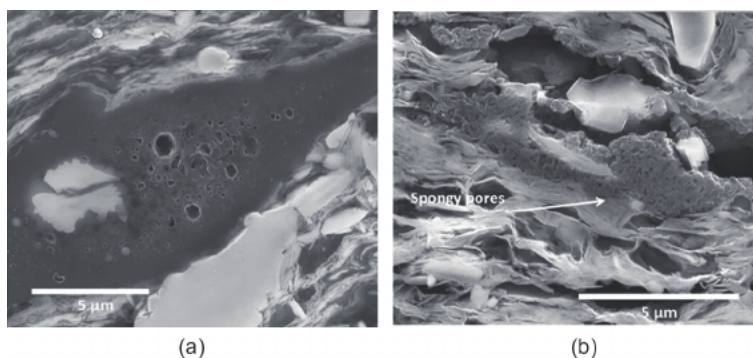


Figure 18.
SEM photomicrographs of organic matter from the Kimmeridge clay (United Kingdom): A - bubbly organic pores and B - spongy organic pores [99].

In addition to thermal maturity, organic richness has been considered an important controlling factor in the availability of organic pores. In general, a positive correlation appears to exist between organic porosity and carbon content for TOC levels less than 5.5 wt.% [110]. At the higher levels of organic enrichment, the lack of a correlation may be a result of pore collapse facilitated by greater organic matter connectivity and a less-developed mineral framework. It should also be noted that the greater the organic matter network, the greater the potential for interconnectivity within the organic pore network.

The nature of organic matter is also considered a controlling factor in organic porosity. For example, in humic kerogen, there appears to be little organic pore development beyond what was initially present [111]. In contrast, porosity increases can be observed in solid bitumen. It was suggested that the ratio of bitumen to kerogen was a key factor in determining organic porosity [112]. The greater the solid bitumen content the greater the organic porosity.

8. Summary and future work

Since the 1970s, numerous geochemical studies have been conducted around the world, including improvements in analytical methods, the establishment of data interpretation guidelines, analogs for geochemical inversion and correlation, and improvements in fundamental understanding of petroleum generation, retention, expulsion, and migration. Application of geochemical characterization and interpretation plays a significant role in reducing risk in petroleum exploration. Nevertheless, many interpretation ambiguities and uncertainties still exist due to complex and unclear subsurface conditions. As advanced analytical data and greater volumes of data become available, integrating geochemistry, geology, data analytics, and modeling may help to further understand petroleum systems with fewer ambiguities and uncertainties. This integration will establish new concepts, workflows and improve estimates of unknown values in time and space.

Acknowledgements

The authors wish to thank Chevron Corporation for permission to publish this work and thank Jessica Little and Michael Hsieh especially for performing Chevron's internal review before submission. We also would like to thank GeoMark for permission of using GC-MS traces in their database in this book chapter to show examples of different biomarker patterns in different types of oils.

References

- [1] Magoon LB, Dow WG. The petroleum system. In: Magoon LB, Dow WG, editors. *The Petroleum System – From Source to Trap*. AAPG Memoir 60; 1994. pp. 3-24
- [2] Dembicki H. Reducing the risk of finding a working petroleum system using SAR imaging, sea surface slick sampling, and geophysical seafloor characterization: An example from the eastern Black Sea Basin, offshore Georgia. *Marine and Petroleum Geology*. 2020;**115**:104276. DOI: 10.1016/j.marpetgeo.2020.104276
- [3] Rudolph KW, Goulding FJ. Benchmarking exploration predictions and performance using 20+ yr of drilling results: One company's experience. *AAPG Bulletin*. 2017;**101**:161-176. DOI: 10.1306/06281616060
- [4] Quirk DG, Archer SG, Keith G, Herrington P, Ramirez AO, Bjørheim M. Can oil and gas exploration deliver on prediction? *First Break*. 2018;**36**:83-88
- [5] Tissot B, Welte DH, Durand B. The role of geochemistry in exploration risk evaluation and decision making. In: *Proceedings of the 12th World Petroleum Congress 12th World Petroleum Congress*; 26 April-1 May 1987. Houston: OnePetro; 1987. pp. 99-112. Paper Number: WPC-22111
- [6] Triebs A. Chlorophyll und häminderivate in organischen mineralstoffen. *Angewandte Chemie*. 1936;**49**:682-686. DOI: 10.1002/ange.19360493803
- [7] Ronov AB. Organic carbon in sedimentary rocks (in relation to presence of petroleum). *Geochemistry* (translated from Russian). 1958;**5**:510-536
- [8] Klemme H, Ulmishek G. Effective petroleum source rocks of the world: Stratigraphic distribution and controlling depositional factors. *AAPG Bulletin*. 1992;**75**:1809-1851. DOI: 10.1306/0C9B2A47-1710-11D7-8645000102C1865D
- [9] Bissada KK. Geochemical constraints on petroleum generation and migration – A review. In: *Proceedings 2nd ASCOPE Conference*; October 1981. Manila, Philippines: ASCOPE; 1982. pp. 69-87
- [10] Momper JA. Oil migration limitations suggested by geological and geochemical considerations. In: *Physical and Chemical Constraints on Petroleum Migration*. AAPG Continuing Education Course Note Series Nr. 8, B1–B60, Tulsa. 1978
- [11] Katz BJ. An alternative view on indo-Australian coals as a source of petroleum. *APEA Journal*. 1994;**34**:256-267
- [12] Leythaeuser D, Schaefer RG, Yukler A. Role of diffusion in primary migration of hydrocarbons. *AAPG Bulletin*. 1982;**66**:408-429. DOI: 10.1306/03B59B2A-16D1-11D7-8645000102C1865D
- [13] Gasparik M, Bertier P, Gensterblum Y, Ghaznizadeh A, Kroos BM, Littke R. Geological controls on the methane storage capacity in organic-rich shale. *International Journal of Coal Geology*. 2014;**123**:34-51. DOI: 10.1016/j.coal.2013.06.010
- [14] Tissot B, Durand B, Espitalié J, Combaz A. Influence of nature and diagenesis of organic matter in formation of petroleum. *AAPG Bulletin*. 1974;**58**:499-506
- [15] Saxby JD, Shibaoka M. Coal and coal macerals a source rocks for oil and gas.

- Applied Geochemistry. 1986;1:25-36.
DOI: 10.1016/0883-2927(86)90035-1
- [16] Vandembroucke M. Kerogen: From types to models of chemical structure. *Oil & Gas Science and Technology - Review IFP*. 2003;58:243-269
- [17] Orr WL. Kerogen/asphaltene/sulfur relationships in sulfur-rich Monterey oils. *Organic Geochemistry*. 1986;10:499-516.
DOI: 10.1016/0146-6380(86)90049-5
- [18] Tissot B, Deroo G, Herbin JP. Organic matter in Cretaceous sediments of the North Atlantic contributions to sedimentology and paleogeography. In: Talwani M, Hay W, Ryan WBF, editors. *Deep Drilling Results in the Atlantic Ocean: Continental Margins and Paleoenvironment*. Vol. 3. AGU Maurice Ewing Series. Malden, MA, USA: Wiley; 1979. pp. 362-374
- [19] Katz BJ. Limitations of 'Rock-Eval' pyrolysis for typing organic matter. *Organic Geochemistry*. 1983;4: 195-199
- [20] Sebag D, Garcin Y, Adatte T, Deschamps P, Ménot G, Verrecchia EP. Correction for siderite effect on rock-Eval parameters: Application to the sediments of Lake Barombi (Southwest Cameroon). *Organic Geochemistry*. 2018;1123:126-135. DOI: 10.1016/j.orggeochem.2018.05.010
- [21] Ordoñez L, Vogel H, Sebag D, Ariztegui D, Adatte T, Russell JM, et al. The Towuti drilling project scientific team. Empowering conventional Rock-Eval pyrolysis for organic matter characterization of the siderite-rich sediments of Lake Towuti (Indonesia) using end-member analysis. *Organic Geochemistry*. 2019;134:32-44.
DOI: 10.1016/j.orggeochem.2019.05.002
- [22] Dembicki H, Horsfield B, Ho TTY. Source rock evaluation by pyrolysis-gas chromatography. *AAPG Bulletin*. 1983;67:1094-1103.
DOI: 10.1306/03b5b709-16d1-11d7-8645000102c1865d
- [23] Horsfield B. Practical criteria for classifying kerogens. Some observations from pyrolysis-gas chromatography. *Geochimica et Cosmochimica Acta*. 1989;53:891-901. DOI: 10.1016/0016-7037(89)90033-1
- [24] Maende A, Pepper A, Jarvie DM, Weldon DW. Advance pyrolysis data and interpretation methods to identify unconventional reservoir sweet spots in fluid phase saturation and fluid properties (API gravity) from drill cuttings and cores. In: *AAPG Annual Convention and Exhibition*. Houston: AAPG; 2017 Search and Discovery #80596
- [25] Jarvie DM, Hill R. Understanding unconventional petroleum system assessment. In: *West Texas Geological Society Fall Symposium*. Midland: AAPG; 2011 Search and Discovery #40840
- [26] Boyd PA, Whitfill DL, Carter TS, Allamon JP. Low-viscosity based fluid for low-toxicity oil-mud systems. *SPE Drilling Engineering*. 1987;2:218-228
- [27] Rodriguez ND, Katz BJ. The effect of oil-based drilling mud (OBM) on the assessment of hydrocarbon charge potential. *Marine and Petroleum Geology*. 2021;133:105312. DOI: 10.1016/j.marpetgeo.2021.105312
- [28] Parrish JT. Upwelling and petroleum source beds with reference to Paleozoic. *AAPG Bulletin*. 1982;66:750-774
- [29] Demaison GJ, Moore GT. Anoxic environments and oil source bed genesis. *Organic Geochemistry*. 1980;2:9-31.
DOI: 10.1016/0146-6380(80)90017-0

- [30] Glenn CR, Arthur MA. Sedimentary and geochemical indicators of productivity and oxygen contents in modern and ancient basins: The Holocene Black Sea as the “type” anoxic basin. *Chemical Geology*. 1985;**48**:325-354. DOI: 10.1016/0009-2541(85)90057-9
- [31] Cole JJ, Pace ML. Bacterial secondary production in oxic and anoxic freshwaters. *Limnology Oceanography*. 1995;**40**:1019-1027
- [32] Pelet R. A model of organic sedimentation on present-day continental margins. In: Brooks J, Fleet A, editors. *Marine Source Rocks*. Geological Society of London: Special Publication 26; 1987. pp. 167-180
- [33] Aller RC. Bioturbation and remineralization of sedimentary organic matter: Effects of redox oscillation. *Chemical Geology*. 1994;**1**:331-345. DOI: 10.1016/0009-2541(94)90062-0
- [34] Bralower TJ, Thierstein HR. Organic carbon and metal accretion rates in Holocene and mid-Cretaceous sediments: Palaeoceanographic significance. In: Brooks J, Fleet AJ, editors. *Marine Petroleum Source Rocks*. Geological Society of London: Special Publication 26; 1987. pp. 345-369
- [35] Porter KG, Robbins EI. Zooplankton fecal pellets link fossil fuel and phosphate deposits. *Science*. 1981;**212**:931-933. DOI: 10.1126/science.212.4497.931
- [36] Pedersen TF, Calvert SE. Anoxia vs. Productivity: What controls the formation of organic-carbon-rich sediments and sedimentary rocks? *AAPG Bulletin*. 1990;**74**:454-466. DOI: 10.1306/0C9B232B-1710-11D7-8645000102C1865D
- [37] Barron EJ, Washington WM. Numerical climate modeling: An exploration frontier in petroleum source rock prediction: Results based on Cretaceous simulations. *AAPG Bulletin*. 1985;**69**:448-459
- [38] Emerson S, Hedges JI. Processes controlling the organic carbon content of open ocean sediments. *Paleoceanography*. 1988;**3**:621-634. DOI: 10.1029/PA003i005p00621
- [39] Coleman ML, Curtis DC, Irwin H. Burial rate a key to source and reservoir potential. *World Oil*. 1979;**188**:83-92
- [40] Müller PJ, Suess E. Productivity, sedimentation rate and sedimentary organic matter in the oceans-I. organic carbon preservation. *Deep-Sea Research*. 1979;**26A**:1347-1362
- [41] Ibach LEJ. Relationship between sedimentation rate and total organic carbon content in ancient marine sediments. *AAPG Bulletin*. 1982;**66**:170-188. DOI: 10.1306/03B59A5D-16D1-11D7-8645000102C1865D
- [42] Robinson VD, Liro LM, Robison CR, Dawson WC, Russo JW. Integrated geochemistry, organic petrology, and sequence stratigraphy of the Triassic Shublik formation, Tenneco Phoenix #1 well, north slope, Alaska, USA. *Organic Geochemistry*. 1996;**24**:257-272. DOI: 10.1016/0146-6380(96)00023-X
- [43] Parrish JT, Droser ML, Bottjer DJ. A Triassic upwelling zone: The Shublik Formation, Arctic Alaska, USA. *Journal of Sedimentary Research*. 2001;**71**:272-285
- [44] Bombardiere L, Gorin GE. Sedimentary organic matter in condensed sections from distal oxic environments: Examples from the Mesozoic of SE France. *Sedimentology*. 2002;**45**:771-788. DOI: 10.1046/j.1365-3091.1998.00177.x

- [45] Waples DW. Reappraisal of anoxia and organic richness, with emphasis on Cretaceous North America. *AAPG Bulletin*. 1983;**67**:963-978
- [46] Katz BJ. Controlling factors on source rock development – A review of productivity, preservation, and sedimentation rate. In: Harris N, editor. *The Deposition of Organic-Carbon-Rich Sediments: Models, Mechanism, and Consequences*. Tulsa, Oklahoma: SEPM Special Publication; 2012. p. 82 7-16
- [47] Winters JC, Williams JA, Lewan MD. A laboratory study of petroleum generation by hydrous pyrolysis. In: Bjoroy M, editor. *Advances in Organic Geochemistry*. Vol. 1981. New York: John Wiley; 1983. pp. 524-533
- [48] Lewan MD, Spiro B, Illich H, Raiswell R, Mackenzie AS, Durand B, et al. Evaluation of petroleum generation by hydrous pyrolysis experimentation [and discussion]. *Philosophical Transactions of the Royal Society of London. Series A, Mathematical and Physical Sciences*. 1985;**315**:123-134. DOI: 10.1098/rsta.1985.0033. The Royal Society Publishing
- [49] Cooles GP, Mackenzie AS, Quigley TM. Calculation of petroleum masses generated and expelled from source rocks. *Organic geochemistry*. 1986;**10**:235-245. DOI: 10.1016/0146-6380(86)90026-4
- [50] Pepper AS, Corvi PJ. Simple kinetic models of petroleum formation. Part I: Oil and gas generation from kerogen. *Marine and Petroleum Geology*. 1995;**12**:291-319. DOI: 10.1016/0264-8172(95)98381-E
- [51] Behar F, Vandenbroucke M, Tang Y, Espitalie J. Thermal cracking of kerogen in open and closed systems: Determination of kinetic parameters and stoichiometric coefficients for oil and gas generation. *Organic Geochemistry*. 1997;**26**:321-339. DOI: 10.1016/S0146-6380(97)00014-4
- [52] Jarvie DM, Hill RJ, Ruble TE, Pollastro RM. Unconventional shale-gas systems: The Mississippian Barnett shale of north-Central Texas as one model for thermogenic shale-gas assessment. *American Association of Petroleum Geologists Bulletin*. 2007;**91**:475-499. DOI: 10.1306/1219060606068
- [53] Malloy TB, Bissada KK, Mei M, Darnell L, Wright J. Detailed characterization of hydrocarbons in source rocks and mud rock reservoirs by thermal extraction-evolved product GC-MS and GC-MS/MS analysis. In: *AAPG Annual Convention and Exhibition*. San Antonio: AAPG Datapages; 2019 Search and Discovery Article #90350
- [54] Burnham AK. *Global Chemical Kinetics of Fossil Fuels: How to Model Maturation and Pyrolysis*. Cham, Switzerland: Springer; 2017. p. 315. DOI: 10.1007/978-3-319-49634-4
- [55] Huc AY. Understanding organic facies: A key to improved quantitative petroleum evaluation of sedimentary basins. In: *Deposition of organic facies*. American Association of Petroleum Geologists. 1990;**30**:1-11. DOI: 10.1306/St30517C1
- [56] Mei M, Burnham AK, Schoellkopf N, Wendebourg J, Gelin F. Modeling petroleum generation, retention, and expulsion from the Vaca Muerta formation, Neuquén Basin, Argentina: Part I. integrating compositional kinetics and basin modeling. *Marine and Petroleum Geology*. 2021;**123**:104743. DOI: 10.1016/j.marpetgeo.2020.104743
- [57] di Primio R, Horsfield B. From petroleum-type organofacies to

- hydrocarbon phase prediction. AAPG Bulletin. 2006;**90**:1031-1058. DOI: 10.1306/02140605129
- [58] Burnham AK, Braun RL. Simple relative sorptivity model of petroleum expulsion. *Energy & Fuels*. 2017;**31**:9308-9318. DOI: 10.1021/acs.energyfuels.7b01815
- [59] Hantschel T, Kauerauf AI, editors. *Fundamentals of Basin and Petroleum Systems Modeling*. Berlin, Heidelberg: Springer; 2009. p. 476. DOI: 10.1007/978-3-540-72318-9
- [60] di Primio R, Skeie JE. Development of a compositional kinetic model for hydrocarbon generation and phase equilibria modelling: A case study from Snorre field, Norwegian North Sea. *Journal of Geological Society of London Special Publications*. 2004;**237**:157-174. DOI: 10.1144/GSL.SP.2004.237.01.10
- [61] Walters CC, Freund H, Kelemen SR, Ertas MD, Symington W. Method for Predicting Petroleum Expulsion. U.S. Patent 8352228 B2. Alexandria, Virginia: United States Patent and Trademark Office (USPTO); 2013
- [62] Pribylov AA, Skibitskaya NA, Zekel LA. Sorption of methane, ethane, propane, butane, carbon dioxide, and nitrogen on kerogen. *Russian Journal of Physical Chemistry A*. 2014;**88**:1028-1036. DOI: 10.1134/S0036024414060259
- [63] Tzabar N, Brake HJM. Adsorption isotherms and sips models of nitrogen, methane, ethane, and propane on commercial activated carbons and polyvinylidene chloride. *Adsorption*. 2016;**22**:901-914. DOI: 10.1007/s10450-016-9794-9
- [64] Baur F, Katz B. Some practical guidance for petroleum migration modeling. *Marine and Petroleum Geology*. 2018;**93**:409-421. DOI: 10.1016/j.marpetgeo.2018.03.003
- [65] Dahlberg EC. *Applied Hydrodynamics in Petroleum Exploration*. 2nd ed. NY: Springer; 1982. p. 161
- [66] Pratsch JC, Gasfelds NW. German Basin: Secondary gas migration as a major geologic parameter. *Journal of Petroleum Geology*. 1983;**5**:229-244. DOI: 10.1111/j.1747-5457.1983.tb00569.x
- [67] Bissada KK, Katz BJ, Barnicle SC, Schunk DJ. Origin of hydrocarbons in Gulf of Mexico basin: A reappraisal. In: Schumacher D, Perkins BF, editors. *Gulf Coast Oils and Gases—Their Characteristics, Origin, Distribution, and Exploration and Production Significance*. Austin: Society of Economic Paleontologists and Mineralogists Foundation, Gulf Coast Section, 10th Annual Research Conference Proceedings; 1990. pp. 163-171
- [68] Clayton JL, Spencer CW, Koncz I, Szalay A. Origin and migration of hydrocarbon gases and carbon dioxide, Békés Basin, southeastern Hungary. *Organic Geochemistry*. 1990;**15**:233-247. DOI: 10.1016/0146-6380(90)90002-H
- [69] Katz BJ, Robison VD. Oil quality in deep-water settings: Concerns, perceptions, observations, and reality. *AAPG Bulletin*. 2006;**90**:909-920. DOI: 10.1306/01250605128
- [70] Whelan JK, Kennicutt MC, Brooks JM, Schumacher W, Eglinton LB. Organic geochemical indicators of dynamic fluid flow processes in petroleum basins. *Organic Geochemistry*. 1994;**22**:587-615. DOI: 10.1016/0146-6380(94)90127-9
- [71] Philp RP, Oung JN. Biomarkers, occurrence, utility and detection. *Analytical Chemistry*. 1988;**60**:887-896. DOI: 10.1021/ac00166a720
- [72] Bissada KK, Elrod LW, Robison CR, Darnell LM, Szymczyk HM,

- Trostle JL. Geochemical inversion - a modern approach to inferring source-rock identity from characteristics of accumulated oil and gas. *Energy Exploration & Exploitation*. 1993;**11**:295-328. DOI: 10.1177/0144598793011003-405
- [73] Didyk BM. Organic geochemical indicators of palaeoenvironmental conditions of sedimentation. *Nature*. 1978;**272**:216-222. DOI: 10.1038/272216a0
- [74] Reed ID, Illich HA, Horsfield B. Biochemical evolutionary significance of Ordovician oils and their sources. *Organic Geochemistry*. 1986;**10**:347-358. DOI: 10.1016/0146-6380(86)90035-5
- [75] Philp RP, Lewis CA. Organic geochemistry of biomarkers. *Annual Review of Earth and Planetary Sciences*. 1987;**15**:363-395. DOI: 10.1146/annurev.ea.15.050187.002051
- [76] Seifert WK, Moldowan MJ. Applications of steranes, terpanes and monoaromatics to the maturation, migration and source of crude oils. *Geochimica et Cosmochimica Acta*. 1978;**42**:77-95. DOI: 10.1016/0016-7037(78)90219-3
- [77] Curiale JA, Bromley BW. Migration of petroleum into vermilion 14 field, Gulf Coast, U.S.A.—Molecular evidence. *Organic Geochemistry*. 1996;**24**:563-579. DOI: 10.1016/0146-6380(96)00033-2
- [78] Curiale JA. A review of the occurrences and causes of migration-contamination in crude oil. *Organic Geochemistry*. 2002;**33**:1389-1400. DOI: 10.1016/S0146-6380(02)00109-2
- [79] Jacob H. Classification, structure, genesis and practical importance of natural solid oil bitumen ("migrabitumen"). *International Journal of Coal Geology*. 1989;**11**:65-79
- [80] Landis CR, Castaño JR. Maturation and bulk chemical properties of a suite of solid hydrocarbons. *Organic Geochemistry*. 1995;**22**:137-149. DOI: 10.1016/0166-5162(89)90113-4
- [81] Hackley PC, Araujo CV, Borrego AG, Bouzinos A, Cardott B, Cook AC, et al. Standardization of reflectance measurements in dispersed organic matter: Results of an exercise to improve interlaboratory agreement. *Marine and Petroleum Geology*. 2015;**59**:22-34. DOI: 10.1016/j.marpetgeo.2014.07.015
- [82] Liu ZF. Application of Raman spectroscopy and transmission spectroscopy for shale reservoir characterization: Thermal maturity correlation and organic matter type differentiation [Thesis]. Houston: University of Houston; 2018
- [83] Jewell DM, Albaugh EW, Davis BE, Ruberto RG. Integration of chromatographic and spectroscopic techniques for the characterization of residual oils. *Industrial and Engineering Chemistry Fundamentals*. 1974;**13**:278-282. DOI: 10.1021/i160051a022
- [84] Summons RE, Powell TG. Chlorobiaceae in Palaeozoic seas revealed by biological markers, isotopes and geology. *Nature*. 1986;**319**(6056):763-765. DOI: 10.1038/319763a0
- [85] Bissada KK, Tan JQ, Szymczyk EB, Darnell LM, Mei M. Group-type characterization of crude oil and bitumen. Part I: Enhanced separation and quantification of saturates, aromatics, resins and asphaltenes (SARA). *Organic Geochemistry*. 2016;**95**:21-28. DOI: 10.1016/j.orggeochem.2016.02.007
- [86] Bissada KK, Tan JQ, Szymczyk EB, Darnell LM, Mei M. Group-type

characterization of crude oil and bitumen. Part II: Efficient separation and quantification of normal-paraffins iso-paraffins and naphthenes (PIN). *Fuel*. 2016;**173**:217-221. DOI: 10.1016/j.fuel.2016.01.056

[87] Summons RE, Hope JM, Swart R, Walter MR. Origin of Nama Basin bitumen seeps: Petroleum derived from a Permian lacustrine source rock traversing southwestern Gondwana. *Organic Geochemistry*. 2008;**39**:589-607. DOI: 10.1016/j.orggeochem.2007.12.002

[88] Eiserbeck C, Nelson RK, Grice K, Curiale JA, Reddy CM. Comparison of GC-MS, GC-MRM-MS, and GC×GC to characterize higher plant biomarkers in Tertiary oils and rock extracts. *Geochimica et Cosmochimica Acta*. 2012;**87**:299-322. DOI: 10.1016/j.gca.2012.03.033

[89] Mei M, Bissada KK, Malloy TB, Darnell ML, Szymczyk EB. Improved method for simultaneous determination of saturated and aromatic biomarkers, organosulfur compounds and diamondoids in crude oils by GC-MS/MS. *Organic Geochemistry*. 2018;**116**:35-50. DOI: 10.1016/j.orggeochem.2017.09.010

[90] Liang QY, Xiong YQ, Fang CC, Li Y. Quantitative analysis of diamondoids in crude oils using gas chromatography-triple quadrupole mass spectrometry. *Organic Geochemistry*. 2012;**43**:83-91. DOI: 10.1016/J.ORGGEOCHEM.2011.10.008

[91] Wei ZB, Moldowan JM, Zhang SC, Hill R, Jarvie DM, Wang HT, et al. Diamondoid hydrocarbons as a molecular proxy for thermal maturity and oil cracking: Geochemical models from hydrous pyrolysis. *Organic Geochemistry*. 2007;**38**:227-249. DOI: 10.1016/j.orggeochem.2006.09.011

[92] Mei M, Bissada KK, Malloy TB, Darnell ML, Liu Z. Origin of condensates and natural gases in the Almond Formation reservoirs in southwestern Wyoming, USA. *Organic Geochemistry*. 2018;**124**:164-179. DOI: 10.1016/j.orggeochem.2018.07.007

[93] Peters KE, Walters CC, Moldowan JM, editors. *The Biomarker Guide: Volume 2, Biomarkers and Isotopes in Petroleum Exploration and Earth History*. 2nd ed. New York: Cambridge University Press; 2005. p. 1155

[94] Cameron NR, Brooks JM, Zumbege JE. Deepwater petroleum system in Nigeria: Their identification and characterization ahead of the drill bit using SGE technology. In: *IBC Nigeria Energy Summit*. London: TDI-Brooks; 1999. Available from: <https://www.tdi-bi.com/about-us/publications/nigeria-petroleum/>

[95] Loucks RG, Reed RM, Ruppel SC, Hammes U. Spectrum of pore types and networks in mudrocks and descriptive classification of matrix-related mudrock pores. *AAPG Bulletin*. 2012;**96**:1071-1098. DOI: 10.1306/08171111061

[96] Mastalerz M, Schimmelmann A, Drobniak A, Chen Y. Porosity of Devonian and Mississippian New Albany shale across a maturation gradient: Insights from organic petrology, gas adsorption, and mercury intrusion. *AAPG Bulletin*. 2013;**97**:1621-1164. DOI: 10.1306/04011312194

[97] Loucks RG, Reed RM. Scanning-electron-microscope petrographic evidence distinguishing organic-matter pores associated with deposition organic matter versus migrated organic matter. *GCAGS Journal* 2014; 3: 51-60. Available from: <https://www.gcags.org/Journal/2014.GCAGS.Journal/GCAGS.Journal.2014.vol3.p51-60.Loucks.and.Reed.pdf> [Accessed: January 27, 2022]

- [98] Canter L, Zhang S, Sonnenfeld M, Bugge C, Guisinger M, Jones K. Primary and secondary organic matter habitat in unconventional resources. In: Olson T, editor. *Imaging Unconventional Reservoir Pore Systems*. Tulsa: AAPG Memoir; 2016. p. 112 9-24
- [99] Katz BJ, Arango I. Organic porosity: A geochemist's view of the current state of understanding. *Organic Geochemistry*. 2018;**123**:1-16. DOI: 10.1016/j.orggeochem.2018.05.015
- [100] Pommer M, Milliken K. Pore types and pore-size distributions across thermal maturity, eagle ford formation southern Texas. *AAPG Bulletin*. 2015;**99**:1713-1744. DOI: 10.1306/03051514151
- [101] Wood JM, Sanei H, Curtis ME, Clarkson CR. Solid bitumen as a determinant of reservoir quality in an unconventional tight gas siltstone play. *International Journal of Coal Geology*. 2015;**150-151**:287-295. DOI: 10.1016/J.COAL.2015.03.015
- [102] Dahl J, Moldowan JM, Walls J, Nur A, DeVito J. Creation of porosity in tight shales during organic matter maturation. In: *American Associate of Petroleum Geologists Annual Convention*; 22-25 April 2012. Long Beach, CA: AAPG; 2012 Search and Discovery #40979
- [103] Zargari S, Canter KL, Prasad M. Porosity evolution in oil-prone source rocks. *Fuel*. 2015;**153**:110-117. DOI: 10.1016/j.fuel.2015.02.072
- [104] Reed RM, Loucks R, Milliken KL. Heterogeneity of shape and microscale spatial distribution in organic-matter-hosted pores of gas shales. In: *American Associate of Petroleum Geologists Annual Convention*; 22-25 April 2012. Long Beach, CA: AAPG; 2012 Search and Discovery Abstract #90142
- [105] Reed RM, Loucks RG, Rupel SC. Comment on "formation of nanoporous pyrobitumen residues during maturation of the Barnett Shale (Fort Worth Basin)" by Bernard et al. (2012). *International Journal Coal Geology*. 2014;**127**:111-113. DOI: 10.1016/j.coal.2013.11.012
- [106] Chen J, Xiao X. Evolution of nanoporosity in organic-rich shales during thermal maturation. *Fuel*. 2014;**129**:173-181. DOI: 10.1016/j.fuel.2014.03.058
- [107] Löhr SC, Baruch ET, Hall PA, Kennedy MJ. Is organic pore development in gas shales influenced by the primary porosity and structure of thermally immature organic matter? *Organic Geochemistry*. 2015;**87**:119-132. DOI: 10.1016/j.orggeochem.2015.07.010
- [108] Curtis ME, Sondergeld CH, Rai CS. Investigation of the microstructure of shales in the oil window. In: *Unconventional Resources Technology Conference*. Denver: URTEC #1581844; 2013. DOI: 10.1190/urtec2013-162
- [109] Driskill B, Walls J, DeVito J, Sinclair SW. Applications of SEM imaging to reservoir characterization in the eagle ford shale, South Texas, U.S.a. In: Camp WK, Diaz E, Wawak B, editors. *Electron Microscopy of Shale Hydrocarbon Reservoirs*. Tulsa: AAPG MEMOIR 102; 2013. pp. 115-136. DOI: 10.1306/13391709M1023587
- [110] Milliken KL, Rudnicki M, Awwiller DN, Zhang T. Organic matter-hosted pore system, Marcellus Formation (Devonian), Pennsylvania. *AAPG Bulletin*. 2013;**97**:177-200. DOI: 10.1306/07231212048
- [111] Hou Y, He S, Wang J, Harris NB, Cheng C, Li Y. Preliminary study on the

pore characterization of lacustrine shale reservoirs using low pressure nitrogen adsorption and field emission scanning electron microscopy methods: A case study of the upper Jurassic Emuerhe Formation, Mohe Basin, northeastern China. *Canadian Journal of Earth Sciences* 2015;**52**:294-306. Available from: <https://link.gale.com/apps/doc/A416596805/AONE?u=anon~305edbe&sid=googleScholar&xid=4c5d40cd> [accessed January 27, 2022]

[112] Suárez-Ruiz I, Juliao T, Suárez-García F, Marquez R, Ruiz B. Porosity development and the influence of pore size on the CH₄ adsorption capacity of shale oil reservoir (upper cretaceous) from Colombia. Role of solid bitumen. *International Journal of Coal Geology*. 2016;**159**:1-17. DOI: 10.1016/j.coal.2016.03.020

Prospectivity Mapping Using Stream Sediment Geochemistry along the Orange River Catchment for Base Metal, Prieska, Northern Cape, South Africa

Nthabiseng Mashale

Abstract

The Areachap Terrane, which is part of the Namaqua Sector of the Namaqua-Natal Belt in the Northern Cape Province, host volcanic-hosted Zn-Cu deposits at volcanic centres. The primary objective was to map Volcanogenic Massive Sulphide (VMS) mineralisation, determine the heavy metal contents of sediments, locate the source of anomalies and delineate targets for follow-up studies. Nine thousand three hundred and fourteen stream sediments samples collected were analysed using XRF. The element associated with their respective lithostratigraphy was calculated using spatial joint analysis tool. ArcGIS was used to display uni-elements maps and relevant multi-element maps. The delineated potential VMS mineralisation target is considered for further follow-up study. The M23 and M24 anomalies are delineated for Cu₂Ni mineralisation. M23 and M24 anomalies are sourced from ultramafic debris transported from the Ghaap Group; however, this potential target will require follow-up studies for verification. The correlation between the Cu-Pb-Zn anomaly with alkali elements (Nb, Zr, Th, and U) and REEs (in Table 9) suggests there is a possibility that the M26–M29 anomaly is alkali-granitic genetic origin. The As, Ba, Ce, Cr, Cu, Hf, Nd, Ni, Rb, Sr., S, V, Zr and Zn contents showed a heterogeneous spatial distribution, reflected by high coefficient of variation and large standard deviation.

Keywords: geochemical signature, mineralisation, base metals, uni-elements maps, multi-element maps, follow-up study

1. Introduction

The Republic of South Africa (RSA) is known to be among one of the world's most active mining countries. RSA hosts several deposits such as gold deposits in the Witwatersrand basin, diamond deposits in Kimberly, Platinum group elements (PGE) in the Bushveld Complex and Manganese deposits in the Griqualand West Basin, all to which, to some extent they control the economy of the country [1].

The Namaqua-Natal Metamorphic Province, particularly the Namaqua Sector has proven to be the remarkable mineralised sector in the country hosting Copperton deposit, which according to [2], and [3] is one of the world's giant Volcanic Hosted Massive Sulphide (VHMS) deposit.

The Namaqua-Natal Metamorphic Province (NNMP) is a tectonostratigraphic province that stretches 1400 km across South Africa, it extensively outcrops in the Northern Cape Province and Kwa-Zulu Natal Province and referred as Namaqua and Natal Sectors respectively and in Namibia. NNMP embrace igneous and metamorphic rocks formed or metamorphosed during the Namaqua Orogeny at 1200 Ma–1000 Ma. It is 400 km wide and has borders with the Kaapvaal Craton to the north and Pan-African (Gariiep and Saldania) belts in the west and south [4, 5].

The Namaqua Sector of the Namaqua-Natal Province is subdivided into a number of distinct, discontinuity-bounded domains: Richtersveld Subprovince, Bushmanland Terrane, Gordonia Terrane, and Kaaien Terrane (**Figure 1**; [6]). The Location of the study area is in western degree of the 2922 Prieska sheet, Northern Cape Province, South Africa (**Figure 1**).

The small portion of Kaapvaal Craton is part of the study area (**Figure 1**). The preserved basin on the Kaapvaal Craton, which is the part of the study area of this research, is Griqualand-West basin. The westernmost of Griqualand West basin exposures at the eastern edge of the Kheis Belt, thrust and fold belt that post-dates younger Olifantshoek red beds. In its extreme, south the Griqualand-West strata are truncated by later dextral shearing on the Brakbosch and Brulpan faults [6].

Geochemical data combined with mineralogical and other additional data sets such as geologic maps, mineral distribution, geophysical methods, among others, provides a foundation for classifying and evaluating mineral resource endowment and natural hazards. A mineral resource produces diagnostic textural, geologic, geophysical, and geochemical signatures when exposed at or near the surface of the earth. Geochemical exploration is based on outlining such dispersion halos and in the present study that will be done by chemical analyses of stream-drainage sediments.

There is different between regional and detailed surveys in terms objective, size of area being surveyed, sampling density, type and of material sampled. Ginsburg [7]

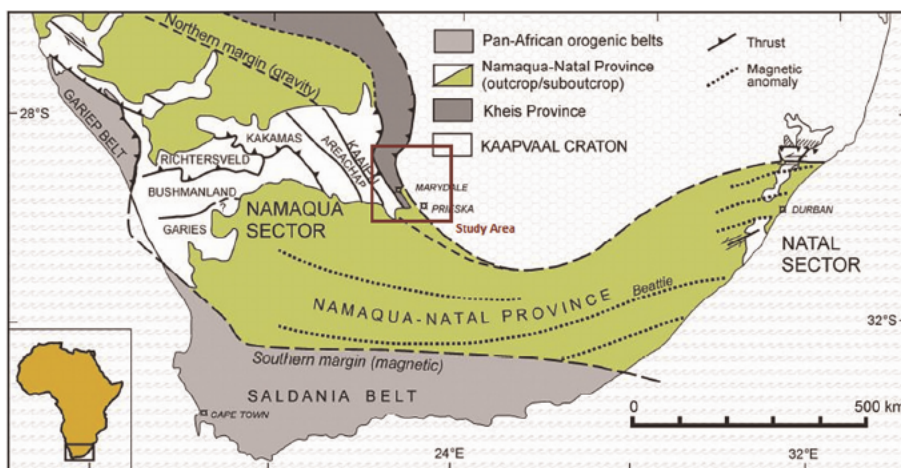


Figure 1. Map of Southern Africa showing Pan-African orogenic belts, NNP, Kheis Province and Kaapvaal craton [6].

recognised three scales of geochemical mapping and surveys depending on purpose and objective, namely, reconnaissance, prospecting and detailed. Regional survey can be conveniently discussed based on the number of stream sediment samples taken per square kilometres [8].

Regional geochemical mapping has been part of the core mapping function of the Council for Geoscience (CGS) since the 1970s. The Regional geochemical mapping program follow a systematic approach focussed on providing high quality- and high density datasets that will contribute to resolving issues relevant to modern South African geological society, namely, exploration, geological mapping, groundwater, environmental studies, and geological modelling. The principal objective of this geochemical orientation survey is to define the patterns of primary and secondary dispersion occurring in the study area particularly those of economically and environmentally interesting elements.

1.1 Research problem

The stream sediments composition of the research are is poorly understood. Mobility of the different elements varies considerably because of factors such as adsorption and Eh-pH conditions. Stream sediments programs worldwide had discovered numerous deposits.

1.2 Justification

The geochemical patterns obtained from this study will enable to link elements deficiencies and abundances with the underlying geology, structures and known mineral occurrences and mines. This will assist in tracing the source of anomalies encountered on stream sediments and delineate targets for follow-up studies within the Orange River catchment area.

1.3 Objectives of the study

1.3.1 Main objectives

The primary aim of this study is to map the VMS mineralisation potential of the Prieska area using the stream sediment data, determine geochemistry of stream sediments within the Orange River catchment area. This will enable the recognition of anomalies within the catchment area and trace their sources.

1.3.2 Specific objectives

The following specific objectives need to be met:

- To determine the solid geochemistry of the sediments from Orange River catchment
- To determine heavy metals content of the sediments
- Locate the source of anomalies and delineate targets for follow-up studies.

1.4 Hypothesis

- Geochemical and mineralogical anomalies of the sediments in the Orange River can be determined
- Metal content of stream Orange River sediments was introduced in solution
- Sources of resulted anomalies within the Orange River catchment can be traced.

1.5 Regional reconnaissance stream sediments survey history around the world

Large areas may be successfully explored using stream sediments geochemistry for indications of individual mineral deposits, groups of occurrences, or favourable geological environments. Sampling density ranges from one sample per 1 km² to one per 25 km² depending upon the type of target and drainage characteristics, and inherent in the reconnaissance concept is the need for more detailed sampling to determine the significance of regional anomalies [9, 10]. The government agencies, Council for Geological Survey and mining companies are mostly responsible to carry out Regional stream sediments surveys. Successful stream sediments surveys conducted around the globe.

The Geological Survey of Zambia in Africa employed regional and provincial scale geochemical mapping in systematic geological mapping. Analyses were for 20 elements by semi quantitative XRF. The Institute of Mining Research at the University of Zimbabwe (formerly known as Rhodesia) had been active in regional geochemical research projects since 1976. Some of the studies done by the institute include a regional stream sediment reconnaissance of 1350 km² of the Sabi Tribal Trust Land at a density of one sample per km² [11], and a survey of 1664 km² near West Nicholson, Zimbabwe, at same density [12] employing multi-element in both cases. In southern Africa, most mining companies devote a greater effort to regional soil sampling than to drainage reconnaissance and it had been estimated that more than 95% of samples collected by the major companies in 1973 were taken from soil grids [13].

In Australia, during 1976, there was a low level of activity as only 4250 stream sediments were collected; the number was expected to decline in 1977. Nevertheless, in the more favourable humid zones most mineral exploration companies make fixed use of regional stream sediment sampling since stream sediments are of limited use in the more arid regions because of low density of drainage and dilution by the wind-blown material. Two size fractions approach may be employed in arid regions, minus-120 mesh and minus-4-plus -16 mesh with coarser fraction containing gossan fragments and multiple grains cemented by metal-rich iron hydroxides [10].

In southern British Columbia portion and Yukon during 1976, Stream sediments sampling took place over an area of 75,000 km² (Cameroon, 1976). According to Meyer et al. [10], Smee and Ballantyne [14] reported that the British Columbia portion of the program covered 46,800 km² at a mean density of one sample per 13 km² and in the Yukon 2200 stations were sampled over an area of 28,490 km², giving the same degree of coverage. More than 90% of stream sediment activities of the Geological Survey of Canada and Federal-Provincial Uranium Reconnaissance Program that commenced in 1975 are related. Rose and Keith [15] concluded that stream sediments were preferable to water for reconnaissance drainage surveys for uranium for eastern Pennsylvania.

2. Methodology

Several techniques including geological mapping and stream sediments geochemistry were used to investigate stream sediments geochemical patterns of the Orange River catchment prospecting area in order to accomplish the goals and objectives set out for this study. A descriptive methodology is summarised in the below flow chart (Figure 2). The steps followed in order to achieve the objectives of this study are desktop study, reconnaissance survey, fieldwork, laboratory work, data analysis and interpretation, discussion, conclusions and recommendations.

2.1 Desktop study

In order to acquire first-hand information about the study area. Prior to field visit, the information from previous work on geology, nature of mineralisation and previous exploration conducted in the Orange River catchment prospect is studied. Information is sources from Books, unpublished technical reports, geological reports, topographical maps, journals and internet sources.

2.2 Fieldwork

A reconnaissance survey was undertaken prior to detailed or actual fieldwork. During this, a snap survey of geology, vegetation, and accessibility of the study area was undertaken. The aim is to locate the ground, target areas indicated by outcrops of

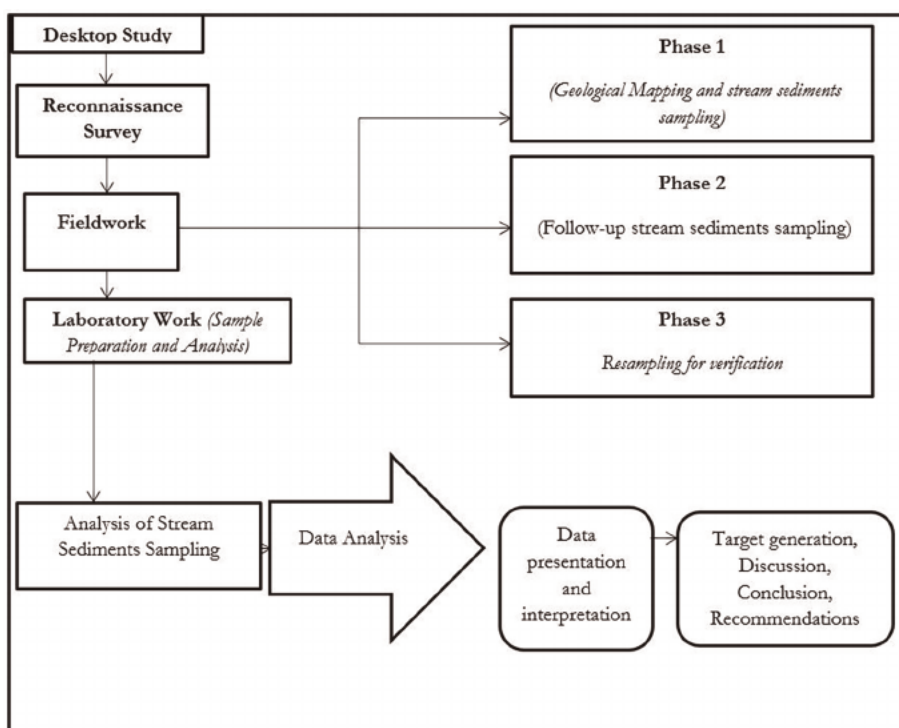


Figure 2. Flow chart indicating methods and procedures applied during the study.

different lithologies. The general attitudes of lithologies at the prospects, rock outcrops, and quantity of samples and duration of fieldwork were established. Additionally, a thorough study of topography, vegetation, pedology, drainage patterns and characteristics of rocks was also to gather as much information as possible in the study area. Stream distribution was also assessed which drain into the Orange River catchment prospect.

Field observations were transferred to a base map before being digitised using ArcGIS 10.3.1. The observations were transferred to a field base map; using diverse colours to discriminate the streams distribution mapped in the area. The spatial extent of each lithology and lithology contacts as well as stream distribution were trace on the map. Field notes includes describing the coordinates and nature of contact with other rock types and soil colour where there is limited outcrops.

2.3 Laboratory work

The sample analysis was conducted by the Council for Geoscience (CGS) laboratory in Pretoria. Sieve shaker, drying oven, atomic absorption spectrometry (Perkin Elmer Analyst 400, AAS), PANanalytical-Axios XRF were used for sample preparation and analysis.

2.3.1 Sample preparation

This section describes the methods used to prepare stream sediments samples collected from the Orange River catchment prospect for laboratory analysis.

2.3.1.1 Drying and milling

Samples are oven dried at 105–110 °C. Once completely dry, samples were first sieved through a 2 mm sieve to remove gravels and organic materials and subsequently sieved through a – 125 µm fraction size and milled to 85% -75 µm. The milled samples were placed in labelled sample bags ready for analysis.

2.3.2 Sample analysis

The prime requirement for mineral exploration survey is the availability of analytical procedures capable of high precision, low detection limit and acceptable accuracy.

2.3.2.1 Stream sediments geochemical analysis using XRF

The PANanalytical-Axios XRF was used for geochemical analysis of stream sediments. The milled samples roasted at 1000 °C for at least three hours in order to oxidise Fe²⁺ and S and to determine loss of ignition (LOI). Glass disks for XRF analysis were prepared by fusing 1 g sample and 8 g of flux (35% LiBO₂ and 64.71% Li₂B₄O₇) at 1050 °C for major element analysis. Major element oxides (SiO₂, TiO₂, Al₂O₃, Fe₂O₃, MnO, MgO, CaO, Na₂O, K₂O, P₂O₅ and Cr₂O₃) and trace element (Ni, Cu, Co, As, Zn, Pb, Cr, Ba, Sc, Sr., V, Th, U, Y, Zr) were analysed.

Trace element analysis was achieved by mixing 12 g milled sample and a 3 g Hoechst wax and then pressing into a powder briquette by a hydraulic press with the applied pressure at 25 ton. The glass disks and wax pellets were analysed by PANalytical-Axios XRF. XRF has the advantage of being non-destructive, multi-elemental, fast and cost

effective compared to other competitive techniques such as Atomic Absorption Spectrometry (ASS) or Inductively Coupled Plasma Spectrometry (ICP OES).

X-rays are produced by irradiating a sample with high energy photons produced by primary X-ray tube. When a high energy primary X-ray collides with an atom, an electron can be ejected from a low energy level creating an electron vacancy. When an electron from a higher energy level fills the vacancy, a secondary X-ray is created characteristic of that element. XRF analysis devices can be largely categorised into wavelength-dispersive X-ray spectrometry (WDX) and energy-dispersive X-ray spectrometry (EDX). WDX disperses the fluorescent X-ray generated in the sample using dispersion crystal and measures it using a goniometer, resulting in a large size. The detector in EDX on the other hand, has a superior energy resolution and requires no dispersion system, which enable downsizing of the device. Interaction of X-rays with sample creates secondary diffracted beams of X-rays related to inter-planar spacing in the crystalline powder according Bragg's Law:

$$n\lambda = 2d\sin\theta \quad (1)$$

Where: n is an integer, λ is the wavelength of X-rays; d is the inter-planar spacing generating the diffraction and is the θ diffraction angle.

The XRF was calibrated by identification of optimum conditions of several variable factors for each element, like identifying correct elemental peak and background, pulse height, collimator mask, counting time, dead time, followed by matrix and inter-element interference corrections. This was achieved by repeated analysis of certified reference material and correcting the variables to yield elemental concentration close to known values. This included 12/76 (amphibolite standard).

The weighted inverse distance interpolation (IDW) method was used to convert point XRF data into continuous geochemical maps using ArcGIS, the IDW parameters used were: power = 2, maximum neighbours = 15, minimum neighbours = 10, cell Size = Maximum of Inputs.

2.3.3 Quality control and quality assurance

It is vitally important that an analysis is precise but the accuracy is not generally so crucial, although some indication of accuracy is needed for most purposes in mineral exploration [16]. Quality assurance program should aim to assess the quality and accuracy at all stages of measurement process, from site selection and sampling through sample handling, preparation and analysis. Subsequently, a quality control/quality assurance See **Table 1** for the results of the reference material and lower limit of detection for each element. The glass disk R422 was analysed firstly with the calibration standards and then every 12 hours during analysis of the sample. The three sediment reference material GSD-9, GSD-11 and GSD-14 were repeatedly analysed every 30 samples to evaluate the precision of the analysis, **Table 1** summaries the results of the reference material and each lower detection limit of each element.

The statistical tests of standard samples repeatability can be based on replicate assays of a certified standard in one laboratory or, conversely, inter laboratory analyses. Blank samples for materials that have very low grade of a metal of interest are usually inserted in a batch of samples being processed. The main purpose of using blanks is to monitor laboratory for a possible contamination of samples, which are mainly caused by poor housekeeping, and insufficient thorough cleaning of equipment.

Oxide (wt %)	GSD-9				GSD-11				GSD-14				
	Lower level of determination	N = 391			N = 525			N = 435					
Element (ppm)	Certified	Average	Standard	%	Certified	Average	Standard	%	Certified	Average	Standard	%	RMS
				RMS				RMS				RMS	
SiO ₂	0.01	64.89	68.20	3.20	4.70	76.25	77.29	3.17	4.10	57.25	53.43	2.51	4.69
TiO ₂	0.01	0.92	0.94	0.01	1.34	0.35	0.35	0.00	1.02	2.40	2.29	0.04	1.84
Al ₂ O ₃	0.01	10.58	11.30	0.72	6.40	10.37	10.41	0.56	5.39	13.39	11.75	0.77	6.56
Fe ₂ O ₃	0.01	4.86	4.82	0.13	2.63	4.39	4.15	0.08	1.96	9.50	9.75	0.17	1.77
MnO	0.00	0.08	0.08	0.00	2.91	0.32	0.31	0.01	3.10	0.16	0.17	0.00	2.52
MgO	0.01	2.39	2.57	0.15	5.64	0.62	0.64	0.06	8.68	3.40	3.27	0.17	5.10
CaO	0.01	5.35	5.99	0.26	4.31	0.47	0.45	0.02	4.70	3.50	3.17	0.15	4.60
Na ₂ O	0.01	1.44	1.68	0.17	10.15	0.46	0.52	0.06	11.73	2.00	2.03	0.17	8.21
K ₂ O	0.01	1.99	2.18	0.03	1.29	3.28	3.43	0.05	1.43	2.30	2.28	0.04	1.60
P ₂ O ₅	0.00	0.15	0.17	0.01	4.56	0.06	0.07	0.01	8.32	0.23	0.22	0.01	5.86
Ag	4.00		5.00	1.00	19.20								
As	4.00	8.40	13.00	4.90	38.00	188.00	195.00	3.00	1.60	18.00	11.00	8.00	71.40
Ba	5.00	430.00	430.00	9.70	2.30	260.00	258.00	7.40	2.90	760.00	810.00	18.10	2.20
Ce	10.00	78.00	79.00	12.20	15.40	58.00	59.00	8.70	14.70	10.00	107.00	11.50	10.80
Co	4.00	14.40	13.00	0.20	1.90	8.50	8.00	0.50	6.70	28.00	28.00	0.60	2.30
Cr	4.00	85.00	89.00	2.60	2.90	40.00	36.00	2.70	7.50	243.00	244.00	7.50	3.10
Cu	2.00	32.10	33.00	1.40	4.10	78.60	78.00	2.00	2.60	66.00	72.00	2.50	3.50
Ga	2.00	14.00	18.00	3.00	16.90	18.50	19.00	3.40	17.20	25.00	30.00	4.00	13.70
Hf	5.00	9.70	11.00	0.70	6.90	5.40	6.00	0.80	14.70	13.00	15.00	1.20	8.00
Mo	2.00	0.64				5.90	7.00	0.50	7.70	2.70	4.00	0.50	13.90

Oxide (wt %)	Lower level of determination	GSD-9			GSD-11			GSD-14					
		Certified	Average	%	Certified	Average	%	Certified	Average	%			
Element (ppm)		Standard	Standard	RMS	Standard	Standard	RMS	Standard	Standard	RMS			
Nb	3.00	17.70	22.00	2.90	13.20	25.00	29.00	2.80	9.70	72.00	86.00	4.90	5.70
Nd	3.00	34.00	37.00	7.80	20.09	27.00	23.00	6.40	27.80	45.00	51.00	10.10	19.70
Ni	2.00	32.30	34.00	1.00	2.80	14.40	18.00	1.20	7.10	87.00	100.00	3.70	3.70
Pb	2.00	23.00	23.00	0.90	8.10	636.00	627.00	14.70	2.30	66.00	68.00	3.20	4.70
Rb	2.00	80.00	84.00	2.20	2.60	408.00	417.00	10.50	2.50	87.00	92.00	3.40	3.70
S	3.00	150.00	217.00	6.70	3.10	170.00	178.00	14.50	8.10	175.00	16.10	9.20	9.20
Sb	3.00	0.80				14.90	11.00	1.30	11.60	2.70	4.00	0.70	18.70
Sc	3.00	11.10	16.00	4.30	26.90	7.40	8.00	3.80	45.20	18.00	21.00	4.30	20.50
Sn	3.00	2.60	5.00	2.10	42.30	370.00	400.00	7.90	2.00	9.50	8.00	3.90	47.70
Sr	2.00	166.00	168.00	1.90	1.10	29.00	34.00	1.10	3.30	216.00	327.00	5.40	230
Ta	3.00	1.30				5.70	5.00	1.40	24.80	5.00	4.00	0.80	19.60
Th	3.00	12.40	11.00	1.90	17.00	23.30	48.00	2.10	4.30	12.40	12.00	2.20	17.40
U	3.00	2.60	4.00	0.80	20.60	9.10	8.00	1.20	15.20	3.00	4.00	1.50	37.20
V	4.00	97.00	105.00	5.40	2.50	46.80	39.00	3.60	9.20	190.00	230.00	20.30	8.80
W	3.00	1.76				126.00	97.00	3.80	3.90	5.60	5.00	0.90	18.10
Y	3.00	26.50	25.00	0.60	2.30	42.70	37.00	2.00	5.50	3.40	34.00	1.50	5.30
Zn	3.00	78.00	72.00	0.60	0.90	373.00	368.00	9.50	2.60	165.00	183.00	5.20	2.80
Zr	3.00	370.00	391.00	9.00	2.30	152.00	156.00	5.60	3.60	524.00	560.00	17.40	3.10

Table 1.
 The Lower limit of detection (LLD) of each element and the reference material obtained results.

2.3.4 Data processing and evaluation

Analytical data processing aims, firstly, at reducing random and/or systematic errors resulting from field survey and/or laboratory analysis, and secondly, at identifying whether the data contain some useful information indicating the source, pathway and trap of coal concentrations in the study area. The careful analysis of such data, using standard computer software packages, is an important and affordable way of adding value to an exploration programme.

2.3.4.1 Statistical data analysis

Statistical methods have been widely applied to interpret analytical data sets and define anomalies. However, such methods need to be used cautiously since the data are typically and spatially dependent on each sample site and a range of different processes that may have influenced the element abundance measured. The data are also imprecise because of unavoidable variability in sampling methods and media and the level of analytical precision.

Moon [16] indicated that the aim of mineral exploration is to define significant anomalies. Anomalies are defined by statistically grouping data and comparing these with geology and sampling information. Strong anomalies detected may be for instance due to a combination of factors such as sampling and analytical errors, or contaminations which do not represent mineralisation. The absence of anomaly on the other hand may not necessarily mean the absence of mineralisation in the area of study. Such absence may be due to low rate of weathering in the area, buried or blind mineralisation, or dilution between source and sample site [17].

The use of descriptive statistics helps us to simplify large amounts of data into a simpler summary. Numerical and graphical methods are the two commonly used methods. Numerical method enables one to compute statistics such as mean and standard deviation while, graphical methods are better suited than numerical for identifying patterns in the data sets. The numerical and graphical methods complement each other and it is therefore wise to use both. Consequently, histograms, and summary statistical information were used in this study to identify patterns in data sets. According to Riemann et al. [18], a graphical inspection of analytical data is necessary as the first step in data analysis. The best means of statistical grouping data is graphical examination using histograms and box plots [19, 20].

3. Data presentation and interpretation

The geology map retrieved from the CGS database, was compiled on ArcGIS software (**Figure 3**). The area is comprised of the Transvaal Sequence, Olifantshoek Supergroup, Kaaien Terrane, Areachap Group and Karoo Supergroup. The Transvaal Sequence is confined to the north-central part of the Kaapvaal Craton [21]. It overlies the Witwatersrand foreland basin (Supergroup) and is overlain by Bushveld Complex [21]. The three basins – the Transvaal basin, and Griqualand West basin, in South Africa, and the Kanye basin in Botswana basins are preserved on the Kaapvaal Craton [21].

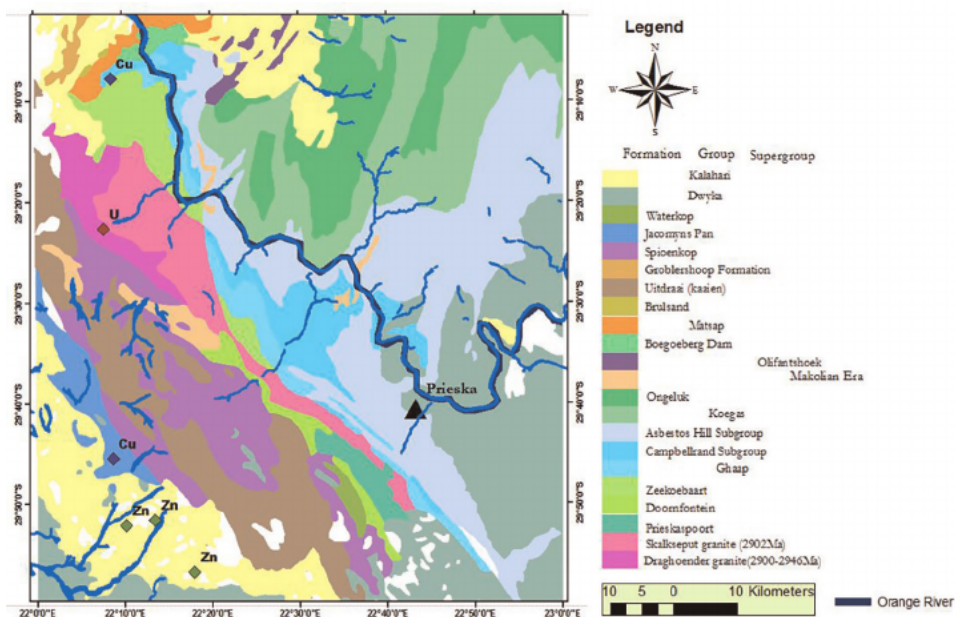


Figure 3.
 The Geology of the Prieska map.

3.1 Univariate stream sediment geochemistry

The geochemical data was transformed into a raster data with a cell size of 1 km using weighted inverse distance interpolation method. A maximum of four points were used to calculate a value for each cell location. First, the raster maps of the uni-elements were visualised in ArcGIS and compared to the underlying geology and known base metal occurrences. Univariate statistical methods was used to extract information from a data set of values for a single element, frequency histograms are created using GIS geostastical analyst tool, to examine the frequency distribution and identify the type of distribution, the all elements Histograms are on none transformation.

The only elements that correlates (**Table 2**) importantly with the known base metals occurrence in Prieska area as discussed in this section. The copper, lead, zinc, gold and silver minerals are associated with Volcanogenic Massive Sulphide (VMS) deposits. Prieska area is underlain by the Areachap Terrane, known to host VMS and Sedimentary exhalative deposit (SEDEX) deposits, including the mined out Copperton deposit, approximately 10 km southwest of the Prieska town. The Areachap terrane is overlain by up to 100 m of Karoo sediments that limited historical exploration.

The elemental distribution maps are plotted using the Jenks natural classification system. The elemental population is classified into five break points;

1. The first break is minimum to mean value, and
2. Second break is from mean to (mean plus standard deviation) value, the first two break are regarded as a background value, values above the threshold calculates **Table 3** are anomalous,

	Ag	As ₂	Ba	Ce	Co	Cc	Cu	Ga	Hf	Mo	Nb	Nd	Ni	Pb	Rb	S	Sb	Sc	Sc	Sn	Sc	Ta	Th	U	V	W	Y	Zn	Zr	
AF 10,000																														
As ₂ 0.1552	10,000																													
Ba 0.0520	-0.0555	10,000																												
Ce 0.0956	0.5085	-0.0218	10,000																											
Co 0.1271	0.0562	0.0767	0.0064	10,000																										
Cr 0.1998	0.4000	-0.0958	0.2664	0.5850	10,000																									
Cu 0.0738	-0.0106	0.5897	-0.0222	0.2059	0.0606	10,000																								
Ga 0.1201	0.1445	0.3487	-0.0953	0.1985	0.0926	0.1297	10,000																							
Hf 0.1611	0.0188	-0.0435	0.6219	0.0443	0.4811	-0.0134	0.1140	10,000																						
Mo 0.1508	0.4587	0.1155	0.4839	0.1453	0.3451	0.2328	-0.0075	0.4829	10,000																					
Nb 0.4435	0.6413	0.1369	0.4409	0.0939	0.4380	0.0356	0.3268	0.3157	0.4147	10,000																				
Nd 0.1338	0.5690	-0.0068	0.3967	-0.0168	0.3239	-0.0245	-0.0169	0.7506	0.3212	0.5731	10,000																			
Ni 0.1609	-0.0154	0.0303	-0.0828	0.7213	0.5889	0.1484	0.2066	0.0004	0.0565	0.0926	-0.0727	10,000																		
Pb 0.2079	0.0909	0.5272	0.1199	0.0348	0.0140	0.3975	0.3629	0.1723	0.1611	0.3920	0.1846	0.0470	10,000																	
Rb 0.0999	0.0098	0.4749	0.0740	-0.1606	-0.2758	0.0678	0.5134	0.0385	-0.0054	0.2702	0.0929	-0.0889	0.4933	10,000																
S -0.0072	-0.0354	0.2343	0.0001	-0.0166	-0.0475	0.1906	-0.0291	-0.0377	0.0375	-0.0501	-0.0048	-0.0014	0.0529	-0.0482	10,000															
Sb -0.0034	0.0161	0.0213	0.0036	-0.0242	-0.0089	0.0064	0.0041	-0.0144	-0.0094	-0.0080	0.0031	-0.0122	-0.0098	0.0575	-0.0063	10,000														
Sc 0.2047	-0.0250	0.0318	-0.1328	0.4429	0.2516	0.0639	0.2282	-0.0301	0.0183	0.1880	-0.1172	0.2640	0.0207	0.0119	-0.0715	0.0271	10,000													
Sn 0.0304	0.0776	0.0155	0.0503	0.0261	0.0482	0.0054	0.0062	0.0402	0.0568	0.0500	0.0601	0.0601	0.0250	0.5404	0.0168	-0.0106	0.0187	-0.0079	10,000											
Sr 0.0695	-0.0067	0.1634	0.0728	0.1555	0.1554	0.0720	0.1295	-0.0078	0.0549	0.0924	0.0699	0.0793	0.0682	-0.0083	0.2750	0.0156	0.0796	-0.0029	10,000											
Ta 0.1460	0.6796	-0.0043	0.3454	0.0778	0.3385	0.0015	0.2528	0.6254	0.3035	0.5409	0.4318	0.0610	0.1471	0.0602	-0.0345	-0.0151	-0.0390	0.0562	0.0001	10,000										
Th 0.2442	0.6040	0.1355	0.4527	0.0881	0.3830	0.0042	0.3247	0.7713	0.3685	0.3119	0.9552	0.0532	0.0380	0.3286	-0.0708	-0.0072	0.0508	0.0870	0.0994	0.5251	10,000									
U 0.4857	0.6433	0.0206	0.4750	0.4511	0.4374	0.0340	0.0623	0.7311	0.4912	0.7532	0.5298	0.0777	0.2401	0.1082	-0.0399	-0.0052	0.1456	0.0738	0.0748	0.4471	0.7055	10,000								
V 0.2149	0.4729	0.1704	0.3644	0.4582	0.6379	0.1149	0.4151	0.6194	0.2823	0.6647	0.5072	0.3049	0.2850	0.1388	-0.0441	0.0091	0.2151	0.0459	0.2889	0.4409	0.7084	0.5656	10,000							
W 0.1762	0.7146	-0.0475	0.4144	0.0653	0.3628	0.0655	0.2838	0.6472	0.3569	0.5250	0.4742	0.1001	0.1219	-0.0574	0.0089	-0.0233	-0.1385	0.0592	-0.0880	0.6536	0.4426	0.3475	0.3731	10,000						
Y 0.0760	0.6310	0.1944	0.4462	0.0596	0.2291	0.0368	0.1847	0.6366	0.3524	0.6057	0.4921	-0.0679	0.2747	0.3773	-0.0808	0.0349	0.1034	0.0384	0.1085	0.3644	0.6741	0.6577	0.5464	0.0729	10,000					

	Ag	As ₅	Ba	Ce	Co	Cc	Cu	Ga	Hf	Mo	Nb	Nd	Ni	Pb	Rb	S	Sb	Sc	Sn	Sc	Ta	Th	U	V	W	Y	Zn	Zr
Zn	0,0507	-0,0406	0,6385	-0,0231	0,1166	0,0117	-0,9213	0,1624	-0,0329	0,2150	0,0267	-0,0194	0,0852	0,4360	0,1348	0,1933	0,0016	0,0126	-0,0011	0,0920	-0,0125	0,0093	0,0037	0,1061	0,0443	0,0403	10,000	
Zr	0,1553	0,3292	-0,0691	0,6256	0,0378	0,4734	-0,0244	0,0292	0,9565	0,5239	0,7904	0,7295	-0,0231	0,1445	0,0038	-0,0438	-0,0143	-0,0294	0,0488	-0,0256	0,6015	0,7495	0,7894	0,5776	0,5925	0,6669	-0,0501	10,000
				Very Strong Correlation																								
				Moderate to strong correlation																								
				Moderate Correlation																								

Table 2.
 The summary statistics of all the analysed elements.

Element	Count	Minimum	Maximum	Mean	Standard Deviation	Skewness	&\$\$\$;	Quantile1	Median	Quantile3	Threshold values	Mean + 3 SD	Coefficient Variation
SiO2 (%)	9312	18.993	80.991	47.074	4.408	-0.535	6.054	44.797	47.382	49.804	55.891	60.299	0.093651
TiO2 (%)	9312	0.238	7.230	1.161	0.342	3.891	32.579	0.988	1.095	1.224	1.845	2.188	0.294575
Al2O3 (%)	9312	2.592	19.816	9.756	1.748	-0.076	3.303	8.562	9.753	10.980	13.251	14.999	0.179152
Fe2O3 (%)	9312	2.766	26.504	7.607	1.659	1.579	9.573	6.685	7.328	8.271	10.925	12.584	0.218062
MnO (%)	9312	0.036	2.281	0.133	0.082	6.192	87.683	0.094	0.114	0.141	0.297	0.379	0.617984
MgO (%)	9312	0.000	7.909	1.315	0.761	2.045	10.105	0.830	1.092	1.593	2.838	3.599	0.578966
CaO (%)	9312	0.189	31.877	1.737	1.737	5.547	51.711	1.012	1.240	1.705	5.211	6.948	0.999938
Na2O (%)	9312	0.000	6.769	0.566	0.168	6.231	206.536	0.471	0.555	0.637	0.902	1.070	0.29633
K2O (%)	9312	0.535	3.266	2.067	0.311	-0.249	3.443	1.890	2.059	2.282	2.688	2.999	0.150348
P2O5 (%)	9312	0.029	1.052	0.139	0.051	3.117	35.630	0.107	0.135	0.162	0.240	0.290	0.364042
As (ppm)	9312	4.000	120.910	15.802	13.874	2.235	9.991	6.145	11.450	20.240	43.551	57.425	0.878017
Ag (ppm)	9312	4.000	25.270	5.392	2.452	3.519	19.435	4.000	4.240	6.050	10.296	12.748	0.454685
Ba (ppm)	9312	91.180	4187.720	410.752	76.653	24.597	1080.028	382.565	409.805	439.865	564.058	640.711	0.186616
Ce (ppm)	9312	10.000	864.010	78.027	55.741	4.665	36.596	53.200	64.390	79.425	189.510	245.251	0.714379
Co (ppm)	9312	4.000	56.420	14.733	4.017	1.149	6.949	12.050	14.140	16.790	22.766	26.783	0.272629
Cx (ppm)	9312	49.790	1052.880	141.762	40.500	4.198	49.516	119.470	131.680	151.535	222.762	263.262	0.285688
Cn (ppm)	9312	7.370	2357.040	34.465	31.879	53.683	3534.044	28.510	32.780	37.740	98.223	130.102	0.924974
Ga (ppm)	9312	6.250	46.420	19.769	4.425	0.143	2.650	16.040	19.890	23.160	28.618	33.043	0.223816
Hf (ppm)	9312	5.000	245.440	23.292	14.397	3.954	30.123	15.850	19.820	25.720	52.085	66.482	0.618101
Mo (ppm)	9312	2.000	13.550	2.143	0.568	7.505	84.540	2.000	2.000	2.000	3.279	3.846	0.264826
Nb (ppm)	9312	3.000	112.200	25.264	8.482	2.075	13.720	20.650	24.060	28.115	42.229	50.711	0.335735
Nd (ppm)	9312	3.000	459.830	40.511	27.490	4.003	31.632	26.270	34.815	44.850	95.490	122.980	0.678578

Element	Count	Minimum	Maximum	Mean	Standard Deviation	Skewness	&\$\$\$;	Quantile1	Median	Quantile3	Threshold values	Mean + 3 SD	Coefficient Variation
Ni (ppm)	9312	11.360	460.500	39.559	12.345	7.908	192.598	33.180	37.620	43.905	64.250	76.595	0.31207
Pb (ppm)	9312	2.000	167.110	18.776	5.030	7.963	192.132	16.420	18.745	20.950	28.836	33.866	0.267912
Kb (ppm)	9312	21.170	142.690	86.942	13.467	-0.688	4.017	80.355	88.400	95.525	133.876	127.343	0.154898
Sb (ppm)	9312	3.000	4.300	3.001	0.026	36.635	1554.275	3.000	3.000	3.000	3.052	3.077	0.008499
S (ppm)	9312	54.920	32965.370	233.027	471.570	49.696	3037.767	146.985	195.115	257.120	1176.166	1647.735	2.023673
Sa (ppm)	9312	3.000	230.040	3.611	3.976	31.589	1458.505	3.000	3.000	3.000	11.562	15.538	1.100919
Se (ppm)	9312	3.000	50.180	18.183	5.077	0.135	3.687	14.930	17.930	21.355	28.337	33.413	0.279187
Sr (ppm)	9312	18.170	975.050	113.523	28.744	8.948	201.199	100.590	133.045	123.810	171.010	199.754	0.253195
Ta (ppm)	9312	3.000	61.570	7.556	6.478	2.620	12.424	3.000	5.285	9.130	20.513	26.992	0.857349
Th (ppm)	9312	3.000	132.240	13.868	6.750	4.161	40.510	10.270	12.970	15.890	27.367	34.116	0.486706
U (ppm)	9312	3.000	25.760	4.041	1.842	3.467	22.295	3.000	3.075	4.450	7.726	9.568	0.455809
V (ppm)	9312	16.180	836.190	126.384	33.836	3.657	41.490	108.250	123.520	137.885	194.057	227.893	0.267726
W (ppm)	9312	3.000	51.750	6.318	5.147	2.546	12.203	3.000	3.980	7.850	16.612	21.759	0.814664
Y (ppm)	9312	3.960	112.390	27.021	7.211	2.420	18.762	23.030	26.635	29.860	41.443	48.654	0.266869
Zn (ppm)	9312	11.990	5347.830	66.145	68.394	58.378	4155.871	53.120	62.850	74.285	202.933	271.327	1.034011
Zx (ppm)	9312	111.870	9242.850	1023.432	671.759	3.605	24.477	669.530	855.425	1144.235	2366.950	3038.709	0.656379

Table 3.
Correlation Matrix.

3. From the threshold to mean + 3*standard deviation value is highly anomalous and
4. The fifth break is the value from mean + 3*standard deviation value to maximum value.

The primary aim of the exploration target generation is twofold; to generate new areas for exploration activity where favourable geology and no mineral occurrences are coincident, and secondly a rethink in areas of known mineralisation on the possibilities of other styles or models of mineralisation. The geology of Prieska area and the geochemistry was joined using the Analysis tool spatial joint; the aim is to calculate the mean values of Uni-element of the lithostratigraphic unit. **Table 4** below refers to the lithostratigraphic unit with their associated elements. Based on [22] the five Fuzzy operators are useful for combining exploration datasets, Fuzzy AND, OR, Algebraic product, algebraic sum and γ -operator. In this study Fuzzy OR operation was applied to combine maps of relevant indicator elements associated with the geology (**Table 4**).

The elements of the highest mean averages associated with the Spioenkop Formation is the Cu, Ga, Zn and Rb (**Figure 4**). Cu and Zn correlates very strong at the correlation coefficient of 0.97. The distribution of the two elements strongly correlated with the known VMS Copperton deposit. **Figures 5–7** displays a Fuzzy OR overlap multi-element map of Cu, Ga, Zn and Rb. The map index poorly delineate Spioenkop Formation, the second dispersion occur in Uitdraai Formation, Jacomyns pan Formation, Globershoop, and Spioenkop Formation. The observed mineralisation potential areas are M1 and M2. The M1 anomaly is associated with the known mine area named Copperton Deposit, Prieska mine, the M1 anomaly is overlaying the Kalahari and Dwyka Group The Prieska Cu_Zn is known as the VMS deposit, the most common commodities or minerals exploited in this area are the Zinc, Copper and Sphalerite. The Mine known as a medium scale abandoned mine. The M2 anomaly is in close vicinity to the Orange River catchment, the anomaly is overlaying the Campbellrand subgroup. Campbell Rand Subgroup belongs to the Ghaap Group. The base mineralisation have been recorded in Ghaap Group is Pering deposit far

Geology (lithostratigraphy)	Elements
Zeekobraat	W, Fe
Spioenkop	Cu, Ga, Rb, Zn
Uitdraai	V
Waterkop	Ba
Ongeluk lava Formation	Co, Ni
Prieskaspoort	Cr, S, Sr., Mg
Koegas Group	Nd, Pb, Th
Jacomyns Pan	Ag
Kalahari Group	Sn
Builsand	Hf, Mo, Nb, Sc, Ta, U
Boegoeberg Dam	Zr, As
Asbestos Hill	Ce

Table 4.
Relevant indicator elements associated with the geology.

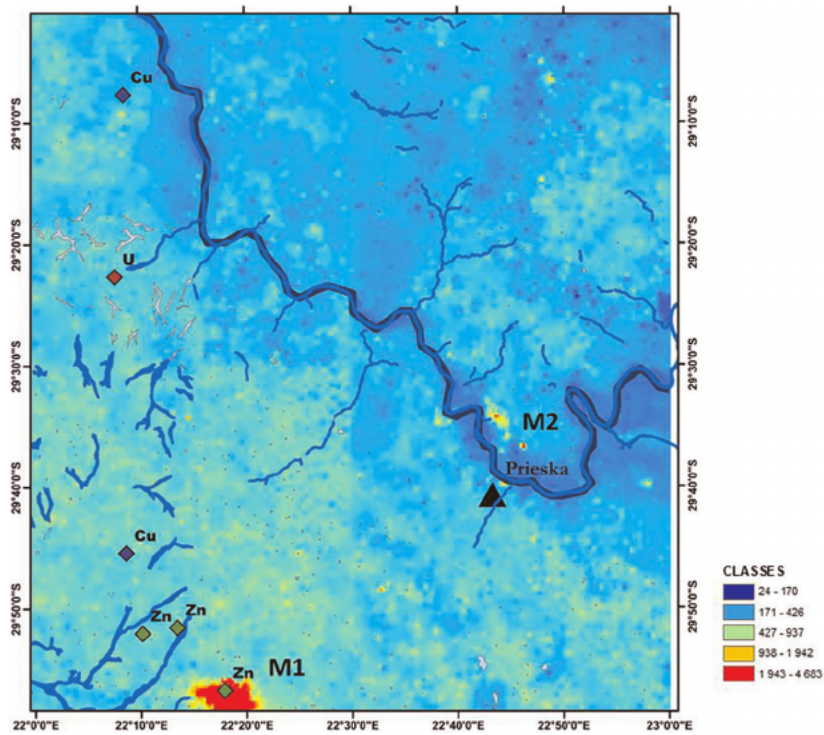


Figure 4.
 Fuzzy OR overlay multi-element map index of Cu, Ga, Zn, and Rb.

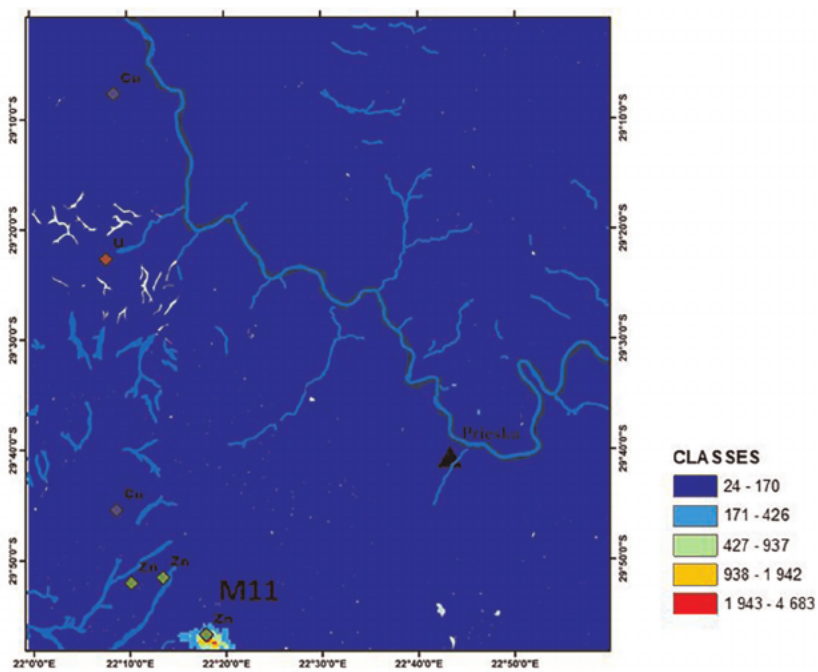


Figure 5.
 The Fuzzy OR overlay map for Cu_Zn index.

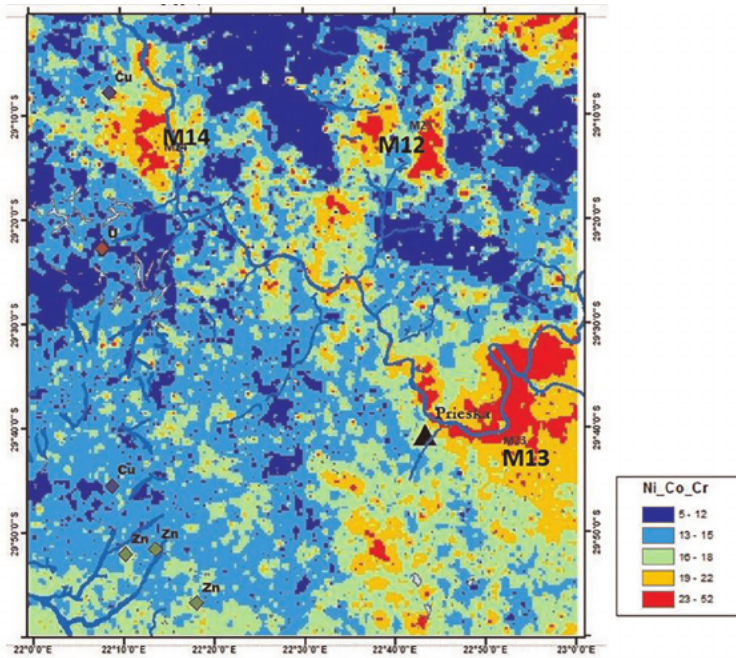


Figure 6.
The Fuzzy OR overlay map for Ni, Co and Cr index.

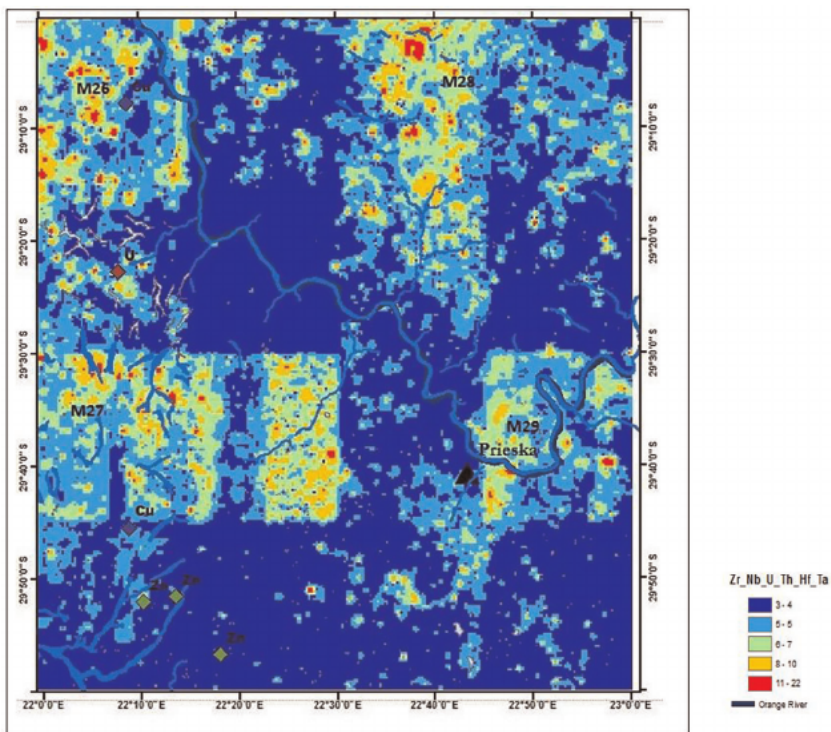


Figure 7.
The Fuzzy OR overlay of Zr_Nb_U_Th_Hf_Ta.

northeast about 150 km from the study area. The Host rocks to Zn–Pb mineralisation on the Ghaap Plateau are stromatolitic dolomites, with minor oolitic dolomites, chert and carbonaceous shale beds of the Campbell Rand Subgroup (Gutzmer, 2006). The occurrence of the M2 potential mineralisation zones requires follow-up studies.

There is a very strong correlation between the Co and Ni, and moderate to strong correlation between Co and Cr indicator elements. The correlations of Co-Ni-Cr are the indicator of mafic- ultramafic geological index. The strong correlation between Co and Ni can also indicate the base metal mineralization. The Ni-Co covers the sulphides and oxides of interest (Co-Ni-Cr) in ultramafic rocks. Co-Ni is a pathfinder of Ni-Cu.

The anomaly M3 – M7 (**Figure 8**) are Co-Ni high values. The M3 potential mineralisation area to the west of Prieska town covers the Dwyka Group, this mineralisation is at the very close vicinity to the Orange River catchment (primary stream) dominant mostly to the south of the catchment. The Co-Ni anomaly (M3) to the north of the Catchment is similar to the Cu-Ga-Zn-Rb anomaly M2, these anomalies cover the Campbellrand Subgroup at the same area, and therefore this outline the new potential of base metal mineralisation The M4 anomaly overlay the Dwyka Group, Asbestos Hills and the Skalkseput Granite. The M4 anomaly trends to the north-west following the Skalkseput Granite lithology, at the M7 the Co-Ni anomaly covers the Skalkseput Granite and is associated with the known occurring Uranium commodity.

The M5 Co-Ni anomaly is in close vicinity with the known small Copper occurrence. The anomaly is evident in and around the Orange River Catchment. This will require follow up study to confirm the parent source of the anomaly, because of its

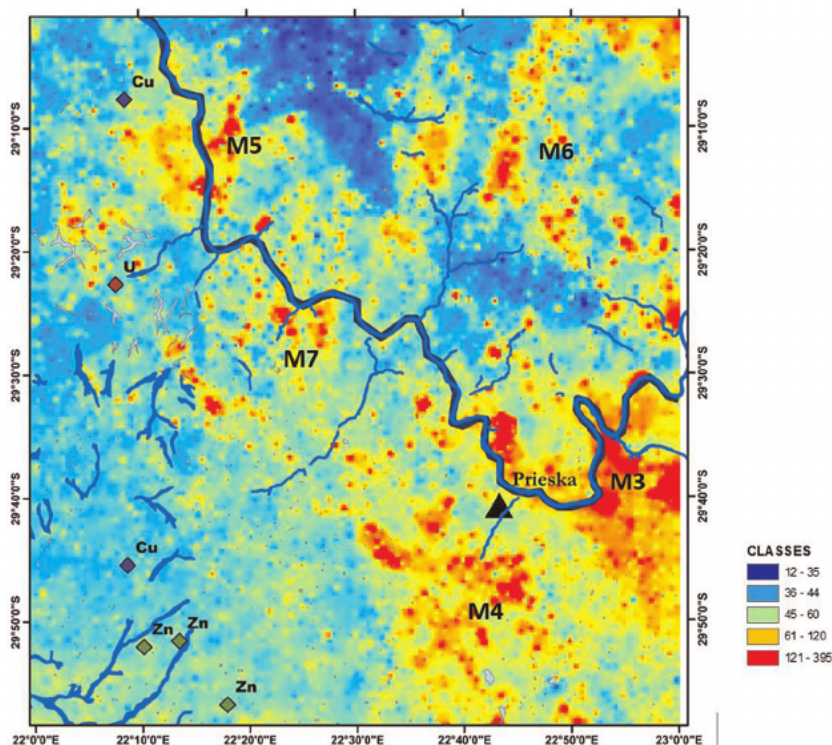


Figure 8.
The Fuzzy OR overlay multi-element map index of Co and Ni.

close vicinity with the known Cu occurrence the Co-Ni correlation may possibly indicate the Base (Cu_Zn) mineralisation. Unlike the M7 anomaly associated with Spioenkop Formation and Ongeluk lava Formation. The M6 anomaly overlay the Ongeluk Lava Formation, and Asbestos Hill.

The elements of the highest mean averages associated with the Brulsand are the Hf, Mo, Nb, Sc, Ta, and U. The Hf, Sc, Mo, Nb, and Ta are transition elements and most of are typically treated as being immobile during metamorphic processes and therefore can be useful in understanding the effects of metamorphism. U strongly correlates with Hf, Ta and Nb, and moderately correlates with Mo. The M8 potential mineralisation (Figure 9) consist of isolated cluster of potential mineralisation zones overlying the Asbestos Hills Subgroup, Koegas Group, Kalahari group, Olifantshoek Supergroup. M9 is associated with known metals occurrences; Cu and U, the isolated cluster of anomalies towards the know Prieska Copperton mine. The M9 potential mineralisation zones on the west of Orange River catchment overlies the Draghoender granite/gneiss, Skalkseput granite, Uitdraai Formation and Zeekoebaart Formation. Granitic rocks rich in pyrochlore, euxenite, brannerite, thorite yield soils rich in Nb, Ta, Ti, rare earths, Sc and Zr, are enriched in dark heavy minerals. The radioactive species originally contained in the parent rocks form a major fraction [23]. The Sc, U, Nb, and Ta are indicators of uranium-bearing minerals in granitic, syenitic, magmatitic, pegmatitic and aplitic bodies and complexes. Strauss and Elsenbroek (2006) found in a study on South African alkali and carbonatite complexes that Nb is by far the strongest and most common indicator for these complexes in soils followed by Zr.

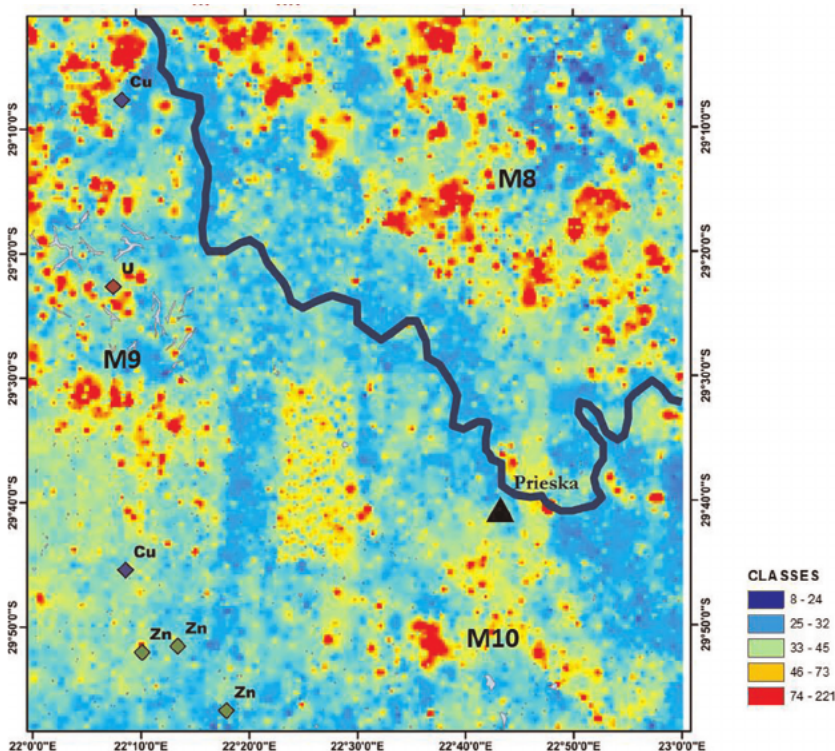


Figure 9. The Fuzzy OR overlay of Mo, Nb, Sc, Ta, and U.

3.2 Stream sediment exploration target generation: economic geology synthesis map of Prieska area

The following geochemical indices are potential target generators for the Prieska area based on the predominant geology in the area coupled with the single element distribution patterns. The Cu_Zn for VMS Zn_Cu deposit, Ni_Co_Cr ultramafic Ni_Cr (\pm Cu) deposit and Zr_Nb_U_Th_Hf-Ta for the heavy mineral placer deposits. First, new raster files for each index element is created by using of the inverse distance weighted interpolation (IDW). Then the indices were calculated using the fuzzy overlay OR function from ARCGIS, the advantage of using fuzzy OR overlay is generally provides a better result in cases where the indicator elements are not always associated and is better suited for the secondary dispersion where associated elements in the primary environment are likely to be separated.

The anomaly (**Figure 5**) delineates the known Copperton mine in Prieska area, the Copperton ore body occurs in a series of quartz-feldspar rocks quartz-biotite gneisses and quartz- plagioclase–amphibole gneisses as Copperton Volcanic Pile.

The anomaly M12 associated with Koegas Group, Ongeluk lava Formation and Asbestos Hill Subgroup (**Figure 6**) is a preferred potential target for ultramafic Ni_Cr (\pm Cu) deposit. The anomaly overlies the banded Iron Formation of the Asbestos Hill Subgroup; the Asbestos Hill Subgroup is Fe-rich. The anomaly M14 is associated with the known Cu occurrence straddles the Campbell Rand Subgroup, and Zeekoebaart Formation is the secondary target. Anomaly M13 is also identified as the secondary potential target for ultramafic Ni_Cr (\pm Cu) associated with Dwyka Group.

Zr_Nb_U_Th_Hf-Ta are high field strength elements associated with the carbonatites deposits and alkaline magmatic complexes, however the carbonatites deposits are unknown to occur around the Prieska geology area. The high field strength elements are primary indicators of the REE deposit. These elements are associated as incompatible ions, within alkaline igneous melts, which by their emplacement is controlled by the failed rift zone or deep-seated suture.

The anomalies of the Zr_Nb_U_Th_Hf-Ta (**Figure 7**) may be due to thorium in waste rock or sediment; dust from mining activities in the surrounding, and possible water contamination from spillage or leakage of chemical solutions used to leach and process ore. Asbestiform amphiboles that are present in waste dumps. The correlation of the Cu-Pb-Zn anomaly with alkali elements (Nb, Zr, Th, and U) and REEs suggests there is a possibility that the M26 –M29 anomaly are alkali-granitic genetic origin. The anomaly could therefore indicate the presence of Cu, Pb, Zn and As sulphides associated with alkali elements and REEs, which makes it a very promising target however the map (**Figure 7**) display a batch effect specifically anomaly M26 and 27, and therefore it is not suitable for interpretation.

4. Conclusions and recommendations

Prieska study area generally forms part of the Namaqua Metamorphic Province and the Griqualand-West Basin. The Kalahari Aeolian sand covers the geology on the area around Prieska Cu-Zn mine. The host sequence in the Copperton district is, from the base: Smouspan Gneiss Member, Prieska Copper Mines Member, and Vogelstruisbult Member. The aeolian sand extensively covers the research area. The secondary dispersion patterns of the elements in the stream sediments may also

destroy the primary association of elements. To overcome this difficulty, a Fuzzy OR overlay of indicator applied. Fuzzy OR generally provides a better result in cases where the indicator elements are not always associated and is better suited for the secondary dispersion where associated elements in the primary environment are likely to be separated.

The descriptive statistics (**Table 3**) results shows that the Ag, Co, Ga, Mo, Nb, Pb, Sb, Sn, Sc, Ta, Th, U, and W concentrations exhibited generally low standard deviation and coefficient of variation values, suggesting a homogenous spatial distribution. In contrast As, Ba, Ce, Cr, Cu, Hf, Nd, Ni, Rb, Sr., S, V, Zr and Zn contents showed a heterogeneous spatial distribution, reflected by high coefficient of variation and large standard deviation. The difference between the median and mean values of high coefficient of variation of the As, Ba, Ce, Cr, Cu, Hf, Nd, Ni, Rb, Sr., S, V, Zr and Zn may be attributed to the extremely high values of these trace elements.

The Fuzzy OR maps give a summary of the potential targets for mineralisation within the study area. Anomaly M1 and M2 associated with Spioenkop Formation though the anomaly does not delineate the Spioenkop Formation but Dwyka Group Sediments, Kalahari Group and Campbell Rand Subgroup. These anomaly signatures are characterised by the one or more of these elements Cu, Ga, Zn, Rb, Pb, Mo, and Ba. Barium is a powerful indicator tool of gossan and be used as an indicator for Zn–Pb deposit. The dataset shows a significant relationship between the Ba and Zn. The relationship between these elements therefore delineate M1 and M2 as potential target for VMS deposit.

The anomaly M2 in close vicinity to the Orange River Catchment, a follow-up study is therefore recommended. The Cu and Zn are generally interpreted as pollution related or may be as a result of metal dispersion from the mine waste. The Zn and Cu high concentrations are not distributed across the Prieska area, the Fuzzy OR overlay of these elements are only elevated in the known Copperton mine area and on the M2 potential VMS mineralisation target area. The anomaly M2 associated with Campbell Rand Subgroup may be as a result of metal dispersion or sourced from the parent underlying rocks.

The Pb and S are also elevated on the known Copperton mine, these elements strongly correlates with the Zn. The Pb and S are likely to be associated with the generic anthropogenic source including sewage discharge, agricultural practises and various kinds of industrial activities. M11 is definitely a VMS mineralisation target, the anomaly overlies the Copperton mine. The high Cu, Zn and Pb are derived from the ore minerals related VMS deposits. The Fe elevated concentration are derived from both primary minerals which are not directly related to the VMS or Co_Ni (\pm Cu) (illustrated in **Figures 4 and 8**) mineralisation within the study area or from ore related minerals of deposits hosted in Banded Iron formation of the Asbestos Hills Subgroup.

The Cr, Ni reflect ultramafic fraction of the stream sediments. The Ni and Cr originate from direct ophiolitic sequences erosion and the recycling of the rocks enriched in ultramafic debris. The M13 and M14 anomaly are traced along the Orange river Catchment, on the Ghaap group which occurs NW to SE of the study area and north of the Orange River Catchment. Ghaap Group consists of shale, sandstone, andesite, and dolomite, and comprised of the magnesium, carbonate-rich Formation such as Vryburg Formation. M13 and M24 potential mineralisation are possibly sourced from ultramafic debris transported from the Ghaap Group by the Orange River Catchment, however this potential target will require follow-up studies for verification. There is a very high Cu-Zn correlation coefficient calculated for samples near the Copperton deposit.

4.1 Recommendations

Indicator elements in stream sediments sample represents either mineralisation or post- mineralisation processes. The processes that affect the indicator elements distribution patterns, these process includes weathering, erosion of ore bodies and adjacent mineralised rock, contamination of pollutants, regolith, topographic gradient vegetation density and/or climate. In this study integration of mineral exploration methods such as remote sensing, geophysics and petrography are recommended, this follow-up studies will assist in determining the extent of the anomaly.

The airborne geophysics studies must be conducted over the research area. Low level airborne electromagnetic (EM) surveys over the target area (M1-M29) especially the M2 and M3 which delineate the possibility of the base metal mineralisation is recommended. The high density stream sediments sampling on the grid and a depth of at least 50 meters to minimise the effect of Aeolian sand cover must be conducted. Petrography is another important tool, to understand the mineralogy of the study area underlying rocks. The detailed analysis of minerals by optical microscopy in thin section and micro-texture and structure is recommended in order to understand the origin and history of the rock.

Remote sensing will also be advantageous in conducting geological traverses of the study area in which anomalies of one or more of the above mentioned elements occur to establish the significance of the anomalies. Remote sensing imagery will also provide information on rock composition or rock alteration which is associated with the indicative of the presence of mineral deposits. Ore deposits are localised along regional and local fracture patterns, the Landsat and radar images are used to map these fracture pattern. Using multiple tools of exploration such as geology, structures, geochemistry, and drainage pattern are recommended for use in ArcGIS as thematic layers to generate the potential mineralisation targets.

References

- [1] Bokana RN. The Lithochemical characterization of the Hondeklouf nickel mineralisation, Kliprand area, Garies terrane, Namaqualand South Africa. Cape Town, South Africa: University of the Western Cape; 2015
- [2] Cornell DH, Hawkesworth CJ, Van Calsteren P, Scott WD. Sm-Nd study of Precambrian crustal development in the Prieska-Copperton region, Cape Province. *Transactions Geological Society of South Africa*. 1986;**89**:17-28
- [3] Bailie R, Gutzmer J. Age and primary architecture of the Copperton Zn-Cu VMS deposit, Northern Cape Province. *South Africa Ore Geology Reviews*. 2011; **39**:164-179
- [4] Cornell DH, Thomas RJ, Moen HFG, Reid DL, Moore JM, Gibson RL. The Namaqua-Natal Province. In: Johnson MR, Anhaeusser CR, Thomas RJ, editors. *The Geology of South Africa*. Geological Society of South Africa, Johannesburg/ Council for Geosciences, Pretoria. *South African Journal of Geology*; 2006. pp. 325-379
- [5] Fransson M. Pb-U zircon dating of metasedimentary rocks in the Areachap, Kakamas and Bushmanland Terranes in Namaqua Province, South Africa (thesis). Göteborgs; 2008
- [6] Sithole N. A study into the main structural features of the Namaqua region and their relation to the intrusion of the Keimoes Suite. Cape Town, South Africa: University of the Western Cape; 2013
- [7] Ginsburg II. *Principles of Geochemical Prospecting*. Vol. 311. New York: Pergamon Press; 1960
- [8] Bradshaw JD, Weaver SD, Laird MG. Suspect terranes and Cambrian tectonics in northern Victoria Land, Antarctica. In: Howell DG, editor. *Tectonostratigraphic Terranes of the Circum-Pacific Region*, Earth Sci. Ser., vol. 1. Houston, Tex: Circum-Pac. Council for Energy and Miner. Resour; 1972. pp. 467-479
- [9] Fletcher WK, Lahiri R, Caughlin BL, Blok H. Use of a sensitive analytical method and the silt-clay fraction of stream sediments in exploration for gold in northern Thailand. *Journal of Geochemical Exploration*. 1995;**55**:301-307
- [10] Meyer WT, Theobald PK Jr, Bloom H. Stream Sediment Geochemistry; Geophysics and Geochemistry in the Search for Metallic Ores. In: Hood PJ, editor. *Geological Survey of Canada, Economic Geology Report*. Vol. 31. 1979. pp. 411-434
- [11] Topping NJ. Regional geochemical drainage reconnaissance in the tribal trust lands; In: Viewing KA, Tripp RB, Curtin GC, Day GW, Karlson RC, editors. *7th Annual Report, Institute Mining Res. Univ. Rhodesia*; 1976. pp. 49-51
- [12] Mayfield I. Regional geochemical drainage reconnaissance near west Nicholson. In: Viewing KA, editor. *7th Annual Report*. Rhodesia: Institute Mining Resources University; 1976. pp. 51-53
- [13] Buhlmann L, Philpott DE, Scott MJ, Sanders RN. The status of exploration geochemistry in southern Africa, in *Geochemical Exploration 1974*. Amsterdam: Elsevier Publ. Co.; 1975. pp. 51-64
- [14] Smee BW, Ballantyne SB. Examination of some Cordilleran uranium occurrences. In: Report of

Activities, Part C, Geological Survey
Canada, Paper. 76-1C. 1976. pp. 255-258

[15] Rose AW, Keith ML. Reconnaissance
geochemical techniques for detecting
uranium deposits in sandstones of
northeastern Pennsylvania. *Journal of
Geochemical Exploration*. 1976;**6**:119-138

[16] Moon CJ. *Exploration Geochemistry*.
In: Moon CJ, Whitley and MKG, Evans
AE, editors. *Introduction to Mineral
Exploration*. Second ed. Oxford:
Blackwell Publisher; 2006. p. 499

[17] Carranza EJM. *A Catchment Basin
Approach to the Analysis of
Reconnaissance Geochemical-Geological
Data from Albay province, Phillipines
(thesis)*. Delft, ITC; 1994. p. 206

[18] Reimann C, Filzmoser P, Garret RG.
Background and threshold: Critical
comparison of methods of
determination. *Science of the Total
Environment*. 2005;**346**:1-16

[19] Garret RG. The role of computers in
exploration geochemistry. In: Garland
GD, editor. *Proceedings of Exploration
87, Ontario Geological Survey*. Vol. 3.
Toronto; 1989. pp. 586-608

[20] Howarth RJ. Statistical Applications
in geochemical prospecting: A survey of
recent developments. *Journal of
Geochemical Exploration*. 1984;**21**:41-61

[21] Eriksson PG, Altermann W,
Catuneanu O, der Merwe V, Bumby AJ.
Major influences on the evolution of the
Kapaal craton. *Sedimentary Geology*.
2001;**141-142**:205-231

[22] An P, Moon WM, Rencz AN.
Application of fuzzy theory for
integration of geological, geophysical
and remotely sensed data. *Canadian
Journal of Exploration Geophysics*. 1991;
27:1-11

[23] Boyle RW. Geochemical prospecting
for thorium and uranium deposits.
Developments in Economic Geology.
1982;**16**:42

Proterozoic Newer Dolerite Dyke Swarm Magmatism in the Singhbhum Craton, Eastern India

Akhtar R. Mir

Abstract

Precambrian mafic magmatism and its role in the evolution of Earth's crust has been paid serious attention by researchers for the last four decades. The emplacement of mafic dyke swarms acts as an important time marker in geological terrains. Number of shield terrains throughout the world has been intruded by the Precambrian dyke swarms, hence the presence of these dykes are useful to understand the Proterozoic tectonics, magmatism, crustal growth and continental reconstruction. Likewise, the Protocontinents of Indian Shield e.g. Aravalli-Bundelkhand, Dharwar, Bastar, and Singhbhum Protocontinent had experienced the dyke swarm intrusions having different characteristics and orientations. In Singhbhum craton, an impressive set of mafic dyke swarm, called as Newer dolerite dyke swarm, had intruded the Precambrian Singhbhum granitoid complex through a wide geological period from 2800 to 1100 Ma. Present chapter focuses on the published results or conclusions of these dykes in terms of their mantle source characteristics, metasomatism of the mantle source, degree of crustal contamination and partial melting processes. Geochemical characteristics of these dykes particularly Ti/Y, Zr/Y, Th/Nb, Ba/Nb, La/Nb, $(La/Sm)_{PM}$ are similar to either MORB or subduction zone basalts that occur along the plate margin. The enriched LREE-LILE and depletion of HFSE especially Nb, P and Ti probably indicate generation of these dykes in a subduction zone setting.

Keywords: geochemistry, newer dolerite dykes, Singhbhum craton, India

1. Introduction

Precambrian mafic magmatism and its role in the evolution of Earth's crust has received particular attention of the geoscientists during the last three decades because it has not only been influenced by progressive secular compositional variation and mantle sources/reservoirs but also by onset of plate tectonics. Study of dykes is useful for recognition of Large Igneous Provinces (LIP) and rebuilding of different continents which may have displaced through geological time [1]. All protocontinents of India such as Aravalli-Bundelkhand, Dharwar, Bastar and Singhbhum retain dykes of varied orientations, therefore, these dykes or dyke swarms represent a main thermal episode during the Proterozoic or Precambrian times [2]. Geochemical and isotope studies of these dykes offer an opportunity in understanding the geochemical evolution of mantle through space and time [3, 4].

Singhbhum Craton is a book that records complex geological and tectonic processes from Paleoproterozoic to Neoproterozoic [5, 6]. Several dykes of mafic to acidic compositions are intruding the Singhbhum Granitoid Complex, which are collectively referred to as the Newer dolerites dykes (NDD) in the geological literature [7, 8]. Being the latest magmatic episode of the Singhbhum Granitoid Complex, Newer dolerite dykes provide the path in understanding the Proterozoic geodynamic evolution of the Singhbhum Craton [9]. The present work contributes in understanding the mantle source characteristics and tectonic setting of the NDD.

2. General geology

Mahanadi Graben and Sukinda thrust borders the Eastern Indian shield in the west and granulite terrain of Eastern Ghats along with recent alluvium surrounds this shield in the south, whereas, Gangetic alluvium and Quaternary sediments of Bengal basin exist in north and east of this shield (**Figure 1**). The major divisions of this shield includes: Chotanagpur Granite Gneiss Complex, Singhbhum Mobile Belt and Singhbhum Craton. The general geological features of each of the above geological provinces are briefly discussed in the following sections.

2.1 Chotanagpur granite gneiss complex

Chotanagpur Granite Gneiss Complex (CGCC) exists in West Bengal and Jharkhand states of India and covers an area of about 80,000 km² (Latitudes 23°00'N to 25°00'N; Longitudes 83°45'E to 87°45'E). It is mostly made of granites, granite-gneisses, migmatites, dolerite dykes and pegmatite, aplite and quartz veins. From the structural patterns, worked out in different parts of the CGGC, it is clear that the region has undergone polyphase deformation producing distinctive folds and related linear fabrics [8].

2.2 Singhbhum mobile belt

The formations occurring in between the Singhbhum Granitoid Complex (SGC) and CGGC are collectively recognized either as the Singhbhum Mobile Belt (SMB) or Singhbhum Group. The SMB (**Figure 2**), has been divided into five litho-stratigraphic domains from north to south [11, 12] like (a) volcano-sedimentary belt, (b) Dalma metavolcanic belt, (c) Chaibasa and Dhalbhum Formations, (d) the rocks occurring in the SSZ and (e) Dhanjori and/or the Ongarbira metavolcanic rocks.

2.3 Singhbhum craton

The Singhbhum Craton (SC) records a long history of crustal evolution from Mesoarchean to Mesoproterozoic. It is an extensive terrain of granite and gneissic complex with subordinate metabasic and minor metasedimentary rocks (**Figure 2**). Some important geological units are briefed below:

2.3.1 Older metamorphic group

Older Metamorphic Group (OMG) occurs near Champua (Latitudes 22°04'N; Longitudes 85°40'E) and as enclaves in the SGC. This group had experienced amphibolite facies metamorphism and is made of pelitic schists, garnetiferous quartzite, calc-magnesian metasediments and sill like mafic rocks [5]. Goswami

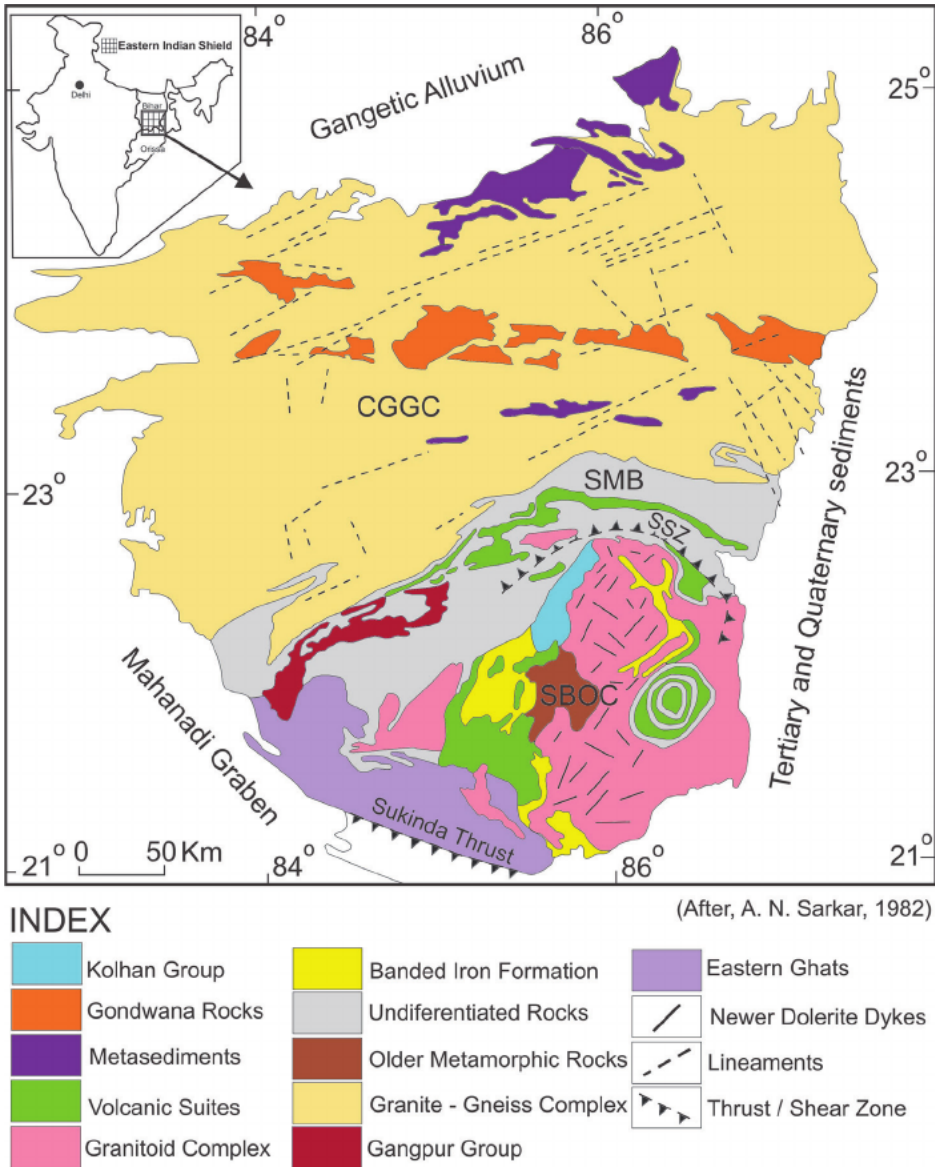


Figure 1. Simplified geological map of eastern Indian shield illustrating the three geological provinces viz. Chotanagpur granite gneiss complex (CGGC), Singhbhum Mobile Belt (SMB) and Singhbhum craton (SC). SSZ – Singhbhum shear zone [9].

et al. [13] and Mishra [14], have dated detrital zircons and recognized an older limit of 3.5Ga age for these supra-crustals. On the bases of Pb/Pb whole rock dating, Moorbath and Taylor [15] has established 3378 ± 98 Ma age for these supra-crustals. This age matches with Sm/Nd (TDM model) ages of 3.41, 3.39 and 3.35 Ga [15]. Sharma et al. [16], however, pointed out that protoliths of OMG amphibolites are 3305 ± 60 Ma old and therefore OMTG which intrude OMG cannot be older than 3300 Ma. The younger 3.40, 3.35 and 3.20 Ga ages have been interpreted as metamorphic events [17, 18].

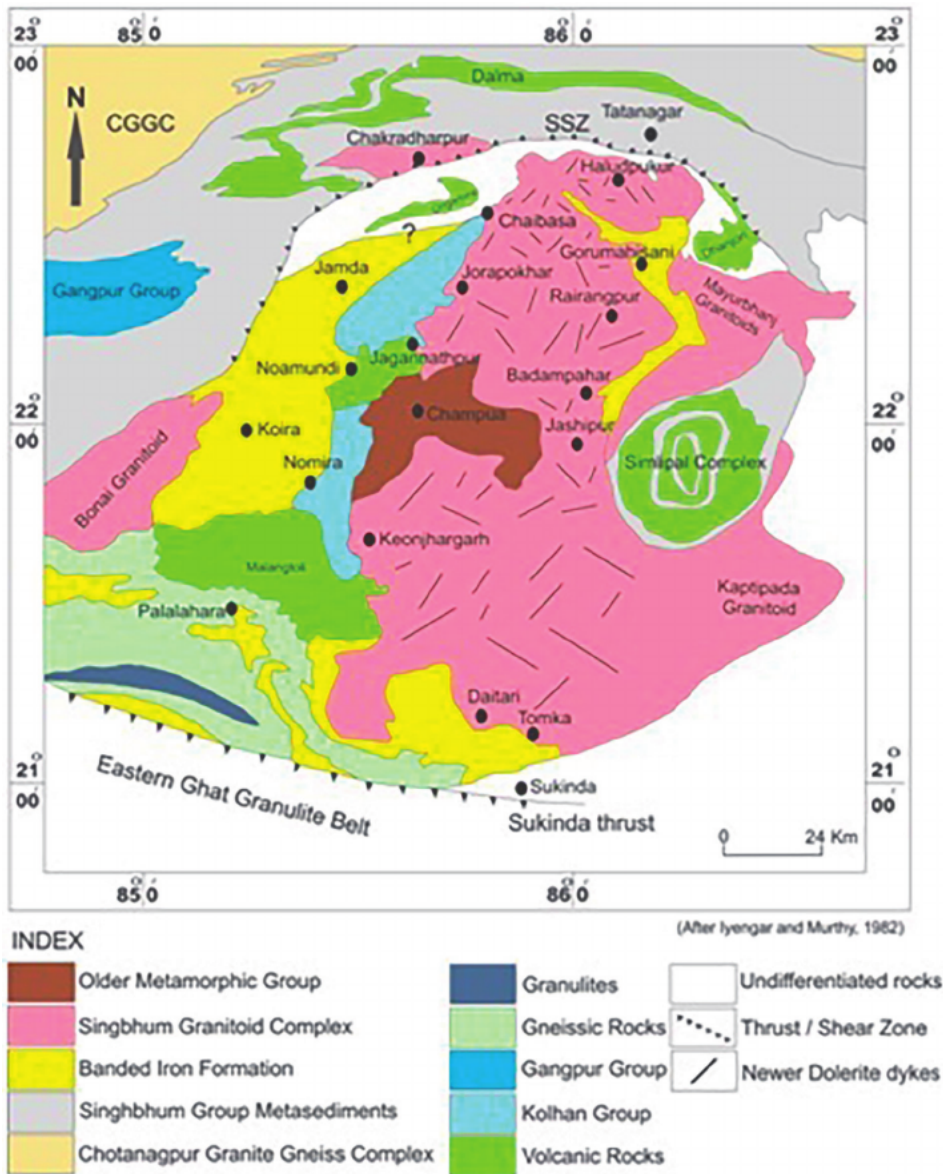


Figure 2. Simplified geological map of the Singhbhum craton [10].

2.3.2 Singhbhum granitoid complex

It has been suggested that SGC (Latitudes 21°00' and 22°45' N; Longitudes 85°30' and 86°30' E) is composed of 12 distinct units that were emplaced in three successive magmatic phases [5]. The K-poor, granodiorite trondhjemite early (phase I) has been dated as 3.25 ± 0.05 Ga [19]. The II and III phases are made of granodiorite that grade to monzogranite and granite and these phases are dated as 3.06 Ga (Pb/Pb whole rock) and 2.9 Ga (Rb/Sr whole rock) respectively [5]. The other granitic bodies that occur in

SC show ages similar to that of SGC, for example, Bonai granites (3369 ± 57 Ma) [20] and Katipada tonalite (3275 ± 81 Ma) [21]. Recent U–Pb zircon studies have revealed that rocks of the SG batholith were emplaced between ~ 3.45 Ga and ~ 3.32 Ga [22].

2.3.3 Banded iron formations

BIF is considered to have been deposited in three interconnected basins [5]. These basins are: (i) Noamundi (Latitudes $22^{\circ}09'N$: Longitudes $85^{\circ}31'E$) – Koira (Latitudes $21^{\circ}54'N$: Longitudes $85^{\circ}15'E$) basin of west Singhbhum district and Keonjhar, (ii) Gorumahisani (Latitudes $22^{\circ}18'30'N$: Longitudes $86^{\circ}17'E$) – Badampahar (Latitudes $22^{\circ}04'N$: Longitudes $86^{\circ}07'E$) basin along the eastern border of the Singhbhum Granitoid Complex and (iii) Daitari-Tomka basin in the southern parts of the Singhbhum Craton. In the Noamundi–Koira BIF, rocks are made up of shale, phyllite, the middle formation of banded hematite jasper and an upper formation of magniferous shale, chert, manganese formation and shale. A granite body intruding BIF near Sulaipat has been dated as 3.12 ± 0.01 Ga [23]. Some mafic and ultramafic rocks referred to as Gorumahisani Greenstones are associated with this Gorumahisani-Badampahar BIF sequence [24].

2.3.4 Bonai volcanic suite

Bonai volcanics show sub-aerial and sub-marine features in the west and east parts of its extension respectively [24, 25]. These volcanics are made of mafic rocks, tuffs and subordinate silica volcanic clastic interbeds. It has been inferred that these volcanics show island arc basalt characteristics [24].

2.3.5 Jagannathpur volcanic suite

These volcanics are exposed around Noamundi upto Jagannathpur and are younger than BIF of Noamundi-Koira belt [24]. Significantly, NDD are not cutting across the Jagannathpur Suite. It, therefore, appears that it is either equivalent in age or younger than the NDD. Alvi and Raza [26] found these to be calc-alkaline basalts and suggested that these lava flows represent an early arc volcanism. The Jagannathpur lavas have been dated around 1629 ± 30 Ma by K/Ar method [5] and 2250 ± 81 Ma by Pb/Pb whole rock isochron method [27].

2.3.6 Gorumahisani volcanic suite

It is associated with Gorumahisani-Badampahar BIF along the eastern border of SBGC. The rocks of this volcanic suite are intruded by Kumhardubi (Latitude $22^{\circ}17'N$: Longitude $86^{\circ}19'30''$) - Dublarbera (Latitude $22^{\circ}29'30''N$: Longitude $86^{\circ}17'E$) gabbro-anorthosite, Rangamatia (Latitude $22^{\circ}29'15''N$: Longitude $86^{\circ}17'30''E$) Leucotonalite, Katupith (Latitude $22^{\circ}18'N$: Longitude $86^{\circ}17'30''E$) Leucogranite and NDD swarm.

2.3.7 Simlipal complex

Recently Kar et al. [28] suggested that the circular shape of Simlipal complex is only a topography controlled rather than an existence of alternate bands of mafic volcanic and quartzites. Further, they suggested that the Simlipal complex overlies the weakly metamorphosed basement heterolith unit (Lulung Formation) which is overlain by Barehipani Formation and Jurunda Formation. Paleoproterozoic age for this complex has been given by Saha [5]. Further, Iyengar et al. [29] suggested 2084 ± 70 Ma age for Simlipal complex by following the Rb–Sr whole rock method.

2.3.8 Kolhan group

This group exists on the western margin of the SBC and its length is around 100 km with a width of about 12 km. Saha [5] correlated Chaniakpur-Keonjhar, Mankarchua and Sarpalli-Kamakhyanager formations with Kolhan Group. The Singhbhum granite Basement, Dongoaposi (Jagannathpur) lavas and the Iron Group surround Kolhan basin on the NE, S-SE and west respectively [30]. The Kolhan shales north of Hat Gamaria are intruded by three parallel sills of the NDD. South west of Jagannathpur, flat lying Kolhan shales overlie the Jagannathpur lava.

3. Petrography

NDD have experienced low grade regional metamorphism in the vicinity of Singhbhum Shear Zone, however they are fresh to least effected in the western and central parts of the Singhbhum Granitoid Complex. NNE–SSW trending ultramafic-mafic dyke exposed near Keshargaria is medium to coarse grained rock with green to dark green color. The ultramafic dykes which consist of olivine (25–52%) and pyroxenes (45–65%) are present. Mafic dykes are mainly massive, sometimes coarse grained and their color varies from black to greenish gray. The essential constituents of dolerite type of dykes includes pyroxenes, plagioclases and quartz with little amphiboles. Clinopyroxene is mainly augite in the form of euhedral to subhedral prismatic phenocrysts and also as granular aggregates in the groundmass. Rarely, clinopyroxene shows alteration to pale-green amphibole and/or biotite around the grain boundaries. Quartz (0.5 to 3%) is present as subhedral to anhedral crystals. Accessory minerals are opaques, apatite, and rutile. Opaque minerals (0.5 to 5%) include magnetite and Cr-Spinel. Norite samples consist dominantly orthopyroxene (hypersthene) and plagioclase (labradorite) together with subordinate diopsidic augite and small amounts of quartz. In Quartz dolerites relatively greater proportion of anhedral quartz is noticed. The major constituents in quartz dolerite are calcic plagioclase, clinopyroxene (diopside-augite) and subordinate amount of orthopyroxene (hypersthene, enstatite). Coarse grained gabbroic variety of the NDD is mostly coarse grained dark colored. Under microscope, they show overall hypidiomorphic texture with local development of subophitic texture. They show subhedral laths of labradorite plagioclase and augite. Orthopyroxene is rarely found within this petrographic variant.

4. Geochemistry

While observing geochemical characteristics, NDD have been classified as (i) ultramafic dykes {having MgO >30.0 wt. %, SiO₂ < 45.0 wt. %, Al₂O₃ < 5.0 wt. % and alkalis <1.0 wt. %}; (ii) Group I dykes {having MgO 12–22 wt. %, SiO₂ 45–53 wt. %, Al₂O₃ < 11.0% and total alkalis <3.0%}; (iii) Group II dykes {having MgO 7.0–19.0 wt.%, SiO₂ 51–60 wt. %, Al₂O₃ 10–12 wt. % and alkalis 1.0–3.50 wt. %}; (iv) Group III {having MgO 6.0–12 wt. %, SiO₂ 51.0–70.0 wt. %, Al₂O₃ 10.0–12.5 wt. % and total alkalis 2.0–4.5 wt. %}. Group I dykes contain lower MgO and MnO and higher SiO₂, TiO₂, Al₂O₃, P₂O₅ and alkalis as compared to Ultramafic dykes. Group II contains high TiO₂, Fe₂O₃, MgO and P₂O₅ contents and lower SiO₂ and Alkalis relative to group III dykes. In Total Alkali-Silica relationships the NDD show chemical variation from

ultramafic to dacite through basalt and basaltic andesite (Figure not shown). Some samples show chemical features like $\text{MgO} > 8\%$, $\text{SiO}_2 > 52\%$, $\text{TiO}_2 \leq 0.5\%$ and $\text{CaO}/\text{Al}_2\text{O}_3 < 1$ similar to that found in boninitic rocks [31–34].

In under investigated samples Mg\# ($\text{Mg\#} = \text{molar } 100 \text{ Mg}/(\text{Mg} + \text{Fe}_{\text{total}})$) show variation like 89–85, 79–64, 80–43 and 74–49 in ultramafic dykes, group I, II and III dykes respectively. Such a change in Mg\# is consistent with the fractional crystallization of ferromagnesian minerals [35]. The presence of normative quartz content in studied dolerite samples (excluding ultramafic samples) having $\text{Mg\#} > 70$ may indicate their derivation from multiple parental magmas. Mir and Alvi, [36] have suggested more investigation in terms of isotope geochemistry and radiometric data of ultramafic dykes from Keshergarya village, Singhbhum craton. They suspect their relationship with the mafic members of the NDD. Tholeiitic and calc-alkaline trends are commonly based on AFM ternary plot ($A = \text{Na}_2\text{O} + \text{K}_2\text{O}$, $\text{FeO}^* = \text{total iron as FeO}$, and $M = \text{MgO}$) [37]. In AFM diagram the NDD show tholeiitic trend. Ultramafic dykes concentrate towards MgO corner of AFM diagram (Figure 3).

During the partial melting or fractional crystallization the transitional elements like Nickel (Ni) and Cobalt (Co) are compatible with olivine whereas Scandium (Sc), Chromium (Cr) and Vanadium (V) are compatible with clinopyroxene [39], hence these elements are important in petrogenetic studies of basic rocks. These elements are useful to demarcate the primary nature of magma as it has been noted that primary mid ocean ridge basalt (MORB) magmas retain high concentration of Ni ($> 250\text{--}400$ ppm), Cr (> 600 ppm) and $\text{Mg\#} > 70$ [35]. Mg\# , Ni & Cr varies like {(85–89, 150–304 & 560–2458), (64–79, 45–145 & 255–733), (43–80, 9–73 & 31–524), (49–74, 17–43 & 42–226)} respectively in concern ultramafic dykes, group I, II and III mafic dykes. Such geochemical observations infer that the samples with low Mg\# , Cr and Ni values may have evolved through fractional crystallization of olivine and pyroxene [35]. Further, it has been suggested that some dyke samples having similar Mg\# with distinct Ni and Cr contents and some samples having distinct Mg\# with similar Ni and Cr contents indicates that either the diverse extents of partial melting of the same source or heterogeneous mantle sources are responsible for the generation of different phases of

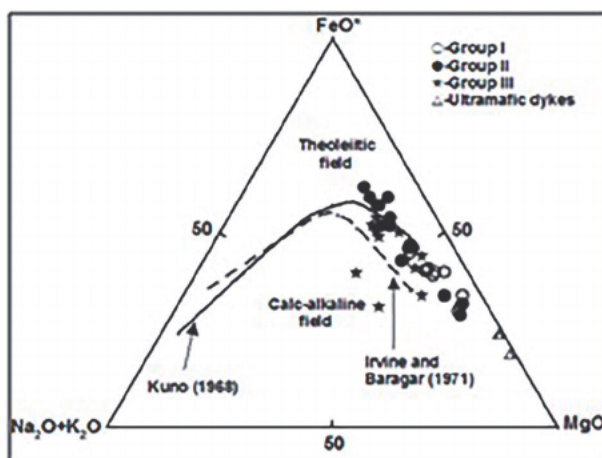


Figure 3. $\text{K}_2\text{O} + \text{Na}_2\text{O}-\text{Fe}_2\text{O}_3-\text{MgO}$ (AFM) diagram showing tholeiitic trend of NDD. Field lines are after Kuno [37] and Irvine and Baragar [38].

the Newer dolerite dykes. Ti/V values ranging from 20 to 50 indicates the low oxygen fugacity (fO_2) i.e. reduced condition of magma generation like MORB setting whereas Ti/V values ranging from 10 to 20 are markers of high fO_2 i.e. oxidizing condition of magma generation like subduction zones or supra-subduction zones settings [40]. In concern Newer dolerite dykes, Ti/V values range from 14 to 30, 9–29, 10–34 and 14–32 in ultramafic dykes, group I, II and III dykes respectively which indicates generation of melts for these dykes had occurred under varied oxidizing conditions.

Mafic intrusions in subduction environments are important for deciphering interaction between subduction slabs and mantle. Such interactions usually result in the mantle wedge being enriched in LILE by introduction of fluids and /melts from the converging lithosphere [41]. Both fluids and melts can be introduced at different depths above a

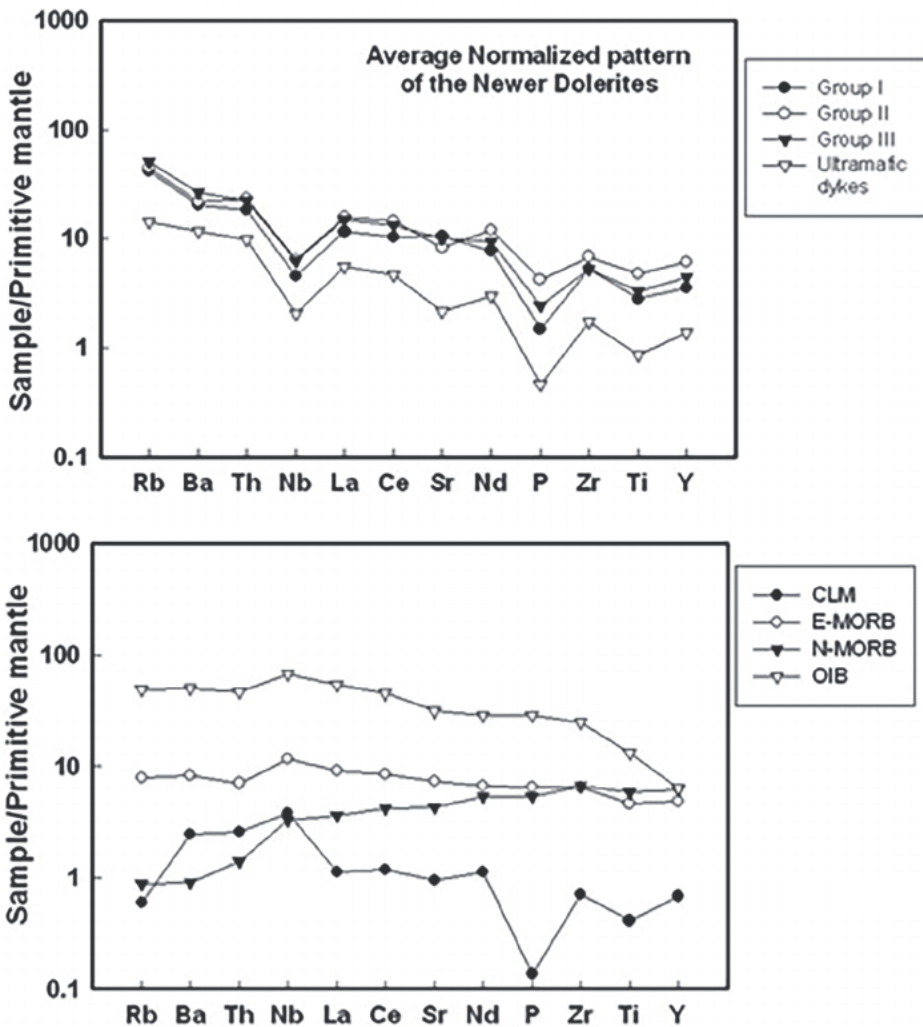


Figure 4. Primitive mantle normalized multi-element spider diagram of NDD. Normalized values are after Sun and McDonald [43]. CLM- continental lithospheric mantle; E-MORB-enriched mid ocean ridge basalts; N-MORB-Normal mid ocean ridge basalts; OIB-Ocean island basalts.

subduction zone [41]. Thus, mafic rocks across subduction zone environments may record variable degrees of mantle source modification by slab derived components [41].

The studied NDD have low K/Rb ratios up to 320 perhaps suggesting the source region of the Newer Dolerites experienced fluid modification [41, 42]. The ratios of elements such as Barium (Ba), Thorium (Th), Zirconium (Zr) and Niobium (Nb) are useful to know about the subduction zone related metasomatism of mantle, hence the values of Ba/Th, Ba/Zr & Ba/Nb in ultramafic dykes, group I, II and III dykes range like {(59–197, 3–6 & 38–119), (35–365; 1–5 & 18–195), (34–231, 1–6 & 10–76) and (37–228, 2–14 & 20–106)} respectively. Such values are higher than that of the average values of the continental crust which in turn points towards the subduction zone related metasomatism of mantle source of these rocks [42]. Two alternative processes could explain the negative Nb anomaly (**Figure 4**) observed in the NDD: (i) metasomatic enrichment of lithospheric mantle [44] and (ii) chemical interaction between lithospheric mantle and asthenosphere-derived magma having incompatible elements but little Nb [45]. However, high La/Nb and La/Ta of Newer dolerite dykes supports the metasomatic enrichment of lithospheric mantle as a reason for Nb anomalies. Hence, the negative anomalies of Nb and Ti on primitive mantle normalized patterns (**Figure 4**) [42], abundance of light rare earth elements (LREE) (Figure not shown), nearly flat sub-parallel pattern of heavy rare earth elements (HREE) (Figure not shown), chondrite normalized ratio of Lanthanum to Ytterbium ($La/Yb_N < 12.0$) and chondrite normalized ratio of Lanthanum to Samarium ($La/Sm_N < 4.0$) of concern NDD supports their affiliation with arc or subduction zone setting [46].

5. Petrogenesis

The petrogenesis of mantle derived magmatic rocks can commonly be traced by their geochemical and isotopic data. The mafic magmatic activity in the form of dykes at intervals throughout the Proterozoic provides a useful window to monitor mantle evolution [47, 48].

From the mentioned geochemical characteristics, it may be inferred that the NDD having $Mg\# < 60$ are evolved members that have been formed through fractional crystallization of Mg-rich minerals like olivine and/or pyroxene [49]. On TiO_2 vs. Al_2O_3/TiO_2 (**Figure 5a**) and CaO/TiO_2 diagrams (**Figure 5b**) NDD plot in MORB, low TiO_2 boninite & high-Mg andesite fields which suggests the compatibility of Ti and retention of Al and Ca in residual phases like pyroxenes, garnet, plagioclase and spinel [50]. Further, these relationships indicate that low TiO_2 samples were derived from relatively more hydrously fractionated magmas and high TiO_2 samples were derived from least hydrously fractionated magmas [51].

Fractional crystallization associated with crustal contamination (AFC) is an important process during magma evolution that may modify both elemental and isotopic compositions [52]. As we know that the concentration of Rubidium (Rb), Barium (Ba), Potassium (K), Sodium (Na) etc. is rich in crustal materials whereas P_2O_5 and TiO_2 is poor in these materials. Hence, any crustal contamination of mafic magma changes the primary geochemistry of magma accordingly [41]. However, in concern samples the low content and range of K_2O and NaO_2 are indications of least crustal contamination in these rocks. In addition to this, the ratio of Cerium to Lead (Ce/Pb) and Niobium to Uranium (Nb/U) are not changed due to partial melting, hence, these ratios can be applied to know about the effects of alteration or crustal

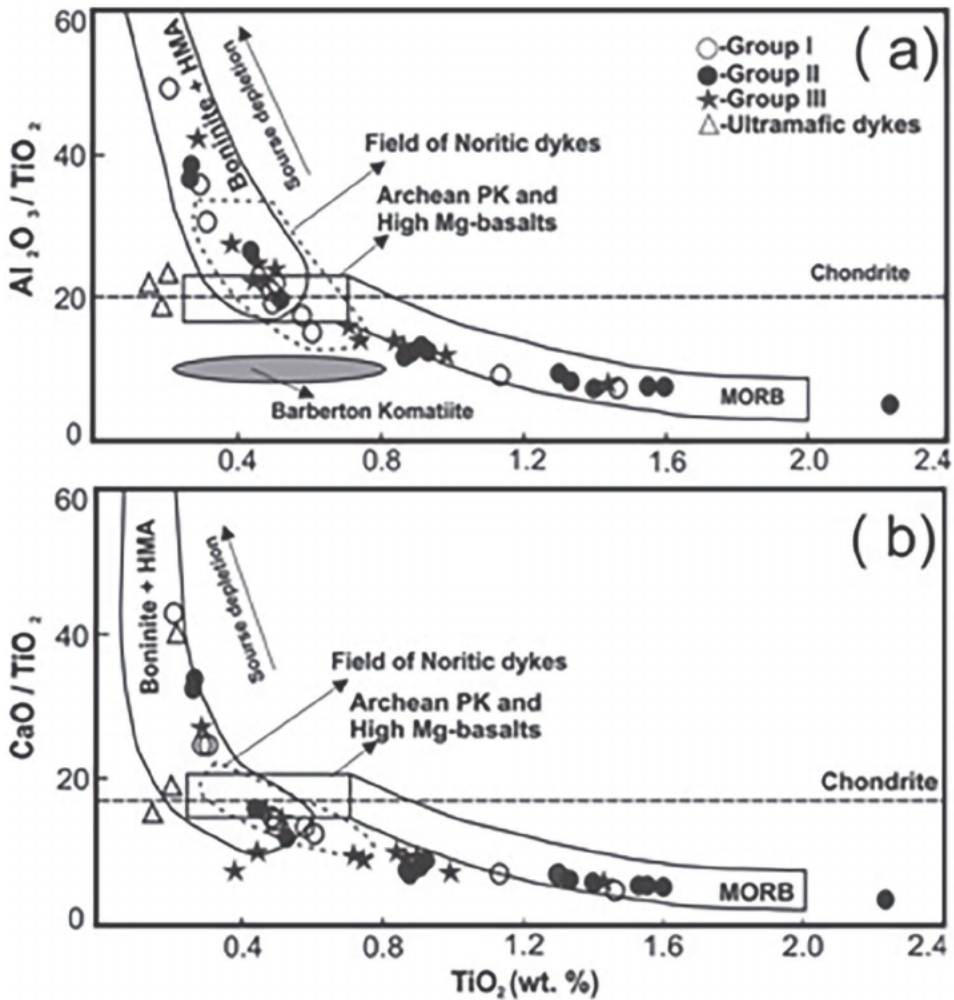


Figure 5. (a) TiO_2 vs. Al_2O_3/TiO_2 and (b) TiO_2 vs. CaO/TiO_2 binary diagrams for NDD. HMA-high Mg Andesites and MORB-Mid Ocean ridge basalts.

contamination of mafic rocks. In concern samples these ratios are higher than that of upper continental crust ($Ce/Pb = 3.2$) and ($Nb/U = 9$) [53]. Therefore, it is suggested that the investigated NDD have least or no contamination of crustal materials.

Trace element ratios, such as La/Yb , Th/Yb , Ba/La and La/Nb are widely used to identify the metasomatic agents and estimate the flux from the subducted slab [54]. All these ratios in case of NDD imply varying inputs of sediment and fluid components from the subducting slab in their formation.

The high $(La/Yb)_N$ and $(Gd/Yb)_N$ in combination with relatively low HREE abundance of the NDD suggest that they may have formed by low degrees of partial melting of a garnet bearing source. Asthenospheric or deep or plume and lithospheric or shallow or non-plume derived mafic melts or basalts can be differentiated or evaluated by geochemical ratios like Lanthanum (La) /Tantalum (Ta) and La/Nb . Thompson and Morrison [55] suggested that values of $La/Ta = 10-12$ and $La/Ta > 30$ indicates that basaltic rocks may have been derived from asthenospheric mantle and lithospheric

mantle respectively. Further, Wang et al. [56] used La/Nb ratio to discriminate asthenospheric mantle and lithospheric mantle sources. They suggested La/Nb <1.5 for asthenospheric mantle derived mafic rocks and La/Nb >1.5 for lithospheric mantle derived mafic rocks. In majority of NDD it has been seen that La/Ta is greater than 30 and La/Nb is greater than 1.5 that reveals their derivation may be from lithospheric mantle source. Moreover, on primitive mantle-normalized multi-element diagram (**Figure 4**), NDD show patterns differed from that of normal mid ocean ridge basalts, enriched mid ocean ridge basalts, ocean island basalts and continental lithospheric mantle and show depletion of Ba, Nb, Sr., P, Ti and richness of Zr. Such geochemical characteristics are similar to that found in arc or back-arc extension basalts [57, 58].

6. Tectonic setting

Keeping in view the importance of dykes or dyke swarms in identification of large igneous provinces, reconstruction of continents, continental rifting and continental-continental collision events [59], the geochemical studies on NDD may have potential in understanding the geodynamic evolution of Singhbhum craton in Precambrian times. The association of mafic dykes with the initiation of sedimentary basins and their geochemistry retaining long term memories of subduction processes in the lithosphere mantle are too well known [60]. Origin of NDD has been either related to arc/back-arc tectonic setting i.e. non-plume source [42, 61–66] or plume source [5, 67]. In addition, Boss [68] suggested both depleted and enriched mantle source for Newer dolerite dykes. However, mantle plume model faces some issues in evaluation of origin of the NDD due to following reasons (i) age of NDD varying from 2800 to 1000 Ma [5, 69, 70] suggests that it is hard to tap a uniform magma source for such a long time interval, (ii) absence of large scale mafic lavas in Singhbhum craton having intraplate setting/geochemistry and (iii) further, the occurrence of voluminous hydrous lithospheric mantle across the cratons developed during the Archaean (~3 Ga) and its role in the Proterozoic magmas [48].

7. Conclusions

Reported age of newer dolerite dykes vary from 900 Ma to 2800 Ma and traverse a number of rock types in some regular sets like NNE–SSW and NW-SE trends. Variations in major elements, particularly SiO₂, Al₂O₃, CaO, TiO₂ contents, and CaO/TiO₂ and Al₂O₃/TiO₂ ratios in these dykes indicates that their Ca and Al are held in the residual mantle phases such as clinopyroxene, plagioclase, spinel and garnet. The overall low Mg #, Cr and Ni values in studied NDD indicate their evolution through fractional crystallization of olivine and pyroxene. A few dyke samples having similar Mg# with distinct Ni and Cr contents and some samples having distinct Mg# with similar Ni and Cr contents indicates that either the diverse extents of partial melting of the same source or heterogeneous mantle sources are responsible for the generation of different phases of the Newer dolerite dykes. In studied NDD low content and narrow range of K₂O and NaO₂ in addition to higher values of Ce/Pb and Nb/U than that of upper continental crust are indications of least crustal contamination in these rocks.

Values of Ba/Th, Ba/Zr & Ba/Nb in NDD are higher than that of the average values of the continental crust which in turn points towards the subduction zone related

metasomatism of mantle source of these rocks. Further, the enriched LREE and flat sub-parallel pattern of HREE along with $La/YbN < 12.0$ and $La/SmN < 4.0$ of concern NDD supports their affiliation with arc or subduction zone setting. Moreover, their primitive mantle-normalized multi-element patterns differed from that of normal mid ocean ridge basalts, enriched mid ocean ridge basalts, ocean island basalts and continental lithospheric mantle and show depletion of Ba, Nb, Sr, P, Ti and richness of Zr. Such geochemical characteristics are similar to that found in arc or back-arc extension basalts.

Acknowledgements

Author is sincerely thankful to the Director, Leh Campus Taru, University of Ladakh for providing facilities in preparation of this book chapter. Author pays thanks to Dr. Malik Zubair A. and Dr. Farooq A. Dar for their valuable suggestions during write up of this book chapter. Constructive comments and valuable suggestions from anonymous reviewers are duly acknowledged.

References

- [1] Bryan SE, Ernst RE. Revised definition of large igneous provinces (LIPs). *Earth Science Review*. 2008;**86**:175-202
- [2] Srivastava RK, Sivaji C, Chalapathi Rao NV. Geochemistry, geophysics and geochronology. In: Srivastava RK, Ch S, Chalapathi Rao NV, editors. *Indian Dykes*. New Delhi: Narosa Publishing House Pvt. Ltd.; 2008. p. 626
- [3] Tarney J. Geochemistry and significance of mafic dyke swarms in the Proterozoic. In: Condie KC, editor. *Proterozoic Crustal Evolution*. Elsevier: Amsterdam; 1992. pp. 151-179
- [4] Hall RP, Hughes DJ. Early Precambrian crustal development: Changing styles of mafic magmatism. *Journal of the Geological Society of London*. 1993;**150**:625-635
- [5] Saha AK. Crustal evolution of Singhbhum-North Orissa, Eastern India. *Memoir, Geological Society of India*. 1994;**27**:341
- [6] Majumdar R, Bose PK, Sarkar S. A commentary on the tectono-sedimentary record of the pre-2.0 Ga continental growth of India Vis-à-Vis a possible pre-Gondwana afro-Indian supercontinent. *Journal of African Earth Sciences*. 2000;**30**:201-217
- [7] Dunn JA. The stratigraphy of south Singhbhum. *Memoir, Geological Survey of India*. 1940;**63**(3):303-369
- [8] Mahadevan TM. *Geology of Bihar and Jharkhand*. Text Book Series. Bangalore: Geological Society of India; 2002. p. 563
- [9] Sarkar AN. Precambrian tectonic evolution of eastern India: A model of converging microplates. *Tectonophysics*. 1982;**86**:363-397
- [10] Iyengar SVP, Murthy YGK. The evolution of the Archaean-Proterozoic crust in parts of Bihar and Orissa, eastern India. *Records, Geological Survey of India*. 1982;**112**:1-5
- [11] Sarkar SC, Gupta A, Basu A. North Singhbhum Proterozoic mobile belt, eastern India: Its character, evolution and metallogeny. In: Sarkar SC, editor. *Metallogeny Related to Tectonics of the Proterozoic Mobile Belts*. Calcutta: Oxford and IBH Publishing Co.; 1992. pp. 271-305
- [12] Gupta A, Basu A. North Singhbhum Proterozoic mobile belt eastern India-a review. *Special Publication, Geological Survey of India*. 2000;**55**:195-226
- [13] Goswami JN, Mishra S, Wiedenbeck M, Ray SL, Saha AK. 3.55 Ga old zircon from Singhbhum-Orissa iron ore craton, eastern India. *Current Science*. 1995;**69**:1008-1011
- [14] Misra S. Precambrian chronostratigraphic growth of Singhbhum-Orissa craton, eastern Indian shield: An alternative model. *Journal of the Geological Society of India*. 2006;**67**:356-378
- [15] Moorbath S, Taylor PN. Early Precambrian crustal evolution in eastern India: The ages of the Singhbhum granite and included remnants of older gneiss. *Journal of the Geological Society of India*. 1988;**31**:82-84
- [16] Sharma M, Basu AR, Ray SL. Sm-Nd isotopic and geochemical study of the Archaean tonalite-amphibolite association from the eastern Indian craton. *Contribution to Mineralogy & Petrology*. 1994;**117**:45-55

- [17] Mishra S, Deomurari MP, Wiedenbeck M, Goswami JN, Ray S, Saha AK. 207Pb/206Pb zircon ages and the evolution of the Singhbhum craton, eastern India: Anion microprobe study. *Precambrian Research*. 1999;**93**:139-151
- [18] Upadhyay D, Chattopadhyay S, Kooijman E, Mezger K, Berndt J. Magmatic and metamorphic history of Paleoproterozoic Tonalite-Trondhjemite-granodiorite (TTG) suite from the Singhbhum craton, eastern India. *Precambrian Research*. 2014;**252**:180-190
- [19] Moorbath S, Taylor PN, Jones NW. Dating the oldest terrestrial rocks – Facts and fiction. *Chemical Geology*. 1986;**57**:63-86
- [20] Sengupta S, Paul DK, De Laeter JR, McNaughton NJ, Bandyopadhyay PK, De Smeth JB. Mid-Archaean evolution of the eastern Indian craton: Geochemical and isotopic evidence from the Bonai pluton. *Precambrian Research*. 1991;**49**:23-37
- [21] Vohra CP, Dasgupta S, Paul DK, Bishoi PK, Gupta SN, Guha S. Rb-Sr chronology and petrochemistry of granitoids from the southeastern part of the Singhbhum craton, Orissa. *Journal of the Geological Society of India*. 1991;**38**:5-22
- [22] Dey S, Topno S, Liu Y, Zong K. Generation and evolution of Palaeoproterozoic continental crust in the central part of the Singhbhum craton, eastern India. *Precambrian Research*. 2017;**298**:268-291
- [23] Chakraborty KL, Majumder T. Geological aspects of the banded Iron formation of Bihar and Orissa. *Journal of the Geological Society of India*. 1986;**31**:305-313
- [24] Banerjee PK. Stratigraphy, petrology and geochemistry of some Precambrian basic volcanic and associated rocks of Singhbhum district, Bihar and Mayurbhanj and Koenjhar districts, Orissa. *Memoir, Geological Survey of India*. 1982;**111**:58
- [25] Bose MK. Precambrian picritic pillow lavas from Nomira, Koenjhar, Eastern India. *Current Science*. 1982;**51**:677-684
- [26] Alvi SH, Raza M. Nature and magma type of Jagannathpur volcanics, Singhbhum, eastern India. *Journal of the Geological Society of India*. 1991;**38**:524-531
- [27] Misra S, Johnson PT. Geochronological constraints on evolution of the Singhbhum Mobile belt and associated basic volcanics of eastern Indian shield. *Gondwana Research*. 2005;**8**:129-142
- [28] Kar A, Ray J, Sinha S, Kar R, Manikyamba C, Paul M, et al. Geology of the Simlipal Volcano-Sedimentary Basin of Singhbhum revisited: A simplistic interpretation. *Journal of the Geological Society of India*. 2022;**98**:329-334
- [29] Iyengar SVP, Chandy KC, Narayanaswamy R. Geochronology and Rb-Sr systematics of the igneous rocks of the Simlipal complex, Orissa. *Indian Journal of Earth Science*. 1981;**8**:61-65
- [30] Mukhopadhyay J, Ghosh G, Nandi AK, Chaudhuri AK. Depositional setting of the Kolhan group: Its implications for the development of a Meso to Neoproterozoic deep-water basin on the south Indian craton. *South African Journal of Geology*. 2006;**109**:183-192
- [31] Srivastava RK. Geochemistry and petrogenesis of Neoproterozoic high-Mg low-Ti mafic igneous rocks in an intracratonic setting, Central India craton: Evidence for boninite

- magmatism. *Geochemical Journal*. 2006;**40**:15-31
- [32] Srivastava RK. Global Intracratonic Boninite-Norite magmatism during the Neoproterozoic: Evidence from the central Indian Bastar craton. *International Geology Review*. 2008;**50**:61-74
- [33] Subba Ra DV, Balaram V, Naga Raju K, Sridhar DN. Paleoproterozoic Boninite-like rocks in an Inter-cratonic setting from northern Bastar craton, Central India. *Journal of the Geological Society of India*. 2008;**72**:373-380
- [34] Mir AR, Alvi SH, Balaram V. Boninitic geochemical characteristics of high-Mg mafic dykes from Singhbhum Granitoid complex, eastern India. *Acta Geochimica*. 2015;**34**(2):241-251
- [35] Wilson M. *Igneous Petrogenesis*. London: Unwin Hyman Ltd.; 1989. p. 466
- [36] Mir AR, Alvi SH. Mafic and ultramafic dykes of Singhbhum craton from Chaibasa, Jharkhand, eastern India: Geochemical constraints for their magma sources. *Current Science*. 2015;**109**(8):1399-1403
- [37] Kuno H. Differentiation of basaltic magmas. In: Hess HH, Poldervaart A, editors. *The Poldervaart Treatise on Rocks of Basaltic Composition*. New York: Interscience; 1968. pp. 623-688
- [38] Irvine TN, Baragar WRA. A guide to the chemical classification of the common rocks. *Canadian Journal of Earth Science*. 1971;**8**:523-548
- [39] Rollinson HR. *Using geochemical data: evaluation, presentation, interpretation*. Essex, U.K.: Longman Scientific Technical; 1993. p. 344
- [40] Shervais JW. Ti-V plots and the petrogenesis of modern and ophiolitic lavas. *Earth & Planetary Science Letters*. 1982;**87**:341-370
- [41] Zhao JH, Zhou MF. Geochemistry of Neoproterozoic mafic intrusions in the Panzhihua district (Sichuan Province, SW China): Implications for subduction-related metasomatism in the upper mantle. *Precambrian Research*. 2007;**152**:27-47
- [42] Mir AR, Alvi SH, Balaram V. Geochemistry of mafic dikes in the Singhbhum Orissa craton: Implications for subduction-related metasomatism of the mantle beneath the eastern Indian craton. *International Geology Review*. 2010;**52**(1):79-94
- [43] Sun SS, Mc Donough WF. Chemical and isotopic systematics of oceanic basalts: Implications for mantle composition and processes. In: Saunders AD, Norry MJ, editors. *Magmatism in the Ocean Basins*. Vol. 42. London, New York, Sydney: Special Publication, Geological Society of London; 1989. pp. 313-345
- [44] Kepezhinskas P, McDermott F, Defant M, Hochstaedter A, Drummond MS, Hawdesworth CJ, et al. Trace element and Sr-Nd-Pb isotopic constraints on a three-component model of Kamchatka arc petrogenesis. *Geochimica et Cosmochimica Acta*. 1997;**61**:577-600
- [45] Gladkochub DP, Wingate MTD, Pisarevsky SA, Donskaya TV, Mazukabzov AM, Ponomarchuk VA, et al. Mafic intrusions in southwestern Siberia and implications for a Neoproterozoic connection with Laurentia. *Precambrian Research*. 2006;**147**:260-278
- [46] Verma SP. Extension-related origin of magmas from a garnet-bearing source in the Los Tuxtlas volcanic field,

Mexico. *International Journal of Earth Science (Geologische Rundschau)*. 2006;**95**:871-901

[47] Ahmad T, Tarney J. Geochemistry and petrogenesis of Garhwal volcanics: Implications for evolution of the north Indian lithosphere. *Precambrian Research*. 1991;**50**:69-88

[48] Radhakrishna T, Joseph M. Geochemistry and petrogenesis of the Proterozoic dykes in Tamil nadu, southern India: Another example of the Archaean lithospheric mantle source. *Geologische Rundschau*. 1998;**87**:268-282

[49] Ringwood AE. *Composition and Petrology of the Earth's Mantle*. London: Mc Graw Hill; 1975. p. 618

[50] Sun SS, Nesbitt RW, Sharaskin AY. Geochemical characteristics of mid ocean ridge basalts. *Earth & Planetary Science Letters*. 1979;**44**:119-138

[51] Pearce JA, Norry MJ. Petrogenetic implications of Ti, Zr, Y and Nb variations in volcanic rocks. *Contribution to Mineralogy & Petrology*. 1979;**69**:33-47

[52] De Paolo DJ. Trace element and isotopic effects of combined wall rock assimilation and fractional crystallization. *Earth & Planetary Science Letters*. 1981;**53**:189-202

[53] Taylor SR, McLennan SM. *The Continental Crust: Its Composition and Evolution*. Oxford: Blackwell; 1985

[54] Hanyu T, Tatsumi Y, Nakai S, Chang Q, Miyazaki T, Sato K, et al. Contribution of slab melting and slab dehydration to magmatism in the NE Japan arc for the last 25 Myr: Constraints from geochemistry. *Geochemistry Geophysics Geosystems*. 2006;**7**(8):1-29

[55] Thompson RN, Morrison MA. Asthenospheric and lower lithospheric mantle contributions to continental extension magmatism: An example from the British Tertiary Province. *Chemical Geology*. 1988;**68**:1-15

[56] Wang XL, Zhou JC, Qiu JS, Jiang SY, Shi YR. Geochronology and geochemistry of Neoproterozoic mafic rocks from western Hunan, South China: Implications for petrogenesis and post-orogenic extension. *Geological Magazine*. 2008;**145**:215-233

[57] Saunders AD, Tarney J. Back-arc basins. In: Floyd PA, editor. *Oceanic Basalts*. Glasgow: Blackie; 1991. pp. 219-263

[58] Holm PE. The geochemical fingerprints of different tectonomagmatic environments using hygromagmatophile element abundances of tholeiitic basalts and basaltic andesites. *Chemical Geology*. 1985;**51**:303-323

[59] Ernst RE, Buchan KL. Large mafic magmatic events through time and links to mantle-plume heads. In: Ernst RE, Buchan KL, editors. *Mantle Plumes: Their Identification through Time*. Vol. 352. Boulder, Colorado: Geological Society America, Special Paper; 2001. pp. 483-575

[60] Goodenough KM, Upton BGJ, Ellam RM. Long term memory of subduction processes in the lithospheric mantle: Evidence from the geochemistry of basic dykes in the Gardar Province of South Greenland. *Journal of the Geological Society of London*. 2002;**159**:705-714

[61] Mir AR, Alvi SH, Balaram V. Geochemistry, petrogenesis and tectonic significance of the newer dolerites from

the Singhbhum Orissa craton, eastern Indian shield. *International Geology Review*. 2011a;53(1):46-60

[62] Mir AR, Alvi SH, Balaram V. Geochemistry of the mafic dykes in parts of the Singhbhum granitoid complex: Petrogenesis and tectonic setting. *Arabian Journal of Geosciences*. 2011;4:933-943

[63] Mir AR, Alvi SH, Balaram V, Bhat FA, Sumira Z, Dar SA. A subduction zone geochemical characteristic of the newer dolerite dykes in the Singhbhum craton, eastern India. *International Research Journal of Geology and Mining*. 2013;3(6):213-223

[64] Bose MK. Proterozoic dykes from Singhbhum granite pluton. In: Srivastava S, Rao C, editors. *Indian dykes*. New Delhi: Narosa Publication; 2008. pp. 413-445

[65] Sengupta P, Ray A, Pramanik S. Mineralogical and chemical characteristics of newer dolerite dyke around Keonjhar, Orissa: Implication for hydrothermal activity in subduction zone setting. *Journal of Earth System Science*. 2014;123(4):887-904

[66] Dasgupta P, Ray A, Chakraborti TM. Geochemical characterisation of the Neoproterozoic newer dolerite dykes of the Bahalda region, Singhbhum craton, Odisha, India: Implication for petrogenesis. *Journal of Earth System Science*. 2019;128:216

[67] Pandey OP, Mezger K, Upadhyay D, Paul D, Singh AK, Söderlund U, et al. Major-trace element and Sr-Nd isotope compositions of mafic dykes of the Singhbhum craton: Insights into evolution of the lithospheric mantle. *Lithos*. 2021;105959:382-383

[68] Bose MK. Mafic-ultramafic magmatism in the eastern Indian craton – A review. *Geological Survey of India*. 2000;55:227-258

[69] Mallick AK, Sarkar A. Geochronology and geochemistry of mafic dykes from Precambrians of Keonjhar, Orissa. *Indian Minerals*. 1994;48:3-24

[70] Kumar A, Parashuramulu V, Shankar R, Besse J. Evidence for a Neoproterozoic LIP in the Singhbhum craton, eastern India: Implications to Vaalbara supercontinent. *Precambrian Research*. 2017;292:163-174

